Dynamo processes and activity cycles of the active stars AB Doradus, LQ Hydrae and HR 1099

Jean-François Donati, A. C. Cameron, Meir Semel, Gaitee Hussain, Pascal Petit, B. D. Carter, S. C. Marsden, M. W. Mengel, Arturo Lopez-Ariste, S. V. Jeffers, et al.

▶ **To cite this version:**

Jean-François Donati, A. C. Cameron, Meir Semel, Gaitee Hussain, Pascal Petit, et al.. Dynamo processes and activity cycles of the active stars AB Doradus, LQ Hydrae and HR 1099. Monthly Notices of the Royal Astronomical Society, 2003, 345, pp.1145-1186. 10.1046/j.1365-2966.2003.07031.x . hal-03801336

HAL Id: hal-03801336
https://hal.science/hal-03801336

Submitted on 13 Oct 2022

HAL is a multi-disciplinary open access archive for the deposit and dissemination of scientific research documents, whether they are published or not. The documents may come from teaching and research institutions in France or abroad, or from public or private research centers.

L'archive ouverte pluridisciplinaire **HAL**, est destinée au dépôt et à la diffusion de documents scientifiques de niveau recherche, publiés ou non, émanant des établissements d'enseignement et de recherche français ou étrangers, des laboratoires publics ou privés.

2003MNRAS.345.1145D

Mon. Not. R. Astron. Soc. **345,** 1145–1186 (2003)

Dynamo processes and activity cycles of the active stars AB Doradus, LQ Hydrae and HR 1099

J.-F. Donati,[1⋆] A. Collier Cameron,[2⋆] M. Semel,[3⋆] G. A. J. Hussain,[2⋆] P. Petit,[1⋆] B. D. Carter,[4 ⋆] S. C. Marsden,[1,4⋆] M. Mengel,[4⋆] A. López Ariste,[3,5⋆] S. V. Jeffers[2⋆] and D. E. Rees[6⋆]

[1]*Laboratoire d'Astrophysique, Observatoire Midi-Pyrénées, F-31400 Toulouse, France*
[2]*School of Physics and Astronomy, University of St Andrews, St Andrews KY16 9SS*
[3]*LESIA, Observatoire de Paris-Meudon, F-92195 Meudon-Cedex, France*
[4]*Faculty of Sciences, The University of Southern Queensland, Toowoomba 4350, Australia*
[5]*High Altitude Observatory–NCAR, PO Box 3000, Boulder, CO 80307, USA*
[6]*CSIRO Division of Radiophysics, PO Box 76, Epping, NSW 2121, Australia*

Accepted 2003 July 18. Received 2003 July 3; in original form 2002 September 27

ABSTRACT

In this paper, we present new brightness and magnetic surface images of the young K0 dwarfs AB Doradus and LQ Hydrae, and of the K1 subgiant of the RS CVn system HR 1099 (=V711 Tauri), reconstructed from Zeeman–Doppler imaging spectropolarimetric observations collected at the Anglo-Australian Telescope during five observing campaigns (totalling 50 nights), from 1998 January to 2002 January. Along with the older images of the same stars (published in previous papers), our complete data set represents the first long-term series on temporal fluctuations of magnetic topologies of very active stars.

All of the magnetic images presented here indicate that large regions with predominantly azimuthal magnetic fields are continuously present at the surfaces of these stars. We take this as further evidence that the underlying dynamo processes that produce them are probably distributed throughout the entire convective zone (and not confined at its base, as in the Sun). We speculate that the radial and azimuthal field maps that we recover correspond, respectively, to the poloidal and toroidal components of the large-scale dynamo field.

We find, in particular, that some signatures, for instance the relative fraction of magnetic energy stored in the large-scale poloidal and toroidal field components, and the polarity of the axisymmetric component of the field, are variable with time, and provide potentially fruitful diagnostics for investigating magnetic cycles in active stars other than the Sun. We report here the detection of partial polarity switches in some of the axisymmetric field components of two of our programme stars (AB Dor and LQ Hya), suggesting that the dynamo operating in these stars may be cyclic.

Key words: line: profiles – stars: activity – binaries: close – stars: magnetic fields – stars: rotation – stars: spots.

1 INTRODUCTION

Zeeman–Doppler imaging or ZDI (Semel 1989; Brown et al. 1991; Donati & Brown 1997) is an innovative tomographic method similar to Doppler imaging (e.g. Vogt, Penrod & Hatzes 1987) that can reconstruct images of the surface magnetic field of rapidly rotating cool active stars, from high-resolution phase-resolved spectropolarimetric observations. As opposed to all other techniques for investigating stellar magnetic fields (e.g. Borra & Landstreet 1980; Robinson 1980; Basri, Marcy & Valenti 1992), which only yield magnetic field parameters averaged over the visible stellar disc (or at least over the visible magnetic regions), ZDI can recover both the location and the shape of magnetic regions at the surface of rapidly rotating cool active stars, but also (to a certain extent) the orientation of field lines within these magnetic regions. In this respect, ZDI represents a very promising opportunity to study the surface magnetic field structures of cool stars other than the Sun, as well as their

⋆E-mail: donati@ast.obs-mip.fr (J-FD); acc4@st-andrews.ac.uk (ACC); semel@obspm.fr (MS); gajh@st-andrews.ac.uk (GAJH); petit@ast.obs-mip.fr (PP); carterb@usq.edu.au (BDC); marsden@usq.edu.au (SCM); mengelm@usq.edu.au (MM); alopez@ucar.edu (ALA); svj1@st-andrews.ac.uk (SVJ); drees@tip.csiro.au (DER)

© 2003 RAS

© Royal Astronomical Society • Provided by the NASA Astrophysics Data System

2003MNRAS.345.1145D

temporal evolution (magnetic cycles) and the underlying dynamo processes, in a manner very similar to that used in the particular case of the Sun (e.g. Stenflo 1992).

ZDI has now been successfully applied to active stars of various evolutionary status, ranging from pre-main sequence to red giant branch stage. Magnetic fields have been detected in approximately 25 stars (e.g. Donati et al. 1997), and mapped for six of them (e.g. Donati et al. 1992, 1999; Donati & Cameron 1997; Donati 1999). The extremely surprising result obtained in these studies is that all such stars feature magnetic regions in which the field is mainly azimuthal, i.e. parallel to the surface and oriented along lines of equal latitude. At first order, the polarity of these azimuthal field regions is independent of longitude, suggesting that they actually reflect the toroidal component of an axisymmetric large-scale dynamo field and that the underlying dynamo processes operate within the bulk of the convective zone (rather than being confined to the interface with the radiative interior as in the Sun).

Monitoring such magnetic structures has already revealed significant long-term evolution possibly attributable to magnetic cycles (Donati 1999). For instance, the field structure of the K1 subgiant of the RS CVn system HR 1099 (=V711 Tauri) has evolved from an almost purely azimuthal field topology at epoch 1990.9 to a mixed field distribution at following epochs, indicating that the underlying activity cycle is probably in the phase of regenerating the poloidal component of the large-scale dynamo field. Similarly, the appearance, at the surface of the young K0 dwarf LQ Hydrae at epoch 1996.99, of a high-latitude azimuthal field feature with a polarity opposite to those detected in all previous maps may suggest that this star has recently undergone a new global polarity switch.

In this paper, we present new spectropolarimetric observations of the young ultrafast rotator AB Dor, of the young K0 dwarf LQ Hya and of the evolved K1 subgiant of the RS CVn system HR 1099, obtained during five major campaigns at the Anglo-Australian Telescope (AAT) with Semel's visitor polarimeter and the UCL echelle spectrograph (UCLES), taking place in 1998 January, 1998 December and 1999 January, 2000 December, 2000 December, 2001 December and 2002 January, and corresponding to a total number of 50 allocated nights. From these observations (detailed in Section 2), we reconstruct new maximum entropy brightness and magnetic surface images (presented in Sections 3–5) for all three stars and five epochs, thus expanding the time series already published by Donati et al. (1992), Donati & Cameron (1997), Donati (1999) and Donati et al. (1999). Finally we briefly discuss in Section 6 some of the implications of these new results for our knowledge of large-scale field structures and dynamo processes in cool active stars.

2 OBSERVATIONS AND MODELLING TOOLS

2.1 Instrumental setup

The observational setup used for this new series of observation is very similar to that described in Donati et al. (1997, 1999), Donati & Cameron (1997) and Donati (1999). It consists of a visitor polarimeter mounted at the Cassegrain focus of the 3.9-m Anglo-Australian Telescope, and collecting stellar light through a 1.8-arcsec circular aperture. Note that the polarimeter used for these runs is completely new and now involves, in particular, quarter-wave and half-wave Fresnel rhombs (e.g. Bennett 1970) to achieve a very achromatic polarimetric analysis. We no longer rotate the quarter-wave retarder, as in the previous setup (e.g. Donati et al. 1997), because of the lateral beam displacement it generates (as a single Fresnel parallelepiped), but rotate instead the half-wave Fresnel rhomb (made of two optically contacted Fresnel parallelepipeds inducing no lateral beam displacement, and placed after the quarter-wave rhomb in the beam) with the same overall result as in the old setup (an exchange of both beams throughout the whole instrument). A double optical fibre then conveys the light from the polarimeter down to the UCL echelle spectrograph, fed through a Bowen–Walraven image slicer device (set in a two slice per fibre configuration). The refocusing optics attendant to the image slicer were the same as those described in Donati et al. (1999), yielding a total slit size of 3.8×0.45 mm^2 at the entrance of the spectrograph, except in 1999 December where the old 1995 December slicer setup was used (see table 1 in Donati et al. 1997).

The other significant change with respect to the set up described in Donati et al. (1999) concerns the CCD detector. In the first four observing seasons reported here, we used a MIT/LL CCD with 2048×4096 15 μm^2 pixel, while an EEV CCD with the same format, but smaller (13.5 μm^2) pixels, was made available to us in the last run. As both chips are larger than the unvignetted field of UCLES camera, we used a smaller window format (2048×2448 pixel for the MIT/LL chip and 2048×2746 pixel for the EEV chip) to reduce read-out time (down to approximately 1 min in fast mode). With the 31.6 groove mm^{-1} grating, up to 52 orders (number 80–131) can be fully recorded on to the MIT/LL detector, ensuring full spectral coverage from 430 to 715 nm in a single exposure with significant overlap (as much as a half free spectral range for the bluest orders) between successive orders. For the EEV chip, the full spectral coverage is slightly smaller (46 orders altogether, ranging from number 84 to 129 and covering from 437 to 681 nm), but this loss of photons is largely compensated by the much higher quantum efficiency of the CCD in most of the spectral window (up to a factor of 2 at 430 nm and a factor of 1.5 at 500 nm). Note that the reduced detector window format ensures that vignetting within the UCLES camera should only be, for each order, approximately 10 per cent larger on both order edges than at the order centre.

With the MIT/LL (respectively, EEV) detector, the slit (convolved with the spectrograph broadening profile) projects on to 29×2.5 pixel (respectively, 33×2.7 pixel), yielding an average spectral resolution of approximately 70 000 and an average pixel size of

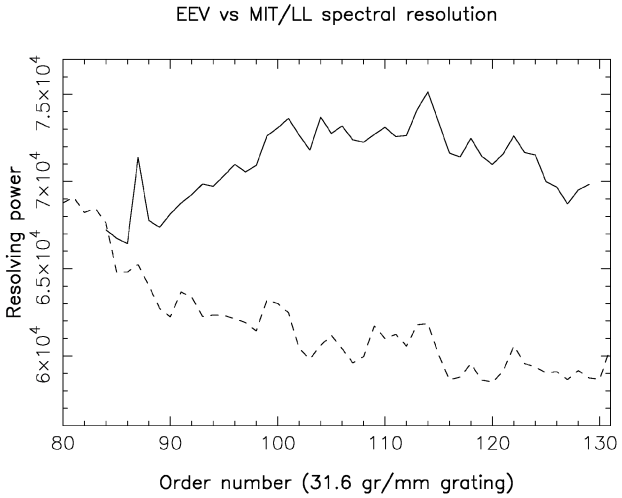

Figure 1. Resolving power of UCLES as a function of the order of number, when using either the EEV (full line) or the MIT/LL chip (dashed line), the 31.6 groove mm^{-1} grating and a 0.45 mm wide slit. The resolution in each order is estimated from the average full width at half maximum of approximately 40 Th lines.

© Royal Astronomical Society • Provided by the NASA Astrophysics Data System

2003MNRAS.345.1145D

Table 1. Journal of observations for AB Dor. The first column lists the date of observation, while columns 2 and 3 indicate the Julian date and Universal Time of the first and last subexposure of each continuous series. Column 4 mentions the total number of individual subexposures/polarization sequences in the associated series of subexposures. Columns 5–8 indicate, for each polarization spectrum, the corresponding total exposure time, peak S/N ratio per pixel (of 1.9 km s^{-1} for the first four runs, and of 1.7 km s^{-1} for the fifth one), S/N ratio in the associated Stokes V least-squares deconvolved spectra (per 2 km s^{-1} velocity bin for the first four runs, and per 1.7 km s^{-1} bin in the fifth one), and multiplex gain in S/N ratio, respectively. Note that whenever more than one polarization sequence is available in a continuous series (i.e. for most AB Dor observations), these columns list the range of variations of these parameters.

Date	JD (245 0000+)	UT (h:m:s)	n_{exp}	t_{exp}	S/N	S/N_{LSD}	Multiplex gain
1998 Jan. 10	824.0520/824.1275	13:14:53/15:03:36	24/6	800	250/280	8800/9500	34/35
	824.1456/824.1961	15:29:37/16:42:23	16/4	800	170/190	5900/6600	34/35
	824.2066/824.2187	16:57:26/17:14:59	5/1	800	170	5600	33
1998 Jan. 11	824.9039/824.9255	09:41:40/10:12:42	8/2	800	180/270	6400/9400	35/36
	824.9530/825.0481	10:52:22/13:09:15	32/8	800	180/310	5100/10 600	22/36
	825.0688	13:39:02	1/0				
1998 Jan. 15	828.9009/828.9226	09:37:21/10:08:35	8/2	800	280	10 000/10 300	36/37
	828.9411/828.9992	10:35:12/11:58:50	20/5	800	270/280	9600/10 100	35/36
	829.0163/829.0380	12:23:30/12:54:47	8/2	800	240	8400/8500	35
	829.0550/829.0732	13:19:11/13:45:27	7/2	400/800	180/280	6700/10 400	37
1998 Dec. 27	1174.9217/1174.9561	10:07:17/10:56:43	12/3	800	210	8200/8300	39/40
	1174.9968/1175.0426	11:55:22/13:01:20	16/4	800	180/240	6300/9300	35/39
	1175.0632/1175.1059	13:30:58/14:32:33	14/3	800	220	8300/8500	38/39
	1175.1201/1175.1417	14:53:00/15:24:01	8/2	800	220/230	8100/8600	37
	1175.1667/1175.2128	16:00:05/17:06:22	16/4	800	110/150	3800/5400	35/38
	1175.2309/1175.2406	17:32:29/17:46:26	4/1	800	130	4800	37
	1175.2498/1175.2730	17:59:44/18:33:11	8/2	800	100/120	3300/4000	33
1998 Dec. 29	1176.9703/1177.1078	11:17:17/14:35:17	32/8	800	31/130	600/4900	19/38
	1177.1328/1177.2027	15:11:12/16:51:57	24/6	800	100/230	3400/8300	34/37
1999 Jan. 02	1181.0005/1181.0586	12:00:40/13:24:25	20/5	800	190/230	6400/8300	34/36
	1181.0754/1181.1454	13:48:35/15:29:23	24/6	800	160/210	6300/7700	36/39
	1181.1629/1181.2207	15:54:36/17:17:49	20/5	800	150/170	5300/6400	35/38
	1181.2391/1181.2654	17:44:19/18:22:13	9/2	800	110/130	3800/4600	35
1999 Jan. 03	1181.9757/1182.0213	11:25:03/12:30:39	16/4	800	160/180	6300/7000	39/40
1999 Dec. 19	1531.9277/1531.9913	10:15:50/11:47:27	20/5	800	280/300	10 400/11 100	36/37
	1532.0174/1532.0666	12:25:02/13:35:55	16/4	800	81/260	1900/9300	23/36
1999 Dec. 21	1534.1334/1534.2168	15:12:05/17:12:15	28/7	800	120/170	3600/5900	30/36
	1534.2355/1534.2477	17:39:07/17:56:45	5/1	800	100	3000	30
2000 Dec. 04	1882.9595/1883.0190	11:01:44/12:27:23	20/5	800	210/230	6300/7100	29/31
	1883.0382/1883.1136	12:54:59/14:43:36	24/6	800	190/220	5200/6200	27/28
	1883.1506/1883.1853	15:36:56/16:26:54	12/3	800	120/130	3200/3500	26/27
	1883.2081/1883.2425	16:59:43/17:49:16	12/3	800	150/160	3900/4100	26/27
2000 Dec. 08	1886.9247/1886.9968	10:11:35/11:55:23	24/6	800	180/220	5400/6800	30/32
	1887.0372/1887.1221	12:53:33/14:55:51	28/7	800	200/220	5900/6600	29/30
	1887.1547/1887.1890	15:42:48/16:32:07	12/3	800	220/240	7100/8000	32/33
	1887.2267/1887.2486	17:26:29/17:57:59	8/2	800	240	8100/8200	34
2001 Dec. 22	2265.9189/2266.0071	10:03:09/12:10:10	28/7	800	240/300	10 000/12 000	40/42
	2266.0280/2266.0897	12:40:21/14:09:12	20/5	800	240/270	10 200/11 400	41/43
	2266.1245/2266.1635	14:59:17/15:55:25	12/3	800	200/220	8000/9000	40/41
	2266.1859/2266.2211	16:27:43/17:18:26	12/3	800	160/170	6000/6500	36/38
	2266.2409/2266.2642	17:46:51/18:20:27	8/2	800	140/160	5000/5800	36
2001 Dec. 25	2269.1011/2269.1475	14:25:39/15:32:22	14/4	400/800	63/110	2200/4200	31/38
	2269.1681/2269.2048	16:02:07/16:54:51	12/3	800	64/100	1700/3600	27/36
	2269.2263/2269.2617	17:25:55/18:16:50	12/3	800	91/100	3200/3700	35/37
2001 Dec. 28	2271.9012/2271.9239	09:37:42/10:10:28	8/2	800	250	10 600/10 700	42/43
	2271.9428/2271.9916	10:37:39/11:47:53	16/4	800	240/280	10 000/11 700	41/43
	2272.0113/2272.0760	12:16:18/13:49:26	20/5	800	250/280	11 200/12 300	43/45
	2272.1101/2272.1461	14:38:35/15:30:24	12/3	800	280/300	11 900/12 700	42
	2272.1643/2272.1995	15:56:37/16:47:18	12/3	800	290/300	11 600/12 200	40/41
	2272.2177/2272.2559	17:13:32/18:08:31	12/3	800	260/290	10 500/11 600	40
2002 Jan. 01	2276.0164/2276.0644	12:23:41/13:32:48	16/4	800	300/310	12 400/12 700	41/42
	2276.0981/2276.1463	14:21:19/15:30:37	16/4	800	300/310	11 800/12 400	38/41
	2276.1656/2276.1880	15:58:25/16:30:39	8/2	800	290/300	11 900/12 200	41

© Royal Astronomical Society • Provided by the NASA Astrophysics Data System

2003MNRAS.345.1145D

Table 2. Same as Table 1 for LQ Hya.

Date	JD (245 0000+)	UT (h:m:s)	n_{exp}	t_{exp}	S/N	S/N_{LSD}	Multiplex gain
1998 Jan. 10	824.0240/824.0368	12:34:37/12:52:57	4/1	1200	170	5900	35
	824.2253/824.2421	17:24:24/17:48:37	5/1	1200	100	3300	33
1998 Jan. 11	825.1914/825.2047	16:35:40/16:54:48	4/1	1200	130	4600	35
1998 Jan. 12	826.0367/826.0497	12:52:51/13:11:38	4/1	1200	140	4800	34
	826.0956/826.1082	14:17:39/14:35:48	4/1	1200	110	3900	35
	826.2231/826.2359	17:21:13/17:39:46	4/1	1200	100	2500	25
1998 Jan. 15	829.0032/829.0124	12:04:35/12:17:50	4/1	800	110	4400	40
	829.1751/829.1842	16:12:05/16:25:18	4/1	800	130	4900	38
1998 Dec. 27	1175.1457/1175.1549	15:29:51/15:43:00	4/1	800	130	4600	35
1998 Dec. 28	1176.0798/1176.0925	13:54:53/14:13:12	4/1	1200	29	800	28
	1176.1018/1176.1145	14:26:35/14:44:52	4/1	1200	73	1700	23
	1176.1537/1176.1663	15:41:16/15:59:29	4/1	1200	67	2000	30
1998 Dec. 29	1177.0472/1177.0578	13:07:54/13:23:11	4/1	970	36	900	25
	1177.2073/1177.2199	16:58:35/17:16:43	4/1	1200	120	4300	36
1998 Dec. 30	1178.0425/1178.0552	13:01:15/13:19:25	4/1	1200	88	2800	32
	1178.1281/1178.1408	15:04:31/15:22:43	4/1	1200	110	4000	36
	1178.2000/1178.2129	16:47:59/17:06:31	4/1	1200	73	2100	29
	1178.2535/1178.2577	18:05:01/18:11:07	2/1	600	30	800	27
1999 Jan. 02	1181.1495/1181.1587	15:35:21/15:48:30	4/1	800	120	4400	37
1999 Jan. 03	1182.0878/1182.0969	14:06:23/14:19:32	4/1	800	110	4200	38
	1182.1398/1182.1489	15:21:20/15:34:29	4/1	800	120	4300	36
	1182.2049/1182.2141	16:55:04/17:08:16	4/1	800	130	4600	35
1999 Dec. 20	1533.0693/1533.0824	13:39:49/13:58:42	4/1	1200	110	3600	33
	1533.1694/1533.1819	16:03:52/16:22:00	4/1	1200	140	4700	34
	1533.2561/1533.2688	18:08:43/18:27:03	4/1	1200	120	4100	34
1999 Dec. 21	1534.0979/1534.1105	14:21:00/14:39:11	5/1	1200	160	5500	34
1999 Dec. 29	1542.0600/1542.0726	13:26:26/13:44:34	4/1	1200	170	5300	31
	1542.2012/1542.2139	16:49:46/17:07:59	4/1	1200	220	8100	37
2000 Dec. 04	1883.1189/1883.1317	14:51:12/15:09:43	4/1	1200	100	2700	27
	1883.1904/1883.2033	16:34:10/16:52:45	4/1	1200	89	2600	29
	1883.2475/1883.2604	17:56:28/18:15:00	4/1	1200	130	4200	32
2000 Dec. 05	1884.1334/1884.1463	15:12:10/15:30:41	4/1	1200	170	5300	31
	1884.2016/1884.2149	16:50:22/17:09:24	4/1	1200	130	4400	34
	1884.2576/1884.2670	18:10:58/18:24:29	4/1	800	100	3500	35
2000 Dec. 06	1885.1266/1885.1419	15:02:15/15:24:17	4/1	800	100	3200	32
	1885.2028/1885.2121	16:51:59/17:05:29	4/1	800	150	5100	34
2000 Dec. 07	1886.1502/1886.1630	15:36:13/15:54:41	4/1	1200	75	1900	25
	1886.2463/1886.2557	17:54:44/18:08:14	4/1	800	50	1000	20
2000 Dec. 08	1887.1262/1887.1358	15:01:42/15:15:36	4/1	800	120	4000	33
	1887.1937/1887.2031	16:39:00/16:52:28	4/1	800	160	5100	32
	1887.2534/1887.2628	18:04:52/18:18:22	4/1	800	170	5500	32
2000 Dec. 09	1888.1143/1888.1237	14:44:33/14:58:04	4/1	800	74	2200	30
	1888.1782/1888.1877	16:16:39/16:30:14	4/1	800	74	2100	28
	1888.2415/1888.2510	17:47:45/18:01:30	4/1	800	100	3100	31
2000 Dec. 10	1889.1123/1889.1217	14:41:39/14:55:11	4/1	800	110	3700	34
	1889.1760/1889.1854	16:13:26/16:27:01	4/1	800	130	4600	35
	1889.2469/1889.2594	17:55:30/18:13:33	4/1	800	110	3600	33
2000 Dec. 11	1890.2175/1890.2321	17:13:09/17:34:14	4/1	1200	52	1100	21
2000 Dec. 12	1891.1119/1891.1248	14:41:12/14:59:47	4/1	1200	100	3000	30
	1891.1882/1891.2016	16:31:04/16:50:19	4/1	1200	130	4400	34
	1891.2617/1891.2716	18:16:51/18:31:10	4/1	900	100	3300	33
2001 Dec. 21	2265.0879/2265.1098	14:06:37/14:38:06	5/1	1200	99	2200	22
	2265.1923/2265.2054	16:36:53/16:55:44	4/1	1200	140	5100	36
	2265.2601/2265.2698	18:14:33/18:28:33	4/1	800	100	4000	40
2001 Dec. 22	2266.0952/2266.1048	14:17:08/14:30:55	4/1	800	110	3300	30
	2266.1697/2266.1793	16:04:24/16:18:13	4/1	800	140	5100	36
	2266.2256/2266.2352	17:24:49/17:38:40	4/1	800	120	4100	34
	2266.2686/2266.2728	18:26:47/18:32:47	2/1	400	83	3000	36
2001 Dec. 23	2267.1688/2267.1791	16:03:06/16:17:54	4/1	800	100	3400	34
	2267.2506/2267.2602	18:00:55/18:14:43	4/1	800	130	4900	38
2001 Dec. 24	2268.1373/2268.1469	15:17:41/15:31:30	4/1	800	110	3900	35

© Royal Astronomical Society • Provided by the NASA Astrophysics Data System

2003MNRAS.345.1145D

Table 2 – *continued*

Date	JD (245 0000+)	UT (h:m:s)	n_{exp}	t_{exp}	S/N	S/N_{LSD}	Multiplex gain
2001 Dec. 25	2269.0874/2269.0969	14:05:48/14:19:36	4/1	800	69	2400	35
	2269.1538/2269.1634	15:41:27/15:55:15	4/1	800	48	1500	31
	2269.2124/2269.2221	17:05:50/17:19:48	4/1	800	80	2800	35
2001 Dec. 26	2270.0796/2270.0893	13:54:35/14:08:33	4/1	800	99	3500	35
	2270.1684/2270.1780	16:02:33/16:16:21	4/1	800	100	3800	38
	2270.2486/2270.2582	17:57:58/18:11:45	4/1	800	100	3600	36
2001 Dec. 27	2271.0908/2271.1006	14:10:42/14:24:49	4/1	800	170	6500	38
	2271.1446/2271.1545	15:28:17/15:42:28	4/1	800	180	6800	38
	2271.2022/2271.2118	16:51:11/17:05:03	4/1	800	180	7200	40
	2271.2496/2271.2592	17:59:24/18:13:18	4/1	800	170	7000	41
2001 Dec. 28	2272.0803/2272.0903	13:55:40/14:10: 2	4/1	800	180	7000	39
	2272.1504/2272.1600	15:36:31/15:50:21	4/1	800	190	8100	43
	2272.2038/2272.2134	16:53:31/17:07:19	4/1	800	200	8300	42
	2272.2604/2272.2703	18:14:58/18:29:13	4/1	800	200	8100	40
2001 Dec. 30	2274.0893/2274.0989	14:08:33/14:22:22	4/1	800	110	3800	35
	2274.1726/2274.1821	16:08:30/16:22:17	4/1	800	88	2900	33
	2274.2387/2274.2615	17:43:40/18:16:36	6/2	400/800	73/82	2600/2700	32/37
2001 Dec. 31	2275.0743/2275.0839	13:46:59/14:00:47	4/1	800	140	6000	43
	2275.1568/2275.1664	15:45:46/15:59:33	4/1	800	180	7100	39
	2275.2370/2275.2469	17:41:19/17:55:33	4/1	800	200	8200	41
2002 Jan. 01	2276.0691/2276.0786	13:39:26/13:53:15	4/1	800	190	7700	41
	2276.1510/2276.1606	15:37:23/15:51:13	4/1	800	190	7600	40
	2276.2345/2276.2441	17:37:43/17:51:32	4/1	800	160	6400	40
2002 Jan. 02	2277.0532/2277.0747	13:16:37/13:47:34	5/1	1600	62	2100	34
	2277.1355/2277.1520	15:15:07/15:38:54	4/1	1600	100	3700	37
	2277.1984/2277.2150	16:45:41/17:09:33	4/1	1600	78	2700	35
	2277.2400/2277.2669	17:45:37/18:24:19	4/1	1600	81	2900	36

1.9 km s^{-1} (respectively 1.7 km s^{-1}). Strangely enough, we observe that the resolving power with the MIT/LL chip is smaller than predicted and varies slightly with wavelength, decreasing from the nominal value at 710 nm (order 80) down to approximately 59 000 at 435 nm (order 131), with a sharp gradient in the 10 reddest orders (see Fig. 1). This effect is probably attributable to crosstalk between adjacent pixels in the MIT/LL CCD detector.

2.2 Data collection and reduction

Out of the 50 nights allocated, approximately 36 could be used to gather some data on our programme stars (those discussed in this paper and some others, the analysis of which will be described in separate contributions), for a total amount of clear (though not necessarily photometric) time of approximately 28 nights (56 per cent of total allocation). While the second (1998 December and 1999 January), fourth (2000 December) and fifth (2001 December and 2002 January) campaign runs were rather productive (with respective fractions of clear time equal to 50, 73 and 77 per cent), the first campaign (1998 January) was only a mild success (with no more than 43 per cent of clear time) while the third one (1999 December) was extremely disappointing (with as low as 27 per cent of clear time).

All frames collected during these campaigns were processed with ESPRIT, a dedicated package for optimal extraction of echelle spectropolarimetric observations (Donati et al. 1997). Altogether, 799, 354 and 352 individual subexposures were collected on AB Dor, LQ Hya and HR 1099, respectively, in different positions of the half-wave Fresnel rhomb (see Section 2.1) and converted to unpolarized (i.e. Stokes *I*) spectra with ESPRIT. By combining groups of two or four successive subexposures (see Donati et al. 1997, for details on the extraction procedure), we also derived 199, 89 and 87 circular polarization (i.e. Stokes *V*) spectra of these three targets. The detailed log of the observations is given in Tables 1–3. A number of these spectra (17 for AB Dor, 20 for LQ Hya, 5 for HR 1099, most of them recorded during twilight) were discarded due to contamination by scattered sunlight. The large spread in signal-to-noise (S/N) ratio values, e.g. ranging from 31 to 330 per 2 km s^{-1} velocity bin in the particular case of our 800 s AB Dor polarization sequences, essentially reflects the relatively poor weather that plagued most of our runs (except the last one). From the peak S/N ratio of 310 per 1.7 km s^{-1} bin obtained from a 800 s exposure on AB Dor, we can nevertheless conclude that the new version of our instrument is roughly as efficient as the previous one (with which we reached maximum S/N ratio values of 430 per 3 km s^{-1} pixel in the same exposure time).

As in previous analyses (Donati & Cameron 1997; Donati 1999; Donati et al. 1999), we used least-squares deconvolution (LSD) to compute 'average' Stokes *I* and *V* spectral line profiles (called LSD profiles in the following) from each unpolarized and circularly polarized spectra. LSD, a technique similar to cross-correlation developed by Donati et al. (1997), extracts profile information from the thousands of moderate to strong spectral lines in the recorded wavelength domain. The most obvious advantage of LSD profiles is that their relative noise level is considerably reduced compared with that of any single line of the original spectrum. Moreover, as demonstrated in Donati & Cameron (1997), LSD conserves the shape of a pure rotational profile to a very good degree of accuracy, implying that any deviation observed in LSD profiles from this reference level can be considered as real and, in our particular case, ready to be interpreted in terms of brightness/magnetic inhomogeneities on stellar surfaces.

© Royal Astronomical Society • Provided by the NASA Astrophysics Data System

2003MNRAS.345.1145D

Table 3. Same as Table 1 for HR 1099.

Date	JD (245 0000+)	UT (h:m:s)	n_{exp}	t_{exp}	S/N	S/N_{LSD}	Multiplex gain
1998 Jan. 10	824.0027/824.0155	12:03:49/12:22:16	4/1	1200	380	14 900	39
1998 Jan. 11	824.9350/824.9476	10:26:26/10:44:35	4/1	1200	310	9700	31
	825.0540/825.0642	13:17:48/13:32:23	4/1	800	230	8500	37
1998 Jan. 12	825.9147/825.9385	09:57:11/10:31:23	5/1	1200	240	8500	35
	826.0561/826.0654	13:20:49/13:34:13	4/1	800	240	9100	38
1998 Jan. 15	828.9273/828.9366	10:15:17/10:28:41	4/1	800	320	14 000	44
	829.0420/829.0512	13:00:26/13:13:40	4/1	800	310	12 900	42
1998 Dec. 27	1175.0480/1175.0579	13:09:09/13:23:19	4/1	800	370	15 500	42
1998 Dec. 28	1175.9207/1175.9377	10: 5:52/10:30:15	5/1	1200	190	3000	16
	1175.9713/1175.9840	11:18:37/11:36:56	4/1	1200	100	2800	28
	1176.0002/1176.0298	12:00:18/12:42:55	8/2	1200	200/210	6100/8100	29/40
1998 Dec. 29	1176.9033/1176.9246	09:40:44/10:11:25	8/2	800	250/300	10 100/12 800	40/43
	1177.0334/1177.0425	12:48:02/13:01:13	4/1	800	150	4500	30
1998 Dec. 30	1177.9177/1177.9303	10:01:29/10:19:40	4/1	1200	320	13 100	41
	1177.9766/1177.9811	11:26:17/11:32:44	2/1	600	170	6400	38
	1178.0256/1178.0375	12:36:49/12:53:58	4/1	800	270	10 600	39
	1178.0770/1178.0862	13:50:56/14:04:08	4/1	800	220	8800	40
1999 Jan. 02	1181.0625/1181.0716	13:30:01/13:43:10	4/1	800	330	14 300	43
1999 Jan. 03	1181.9090/1181.9185	09:48:55/10:02:39	4/1	800	330	12 900	39
	1182.0745/1182.0836	13:47:16/14:00:24	4/1	800	230	10 100	44
1999 Dec. 19	1531.9972/1532.0105	11:55:55/12:15:07	4/1	1200	500	19 100	38
1999 Dec. 20	1532.9094/1532.9224	09:49:30/10:08:13	4/1	1200	450	17 700	39
	1533.0886/1533.1014	14:07:38/14:25:58	4/1	1200	340	13 400	39
1999 Dec. 21	1534.0031/1534.0157	12:04:31/12:22:39	4/1	1200	360	10 300	29
	1534.0297/1534.0423	12:42:48/13:00:57	4/1	1200	380	15 100	40
	1534.1159/1534.1285	14:46:55/15:05:02	4/1	1200	250	6600	26
1999 Dec. 29	1542.0409/1542.0536	12:58:57/13:17:09	4/1	1200	350	12 300	35
2000 Dec. 04	1882.9449/1882.9545	10:40:42/10:54:27	4/1	800	220	9100	41
	1883.0245/1883.0339	12:35:16/12:48:52	4/1	800	280	11 000	39
	1883.1371/1883.1465	15:17:25/15:30:56	4/1	800	230	7800	34
2000 Dec. 05	1883.9217/1883.9345	10:07:11/10:25:40	4/1	1200	460	17 100	37
	1883.9648/1883.9776	11:09:16/11:27:46	4/1	1200	360	15 100	42
	1884.0155/1884.0283	12:22:17/12:40:49	4/1	1200	420	17 800	42
	1884.1520/1884.1649	15:38:52/15:57:26	4/1	1200	450	15 200	34
2000 Dec. 06	1885.1466/1885.1560	15:31:06/15:44:36	4/1	800	290	10 100	35
2000 Dec. 07	1885.9227/1885.9355	10:08:41/10:27:09	4/1	1200	440	15 800	36
	1885.9805/1885.9934	11:31:53/11:50:30	4/1	1200	390	14 800	38
	1886.1312/1886.1442	15:08:57/15:27:43	4/1	1200	350	12 200	35
2000 Dec. 08	1886.9092/1886.9186	09:49:14/10:02:50	4/1	800	390	14 400	37
	1887.0186/1887.0281	12:26:50/12:40:28	4/1	800	380	15 100	40
	1887.1402/1887.1495	15:21:52/15:35:19	4/1	800	330	12 000	36
2000 Dec. 09	1887.8973/1887.9102	09:32:10/09:50:38	4/1	1200	310	12 900	42
	1887.9500/1887.9628	10:47:59/11:06:27	4/1	1200	400	15 000	38
	1888.0151/1888.0244	12:21:41/12:35:11	4/1	800	280	10 300	37
	1888.1284/1888.1378	15:04:57/15:18:25	4/1	800	190	6600	35
2000 Dec. 10	1888.8980/1888.9109	09:33:11/09:51:40	4/1	1200	380	15 300	40
	1888.9476/1888.9605	10:44:29/11:03:03	4/1	1200	380	15 100	40
	1889.0118/1889.0212	12:17:03/12:30:33	4/1	800	340	13 100	39
	1889.1267/1889.1361	15:02:28/15:16:02	4/1	800	290	10 600	37
2000 Dec. 11	1889.9159/1889.9287	09:58:52/10:17:23	4/1	1200	370	14 600	39
	1889.9674/1889.9820	11:13:02/11:34:04	4/1	1200	400	15 400	38
	1889.9880/1890.0120	11:42:43/12:17:15	4/0	2400	460	18 700	41
	1890.0387/1890.0516	12:55:45/13:14:20	4/1	1200	440	17 000	39
	1890.1262/1890.1390	15:01:41/15:20:10	4/1	1200	150	2200	15
2000 Dec. 12	1890.8961/1890.9090	09:30:23/09:48:54	4/1	1200	390	15 100	39
	1890.9466/1890.9595	10:43:04/11:01:41	4/1	1200	430	16 900	39
	1891.0387/1891.0515	12:55:40/13:14:09	4/1	1200	330	12 600	38
	1891.1315/1891.1446	15:09:22/15:28:14	4/1	1200	280	10 100	36
2000 Dec. 14	1893.0472/1893.0565	13:07:56/13:21:25	4/1	400	130	5000	38
2001 Dec. 21	2265.0249/2265.0383	12:35:55/12:55:06	4/1	1200	400	15 500	39
	2265.1187/2265.1319	14:50:59/15:09:54	4/1	1200	360	13 200	37

© Royal Astronomical Society • Provided by the NASA Astrophysics Data System

2003MNRAS.345.1145D

Table 3 – *continued*

Date	JD (245 0000+)	UT (h:m:s)	n_{exp}	t_{exp}	S/N	S/N_{LSD}	Multiplex gain
2001 Dec. 22	2265.9027/2265.9133	09:39:56/09:55:10	4/1	800	380	15 500	41
	2266.0131/2266.0227	12:18:49/12:32:37	4/1	800	380	15 900	42
	2266.1095/2266.1191	14:37:41/14:51:29	4/1	800	280	11 300	40
2001 Dec. 23	2266.8997/2266.9093	09:35:31/09:49:20	4/1	800	450	19 300	43
	2266.9993/2267.0094	11:58:56/12:13:35	4/1	900	280	9200	33
2001 Dec. 25	2269.0715/2269.0811	13:42:56/13:56:47	4/1	800	230	9200	40
2001 Dec. 26	2269.9024/2269.9119	09:39:24/09:53:11	4/1	800	300	12 700	42
	2269.9985/2270.0081	11:57:54/12:11:44	4/1	800	260	10 700	41
2001 Dec. 27	2270.9024/2270.9120	09:39:28/09:53:16	4/1	800	390	16 500	42
	2270.9978/2271.0075	11:56:54/12:10:44	4/1	800	480	20 700	43
	2271.0763/2271.0859	13:49:51/14:03:41	4/1	800	440	18 400	42
2001 Dec. 28	2271.9286/2271.9382	10:17:11/10:31:00	4/1	800	440	18 200	41
	2271.9966/2272.0067	11:55:02/12:09:35	4/1	800	500	21 500	43
	2272.0948/2272.1046	14:16:27/14:30:35	4/1	800	440	17 400	40
2001 Dec. 30	2273.9060/2273.9157	09:44:39/09:58:38	4/1	800	300	10 400	35
	2273.9918/2274.0014	11:48:10/12:01:59	4/1	800	420	18 000	43
2001 Dec. 31	2274.9144/2274.9252	09:56:45/10:12:16	4/1	900	330	14 700	45
	2274.9833/2274.9928	11:35:53/11:49:41	4/1	800	380	16 300	43
	2275.0892/2275.0993	14:08:29/14:23:03	4/1	800	380	15 000	39
2002 Jan. 01	2275.9095/2275.9192	09:49:41/10:03:41	4/1	800	510	23 200	45
	2275.9588/2275.9684	11:00:38/11:14:26	4/1	800	440	19 800	45
	2276.0833/2276.0929	14:00:01/14:13:48	4/1	800	520	20 200	39
2002 Jan. 02	2276.9150/2276.9247	09:57:38/10:11:30	4/1	800	340	15 200	45
	2276.9873/2276.9969	11:41:41/11:55:29	4/1	800	270	11 400	42
	2277.0810/2277.0941	13:56:42/14:15:31	4/1	1200	170	7200	42

The list of spectral lines available for LSD (and in particular their wavelengths, relative central depths and Landé factors) are obtained from a full LTE spectral synthesis using Kurucz's (1993) model atmospheres (a $T_{\rm eff} = 5000$ K and $\log g = 4.5$ atmosphere for AB Dor and LQ Hya, and a $T_{\rm eff} = 4750$ K and $\log g = 3.5$ atmosphere for HR 1099), and selecting only those features where the relative central depth (prior to rotation or macroturbulence broadening) exceeds 40 per cent of the local continuum flux. In our particular case, the total number of spectral features used in the analysis ranged from approximately 3600 up to 4500 depending on the spectral type (lines appearing in two adjacent orders being counted as two different spectral features), yielding multiplex gains for Stokes V profiles of up to 45 in the S/N ratio[1] (see Tables 1–3).

Zeeman signatures are clearly detected in most spectra of all runs, with a mean relative peak-to-peak amplitude of 0.12, 0.25 and 0.15 per cent for AB Dor, LQ Hya and HR 1099, respectively, (similar to what was obtained in previous runs, e.g. Donati et al. 1997). All LSD profiles shown in Sections 3–5 are normalized to mean weights of 0.7 and 500 nm for Stokes I and Stokes V data, respectively, (see Donati et al. 1997, Section 4.1, for the exact definition of these normalizing factors).

A new procedure was also applied to all spectra to correct for small shifts occurring within the spectrograph throughout the night, for various technical reasons (e.g. dewar refill, thermal and mechanical relaxation of components). For this purpose, we use the rich spectrum of telluric lines that plague most spectroscopic data recorded at the AAT. With the help of a specific LSD mask (built from a digitized solar atlas and including approximately 600 lines throughout our domain of interest), we construct a mean LSD telluric line profile and use it as a velocity reference (by assuming that the centroid of this LSD profile coincides with zero radial velocity in the observer's rest frame). Shifts of up to 2 km s^{-1} are found to occur within UCLES throughout the nights, sometimes very progressively between the beginning and the end of the night, sometimes suddenly between two exposures (and not necessarily correlated with a dewar refill or any other obvious human operation within the spectrograph). These shifts are corrected by simply applying a standard velocity correction to the wavelength scale produced by ESPRIT. Using standard stars with sharp spectral lines, we find that radial velocities derived from spectra corrected with this method are stable to better than 0.1 km s^{-1}.

2.3 Brightness and magnetic tomographic imaging of stellar surfaces

To perform brightness and magnetic tomographic imaging of stellar surfaces from sets of rotationally modulated Stokes I and V profiles, we use the image reconstruction code of Brown et al. (1991) and Donati & Brown (1997), which implements Skilling & Bryan's (1984) algorithm for maximum entropy optimization problems.

For brightness imaging, we use the two-component model of Cameron (1992), which aims at reconstructing, for each image pixel of the stellar surface, the local relative area occupied by cool spots. This quantity, varying from 0 (no spot) to 1 (maximum spottedness), is referred to as 'spot occupancy' in the following. LSD profiles of very slowly rotating standard stars (δ Eri, Gl 176.3 and Gl 367) are used as template profiles describing the spectral

[1] In the following text, we define the S/N ratio of Stokes V spectra as $1/n$ where n is the relative noise level per digital channel. Being roughly equal to the square root of the total number of photons collected in the corresponding bin, this parameter is thus nothing more than a circular polarization spectrum quality indicator, and gives, in particular, no information concerning the accuracy to which a potential Zeeman signature may be detected.

© Royal Astronomical Society • Provided by the NASA Astrophysics Data System

2003MNRAS.345.1145D

contribution of the photosphere and spot, respectively, just as in Donati & Cameron (1997), Donati (1999) and Donati et al. (1999). A linear limb-darkening law (with a coefficient of 0.75, appropriate for this wavelength range and photospheric temperatures) is used to simulate the variations of the continuum intensity over the stellar disc, while the variation of the local profile with limb angle is ignored; although pretty rough, this approximation is found to produce almost no difference in the final profiles (and thus no artefacts in the reconstructed image) as long as the equivalent width of the disc integrated synthetic profiles matches precisely that of the observed profiles, as demonstrated through detailed simulations by Unruh & Cameron (1995). Various other imaging tests performed with even rougher assumptions (e.g. Gaussian intrinsic profiles with a linear limb darkening law, Hatzes et al. 1989; Donati & Cameron 1997; Hussain et al. 2000; Petit et al. 2003a,b) demonstrate that the exact shape of the intrinsic profile is not a crucial parameter for Doppler imaging (provided the equivalent width of the synthetic and observed profiles are matched). No simultaneous photometry was available to constrain further the image reconstruction.

For magnetic imaging, we chose the very simple model of Donati & Brown (1997) assuming weak magnetic fields and a constant Gaussian intrinsic profile over the stellar surface. Quite unexpectedly, this model is found to be perfectly adequate for describing LSD Stokes V profiles averaged over several thousand individual spectral features. In particular, Stokes V profiles of very slowly rotating magnetic Ap stars indicate that the weak-field approximation holds true up to fields strengths in excess of 1 kG (Donati & Cameron 1997) and is therefore perfectly suited for our purpose. The quantities we reconstruct are the three components of the magnetic field vector in spherical coordinates (i.e. radial, meridional and azimuthal field), weighted by potential surface inhomogeneities in brightness, local magnetic field occupancy and central depth of the true intrinsic profile.

The peculiarities of magnetic imaging from Stokes V dynamic spectra (with respect to conventional brightness imaging), as well as the capabilities and limitations of this method in the particular case of spotted distributions are outlined in Donati & Brown (1997) and further discussed in Donati (1999, 2001). The essential result is that ZDI is able to recover the *location* of magnetic regions at the stellar surface, and, to a certain extent, the *orientation* of field lines within them. Of particular interest is the point that magnetic regions in which the field is *azimuthal* can be well distinguished from those in which the field is either radial or meridional; however, ZDI from Stokes V data alone suffers potentially important crosstalk from *radial* to *meridional* field components (and vice versa) in the particular case of low-latitude features, especially at low stellar inclination angles. No noticeable distortion is observed on the recovered image from the fact that we select as solution the map with minimal information content, apart from the observation that the strongly limb-darkened features at lowest latitudes tend to be recovered with significantly weaker contrast and spread out over a large range of latitudes.

An important result is that no crosstalk is noted between the reconstructed brightness and magnetic maps, apart from the observation that magnetic fields concentrated in cool spots tend to be outshone by those found in regions at photospheric temperature with the inversion code dimming (and sometimes even suppressing) such cool magnetic features in the reconstructed map.[2] This absence of crosstalk is easily understandable from the fact that brightness features cannot produce circular (nor linear) polarization signatures by themselves but can only change their relative amplitudes and thus do no more than affect the fluxes that the inversion code reconstructs in the magnetic regions. In particular, no magnetic region is generated by our imaging software within regions for which (or at the immediate vicinity of which) no magnetic field is already present in the original maps.

Another behaviour of ZDI worth noting is that it reconstructs only the magnetic features producing clear Stokes V signatures in the data set and ignores all those generating Zeeman signals smaller than the noise level, in agreement with the principles of maximum entropy image reconstruction. This is the case, in particular, for all small bipolar features (i.e. smaller than the resolution element of the imaging process) for which the net circular polarization almost cancels out when averaging over the different polarities. This situation can also be encountered with large-scale magnetic features in very specific circumstances; pairs of low-latitude magnetic field belts of opposite polarities encircling the star and located symmetrically about the equator belong to this category, remaining easily undetected in circular polarization at stellar inclination angles close to 90° (Piskunov & Kochukhov 2002). This latter example is fortunately a rare exception, ensuring that large-scale magnetic structures are recovered in most cases with ZDI. In particular, it does not affect the results presented below, focusing on stars with rotation axes inclined to the line of sight at angles smaller than 60° and for which all large-scale magnetic structures with sufficient visibility to the observer should be recovered by the inversion code.

For additional details on the imaging technique, the reader is referred to Donati & Brown (1997) and Donati (1999, 2001).

3 THE YOUNG ULTRAFAST ROTATOR AB DORADUS

For all reconstructions, we used a stellar inclination angle of 60°. Moreover, we assumed a surface differential rotation rate equal to that measured by Donati & Cameron (1997) and confirmed by Donati et al. (1999). Although some of these data can be used to redetermine the differential rotation parameters and check for potential variability as the star progresses on its activity cycle (as suggested by Cameron & Donati 2002), we decided to keep the description of these results to another paper (Donati, Cameron & Petit 2003). The line-of-sight projected rotational velocity ($v \sin i$) we used in this study (equal to 89 km s^{-1}) is slightly smaller (by 2 km s^{-1}) than the value used in previous studies (e.g. Donati et al. 1999); although this new estimate produces brightness images with slightly larger overall spot coverage, we find that it also generates smaller systematic (i.e. phase-averaged) residuals between observed and synthetic profiles. The radial velocity we derive (see Table 4) is found to vary regularly with time. If we add the radial velocity measurements obtained by reprocessing with the same technique the 1995 December and 1996 December data sets (Donati & Cameron 1997; Donati et al. 1999) both equal 31.4 ± 0.2 km s^{-1}, we find that the full amplitude of the radial velocity variation we observed until now reaches 1.3 km s^{-1}, and is thus sufficiently larger than the

[2] Although this effect can potentially change the overall appearance of the reconstructed magnetic field with respect to that at the stellar surface (especially in polar regions), we prefer not to refer to it as crosstalk, given the fact that what it does is not to confuse a non-magnetic signature for a magnetic one or vice versa, but rather to yield the minimum amount of magnetic field flux compatible with the observed data, in agreement with the principles of maximum entropy image reconstruction.

© Royal Astronomical Society • Provided by the NASA Astrophysics Data System

2003MNRAS.345.1145D

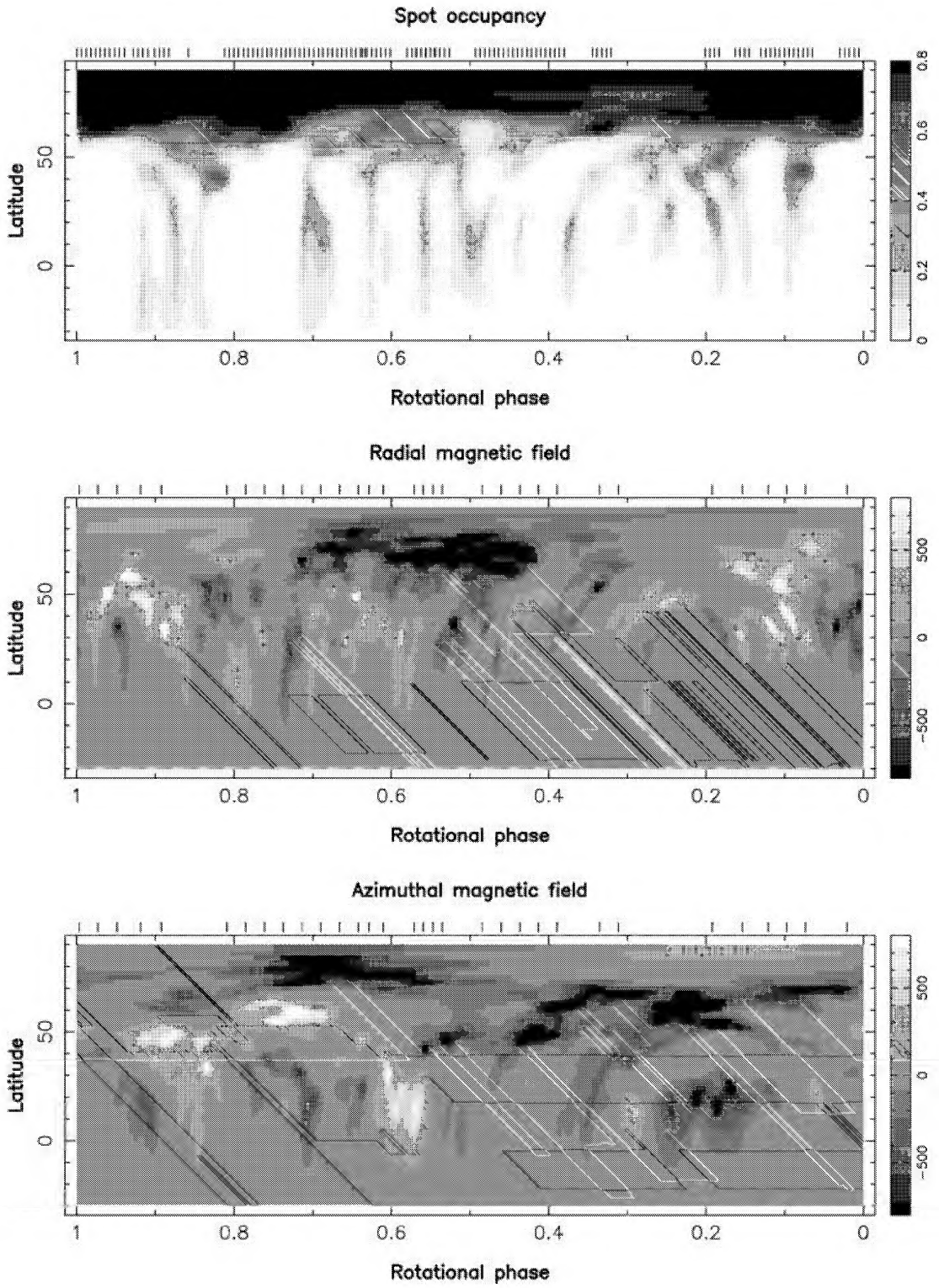

Figure 2. Maximum entropy brightness (upper row) and magnetic (lower rows) rectangular maps of AB Dor at epoch 1998.03. The reconstructed meridional field component is very small and is therefore not shown here. The vertical ticks above each graph depict the rotational phases of individual Stokes *I* and *V* observations. Positive field values correspond to magnetic vectors directed outward and eastward for radial and azimuthal field components, respectively (all labelled in G). Note that the rotational phase runs backwards (i.e. from right to left) on all maps.

© Royal Astronomical Society • Provided by the NASA Astrophysics Data System

2003MNRAS.345.1145D

Table 4. Radial velocities of AB Dor and LQ Hya (columns 2 and 3), systemic velocity of HR 1099 (column 4), and orbital phase of first conjunction of HR 1099 (column 5) in the ephemeris of Fekel (1983), for each of our observing runs. The rms accuracy on radial velocities is of the order of 0.2 km s^{-1} (the stellar lines being broad and time variable), while the error bar on the phase of first conjunction is always smaller than 0.0001.

Epoch	v_{rad} (km s^{-1})			ϕ_0
	AB Dor	LQ Hya	HR 1099	HR 1099
1998.03	31.5	8.4	−14.5	−0.0458
1999.00	31.6	8.4	−14.6	−0.0529
1999.97	31.8	8.2	−14.7	−0.0616
2000.93	32.1	8.4	−14.8	−0.0701
2001.99	32.7	8.6	−14.5	−0.0784

error bar for us to claim that it is real. It very probably reflects the orbital motion of AB Dor recently demonstrated by Guirado et al. (1997), and continuous monitoring should help to determine what the orbital period actually is.

All data sets (phased according to Innis et al.'s 1988 ephemeris HJD = 244 4296.575 + 0.514 79 E) provide very good to excellent sampling of the rotational cycle of AB Dor, except that collected at epoch 1999.97 for which bad weather (see Section 2.2) prevented us from covering more than approximately half the visible surface of AB Dor. The maximum entropy images we reconstruct from the various data sets are shown in Figs 2, 4, 6, 8 and 10 for epochs 1998.03, 1999.00, 1999.97, 2000.93 and 2001.99, respectively, while the corresponding fits are presented in Figs 3, 5, 7, 9 and 11. Unpolarized LSD profiles are fitted to an average accuracy level of approximately 0.07 per cent rms, while Stokes *V* LSD profiles are adjusted at unit reduced χ^2 level.

Note that in some cases (e.g. between phase 0.4 and 0.7 at epoch 2001.99, see Fig. 11), we can clearly see in the observed Stokes *I* LSD profiles a shallow, but significant, absorption feature travelling all the way throughout the line from the blue side to the red side of the profile, which is not reproduced in the synthetic profiles. We consider these spectral features as the first evidence for small regions brighter than the surrounding photosphere (i.e. faculae) located at the surface of AB Dor; indeed only bright surface features can produce such absorption transients in the LSD line profiles, instead of the standard pseudo-emission bumps that cool star spots generate. Being designed for reconstructing only cool surface regions (to prevent bright artefacts from showing up in the image, see Cameron 1992), our code unsurprisingly fails at fitting these absorption trails in the dynamic spectra. Given that there are very few such regions on AB Dor at any given epoch, this is not a significant limitation for the present study, the aim of which is to delineate the structure of the magnetic field and its long-term evolution.

All brightness images are structurally very similar, with a main polar spot and a large number (more than 25 at epoch 2001.99) of small mid- to low-latitude appendages or separate spots, some of them reconstructed very close or even below the equator. They all yield very similar spot coverage, of the order of 8.5 per cent of the total stellar surface, with approximately one-third of the spots located at a latitude lower than 50°. A closer analysis reveals that the relative fraction of the spot coverage associated with low-latitude features (i.e. lower than 50°) with respect to that of circumpolar regions increased slightly but regularly over our observing time-span of 5 yr, from approximately 25 per cent at epoch 1998.03 up to 40 per cent at epoch 2001.99. Looking at the yearly transformation of curves such as that shown in the left-hand panel of Fig. 12 and noticing, in particular, that the peak at high latitude in the distribution of the fractional spot coverage does not become progressively broader with time towards low latitudes, we can conclude that this evolution essentially reflects a global modification of the spot configuration occurring on a long-term basis, with a polar spot becoming progressively weaker with time and more/bigger spots forming at low latitudes, rather than of some slow migration pattern of high-latitude features towards the equator.

The same global similarity with previously reconstructed maps is observed on the magnetic images as well.[3] These maps yield mean quadratic magnetic fluxes (defined here as the local field modulus times the local relative surface area, regardless of the field orientation) of the order of 125 G at most epochs, with a peak to 175 G at epoch 2001.99. Only at epoch 1999.97 is the mean field as low as 60 G, owing to the poor phase coverage that prevented us from reconstructing more than approximately half the visible surface of the star. Comparing with values obtained at epoch 1995.94 and 1996.99 (both equal to approximately 110 G, Donati et al. 1999), we can conclude that the field flux of AB Dor has regularly increased up to now. We also find that approximately 60–70 per cent of the quadratic magnetic flux is recovered at a latitude lower than 50°. The clear difference with the brightness images (for which only one-third of the total spottedness is found at latitudes lower than 50°) may be caused, at least partly, by the fact that some of the magnetic flux located close to the visible pole is obscured by the relative darkness of the huge polar spot. Indeed, almost no magnetic flux is recovered at latitudes higher than 80° (see the left-hand panel of Fig. 12), where the local surface brightness never exceeds 20 per cent of that in the quiet photosphere.

The most striking similarity with previous maps is of course the ring of clockwise field surrounding the rotational pole of AB Dor, showing up very clearly in every single image. However, the latitudinal polarity pattern of the azimuthal field component at lower latitudes that we reported in the previous maps (counterclockwise field at intermediate latitudes and clockwise field close to the equator) seems less obvious in this new sequence of maps. Although we still statistically tend to find regions with strongest positive azimuthal field at intermediate latitudes, we also sometimes find a few of them close to the equator (e.g. at phase 0.58 on epoch 1998.03, or at phase 0.87 on epoch 2000.93), and several regions of intense clockwise azimuthal field at intermediate latitudes (e.g. at phase 0.24 on epoch 2001.99). If we average all maps together and integrate the algebraic azimuthal flux over longitudes (see the dash-dot curve in left-hand panel of Fig. 12), we confirm that there are indeed, statistically at least, two dominant azimuthal field polarities throughout the upper hemisphere of AB Dor, a negative one at a latitude of approximately 70° (the circumpolar ring of clockwise field), and a second negative one at a latitude of approximately 15°. A third one with opposite polarity shows up marginally between the two others, at a latitude of approximately 35°.

This result therefore confirms the suspicion reported in our previous studies, i.e. that the azimuthal field component essentially represents the mainly axisymmetric, dynamo generated, large-scale toroidal field structure, which, for some yet unknown reason, is not

[3] The impression that magnetic maps feature a finer spatial resolution than brightness maps, for instance at epoch 2001.99 (see Fig. 10), is only a visual artefact of the displayed contours, autocorrelation maps of reconstructed images demonstrating clearly that the spatial resolution of magnetic maps is approximately 3 times lower than that of brightness maps, as expected from the much poorer phase sampling of the Stokes *V* data.

© Royal Astronomical Society • Provided by the NASA Astrophysics Data System

2003MNRAS.345.1145D

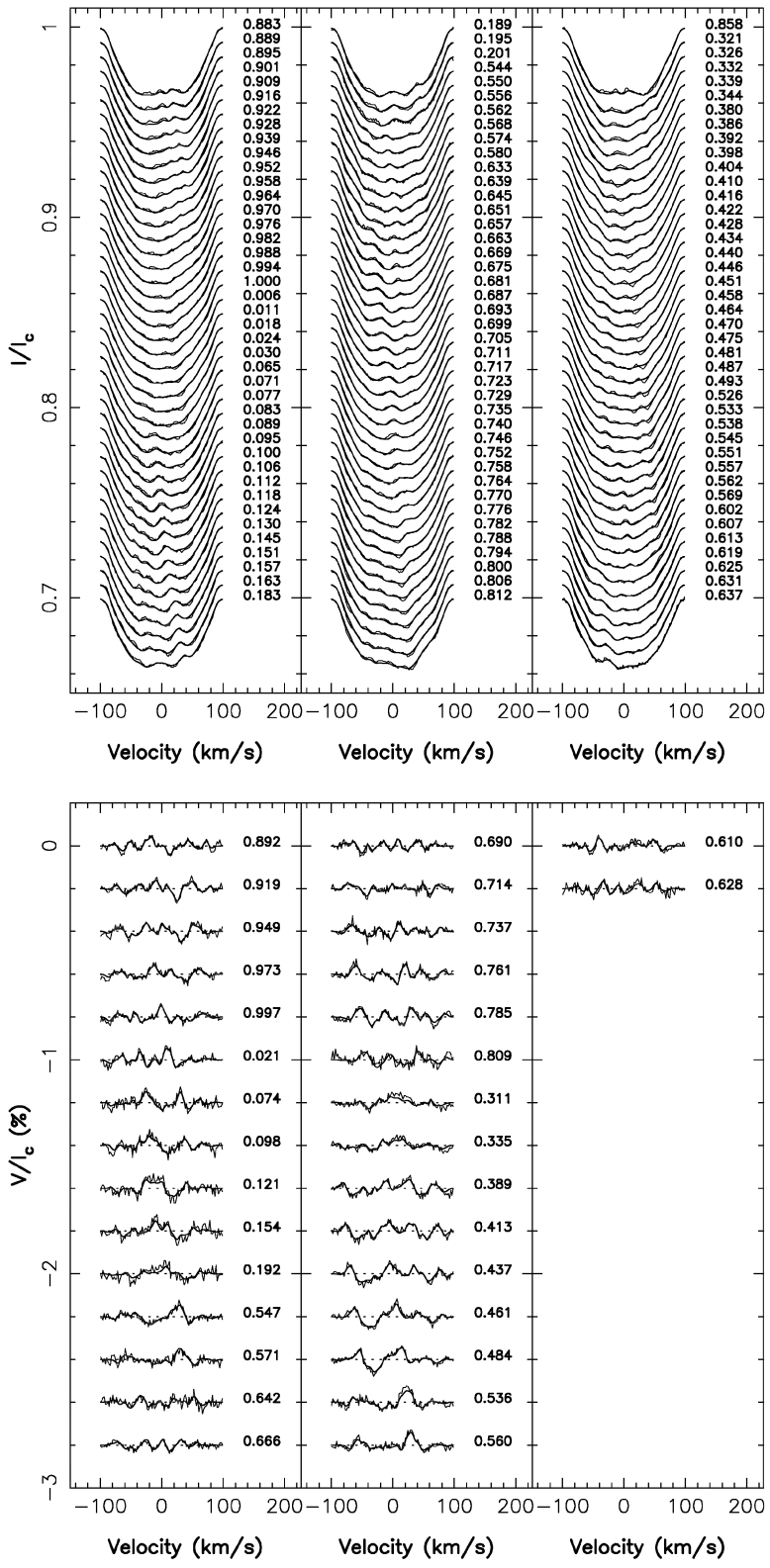

Figure 3. Maximum entropy fit (thick line) to the observed (thin line) Stokes *I* (top panel) and *V* (bottom panel) data sets. Observations are depicted from top to bottom and left to right by increasing UT date (with successive profiles being shifted downwards for graphical purposes). The dotted lines in the bottom panel illustrate the zero circular polarization level of each profile. Rotational phases are indicated to the right of each profile.

© Royal Astronomical Society • Provided by the NASA Astrophysics Data System

2003MNRAS.345.1145D

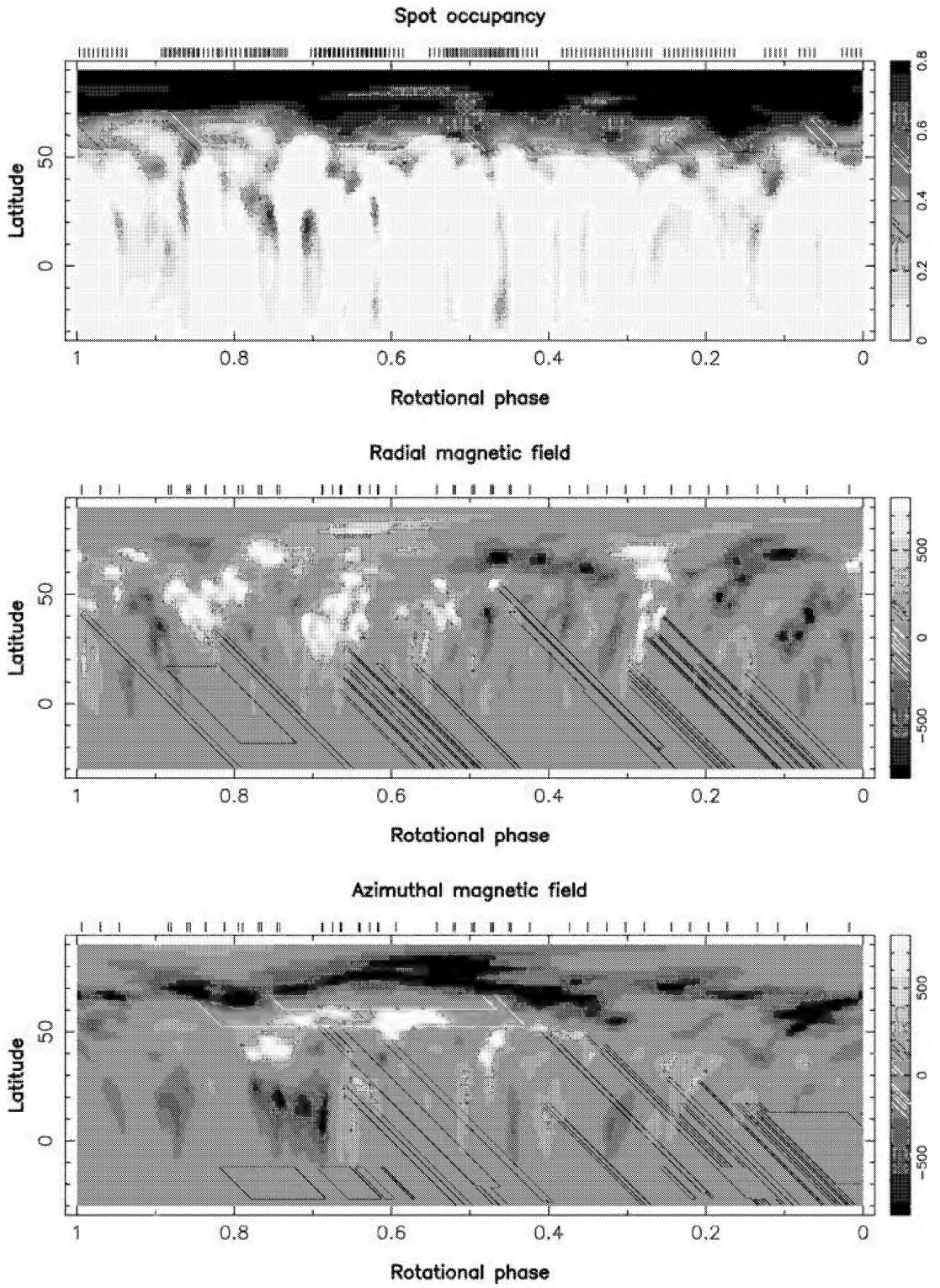

Figure 4. Same as in Fig. 2 for epoch 1999.00.

confined at the base of the convective zone as in the Sun, but readily detectable at photospheric level and thus probably distributed throughout the whole convective zone. We stress, however, that, at each epoch, a significant fraction of the azimuthal field we reconstruct at low to intermediate latitudes does not contribute to this axisymmetric structure, but rather to a more complex, higher-order, component of the large-scale toroidal dynamo field. No temporal evolution of the latitudinal position of these polarities is readily visible from the images; splitting all epochs into two consecutive subsets and comparing the resulting latitudinal magnetic flux distributions

© Royal Astronomical Society • Provided by the NASA Astrophysics Data System

2003MNRAS.345.1145D

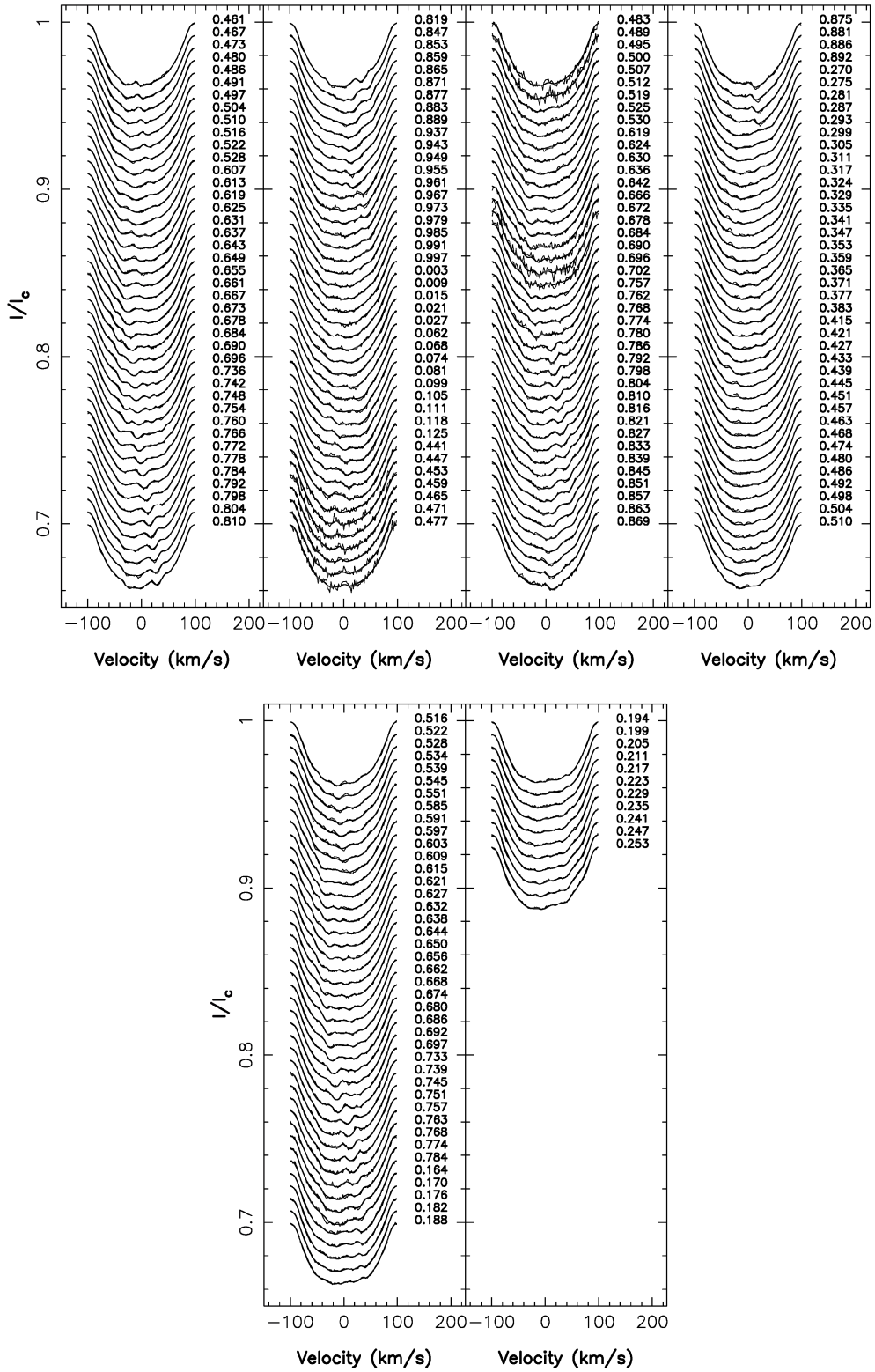

Figure 5. Same as in Fig. 3 for epoch 1999.00.

of the azimuthal field yields no evidence for the potential migration of these rings over the full time-span of our observations.

The radial field maps are also structurally similar to their 1995 and 1996 equivalents, showing no apparent latitudinal polarity pattern. However, if we proceed as we did for the azimuthal field image, i.e. by integrating the radial field images over longitudes to retain only the axisymmetric latitudinal pattern (presumably linked to the poloidal component of the large-scale dynamo field), we observe

© Royal Astronomical Society • Provided by the NASA Astrophysics Data System

2003MNRAS.345.1145D

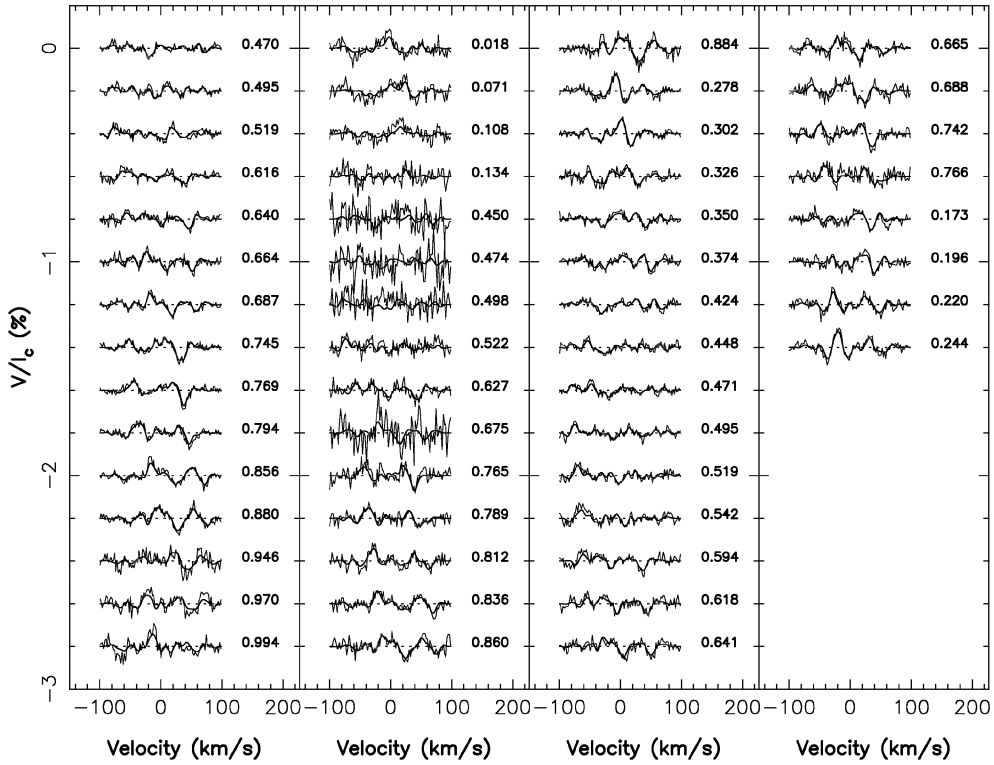

Figure 5 – *continued*

that the polarity at low latitudes remained essentially positive at all epochs, while that at high latitudes switched sign (from negative to positive) sometimes around epoch 1999.5. Note that this sign switch at high latitudes is readily visible in the Doppler images themselves; the prominent spot of negative radial field reconstructed at epoch 1998.03 (at phase 0.55 and latitude 70°) is replaced approximately 3 yr later by a region of positive radial field with similar size (located at phase 0.90 and latitude 65°), while all other maps essentially feature mixed polarity (and usually much smaller sized) radial field regions at such a high latitude. This temporal change of the latitudinal polarity structure of the radial field looks promising for investigations of the long-term, possibly cyclic, evolution of the large-scale dynamo field and is discussed further in Section 6.

Another quantity worth computing is the fraction of the total magnetic energy stored in the various field components. We find that on average, the radial field component contains approximately 40 per cent of the reconstructed magnetic energy, varying from approximately 35 to 45 per cent depending on the epoch. As our imaging technique is not very sensitive to meridional fields for stars with high inclination angles (Donati & Brown 1997), we find, unsurprisingly, that the azimuthal field component contains approximately 60 per cent of the total magnetic energy. At two different epochs since the beginning of our observations, however, (in 1995.94 and 1999.97), the radial field component is found to dominate the magnetic energy budget, including as much as 55 per cent of the total magnetic energy. The first question that arises is of course to know whether the quantities we estimated, and in particular their temporal fluctuations, are indeed representative of some real process going on at the surface of the star, or only reflect the intrinsic limitations of the imaging code (recalled in Section 2.3). One could for instance argue that a lot of the magnetic field present at the surface of the star (possibly even the major fraction of it) is concentrated in cool regions or in small-scale bipolar features that are not reconstructed (or at least strongly dimmed) in our images. Although this is indeed possible, it does not necessarily imply that the relative amounts we derive for the magnetic energies stored in each field component and their fluctuations with time are meaningless; one could fairly reasonably imagine that both small- and large-scale magnetic features follow the same variational laws (as for instance on the Sun where the Hale polarity law applies for large active regions and for small ephemeral features), with their respective weights being dictated by some constraint of physical origin (e.g. that the distribution of the spatial scales of magnetic features is a fractal of fixed dimension). Another concern deals with the possible impact of phase coverage on the derived ratio of reconstructed radial and azimuthal magnetic field energies; simulations indicate that only very weak dependence should be observed, validating our result that the large-scale magnetic structures are probably indeed truly variable along the lines described above, even in the case of epoch 1999.97 at which the data set is sparser than usual. Although we keep further discussion on this subject for Section 6, we already stress the fact that this temporal fluctuation between the azimuthal and the radial components of the medium- to large-scale magnetic field that our data suggest represents an interesting discovery and a potentially fruitful source of information for our understanding of how dynamos operate in cool stars other than the Sun.

If we now look at how the brightness and quadratic magnetic flux distributions depend on longitude once integrated over latitudes 0°–50° (i.e. keeping the polar regions out to concentrate on low-latitude features and avoid contamination from the tilted polar spot, see below), we find that both curves usually show one main peak roughly centred on the same longitude (see, for instance, the right-hand panel of Fig. 12 in the particular case of epoch 2001.99). At some particular epochs (e.g. 1998.03), one of these distributions may even feature

© Royal Astronomical Society • Provided by the NASA Astrophysics Data System

2003MNRAS.345.1145D

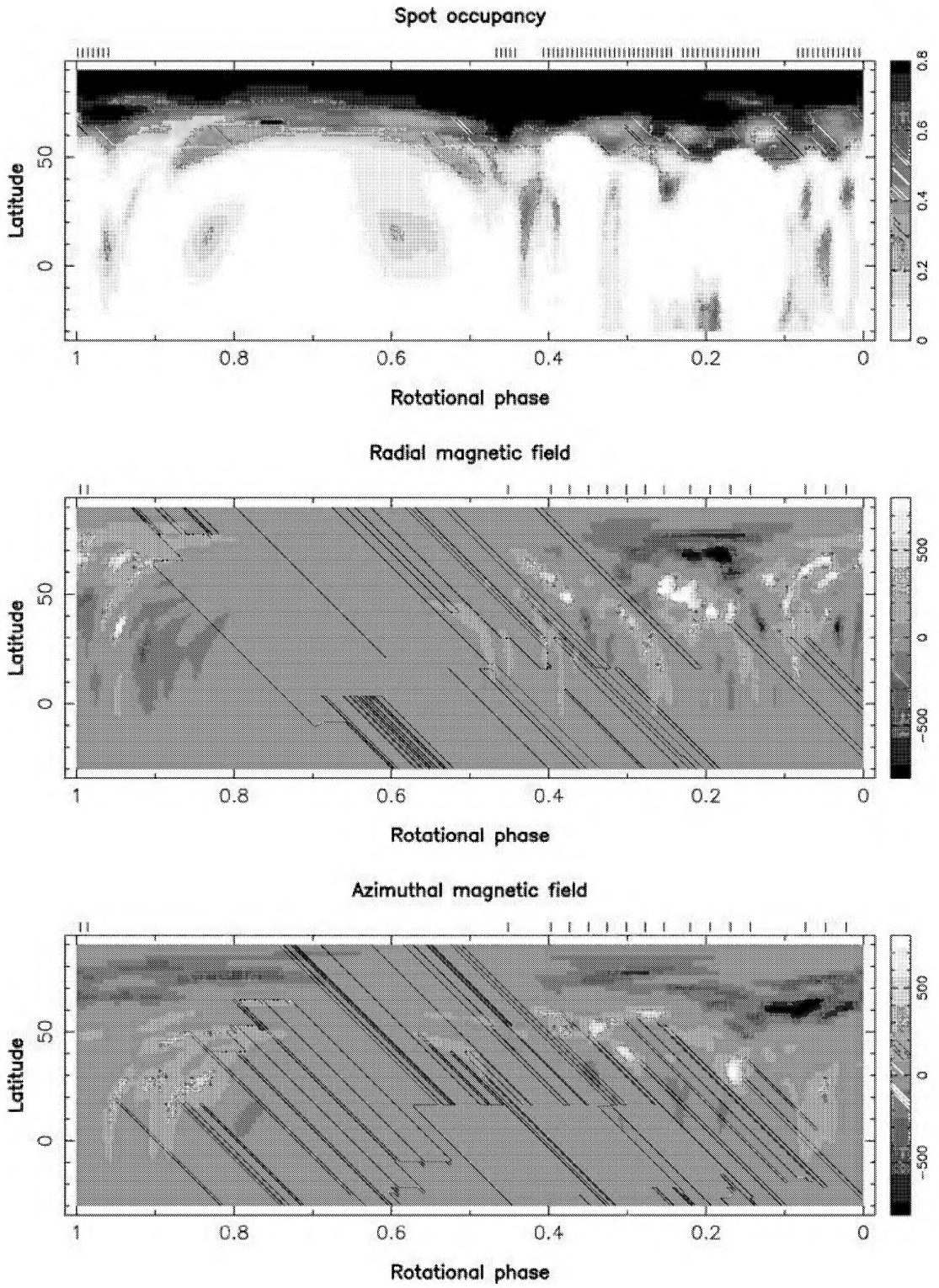

Figure 6. Same as in Fig. 2 for epoch 1999.97.

a second, usually weaker, peak. Concentrating on the longitudinal pattern of the magnetic flux, we find that the main peak, whenever clearly visible (i.e. at epochs 1995.94, 1996.99, 1998.03, 2000.93 and 2001.99), is located at phase 0.81, 0.69, 0.70, 0.97 and 0.37, respectively. We interpret these coincident peaks in both brightness and magnetic flux distributions with longitudes as evidence for 'active longitudes' at the surface of AB Dor, presumably linked to an angular tilt in the dipolar component of the large-scale dynamo field. Note that such active longitudes are not necessarily equivalent to (and in particular are not defined in the same way as) those invoked

© Royal Astronomical Society • Provided by the NASA Astrophysics Data System

2003MNRAS.345.1145D

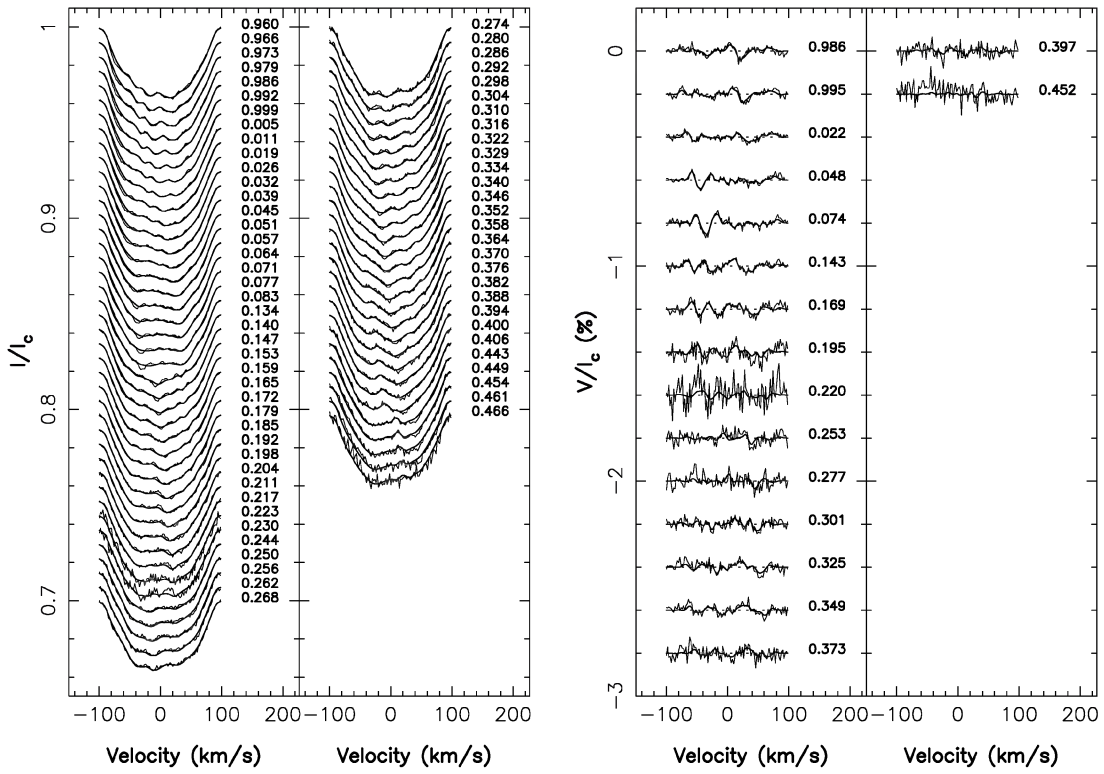

Figure 7. Same as in Fig. 3 for epoch 1999.97.

by other authors (e.g. Jetsu, Pelt & Tuominen 1993; Berdyugina, Pelt & Tumoninen 2002), for whom they represent longitudes at which cool spots tend to form more often. We speculate that these phases of enhanced activity probably relate to the open field regions of the global magnetic topology of AB Dor that Jardine, Cameron & Donati (2002) recently demonstrated. The long-term evolution of this active longitude does not, however, seem to follow any obvious trend up to now. A more detailed analysis, involving in particular spherical harmonics reconstruction of the magnetic field map (e.g. Donati 2001) and field extrapolation (e.g. Jardine et al. 2002), is probably required to investigate this issue properly.

In addition to this, at most epochs we observe a clear angular off-centring of the azimuthal field ring encircling the rotational pole of AB Dor, and a tilt of the cool polar spot, by approximately 10°. One can reasonably wonder whether these tilts of both the brightness and magnetic distributions are somehow related to the active longitude mentioned above. However, we observe that, for most epochs, the phases towards which the azimuthal field ring and the polar spot are tilted are mutually incompatible (being, respectively, equal to 0.45 and 0.88 at epoch 1996.99 for instance, Donati et al. 1999); moreover, both often also disagree with the phase of enhanced activity that we determined previously (equal to 0.69 at epoch 1996.99). The reason for this apparent contradiction, suggesting in particular, that the large-scale brightness and magnetic field distributions may be misaligned, is not yet clear.

4 THE YOUNG K0 DWARF LQ HYDRAE

For all reconstructions presented herein, we assumed for LQ Hya the same inclination angle as that used in Donati (1999), equal to 60°. As for AB Dor, the line-of-sight projected rotational velocity we used in this study (26 km s^{-1}) is slightly smaller than what we used in our previous investigation (Donati 1999, where $v \sin i$ was set to 26.5 km s^{-1}); we find, in particular, that this value enables us to obtain a better fit to the data and to minimize systematic residuals, at the cost of producing brightness images with slightly larger spot coverage. The radial velocity we derive for LQ Hya is remarkably constant. If we incorporate the values derived by reprocessing with the same software the data secured during the 1995 December and 1996 December runs (both equal to 8.5 ± 0.2 km s^{-1}), we find that LQ Hya drifts away from the Sun at a velocity of 8.4 ± 0.2 km s^{-1}. In particular, it implies that LQ Hya is very likely not a binary star. All data were phased according to the ephemeris of Strassmeier et al. (1993) (HJD = 244 8270.0 + 1.606 E) in order to remain consistent with the previous studies of the same kind (Donati 1999). To make our results more easily comparable with those of other studies (e.g. Berdyugina et al. 2002) using a different ephemeris (that of Jetsu et al. 1993), we provide a list of all phase shifts (see Table 5) to allow any potential reader to compare the results of both studies more easily.

Table 5. Approximate phase shifts to be subtracted to our sets of phases to convert them into those produced by Jetsu et al.'s ephemeris (1993). Note that we also provide these shifts for the images published in Donati (1999).

Epoch	Mean Julian date	Phase shift
1991.96	244 8609	0.68
1992.94	244 8967	0.35
1993.99	244 9348	0.07
1995.94	245 0062	0.42
1996.99	245 0445	0.15
1998.03	245 0826	0.87
1999.00	245 1178	0.53
1999.97	245 1537	0.21
2000.93	245 1887	0.88
2001.99	245 2271	0.60

© Royal Astronomical Society • Provided by the NASA Astrophysics Data System

2003MNRAS.345.1145D

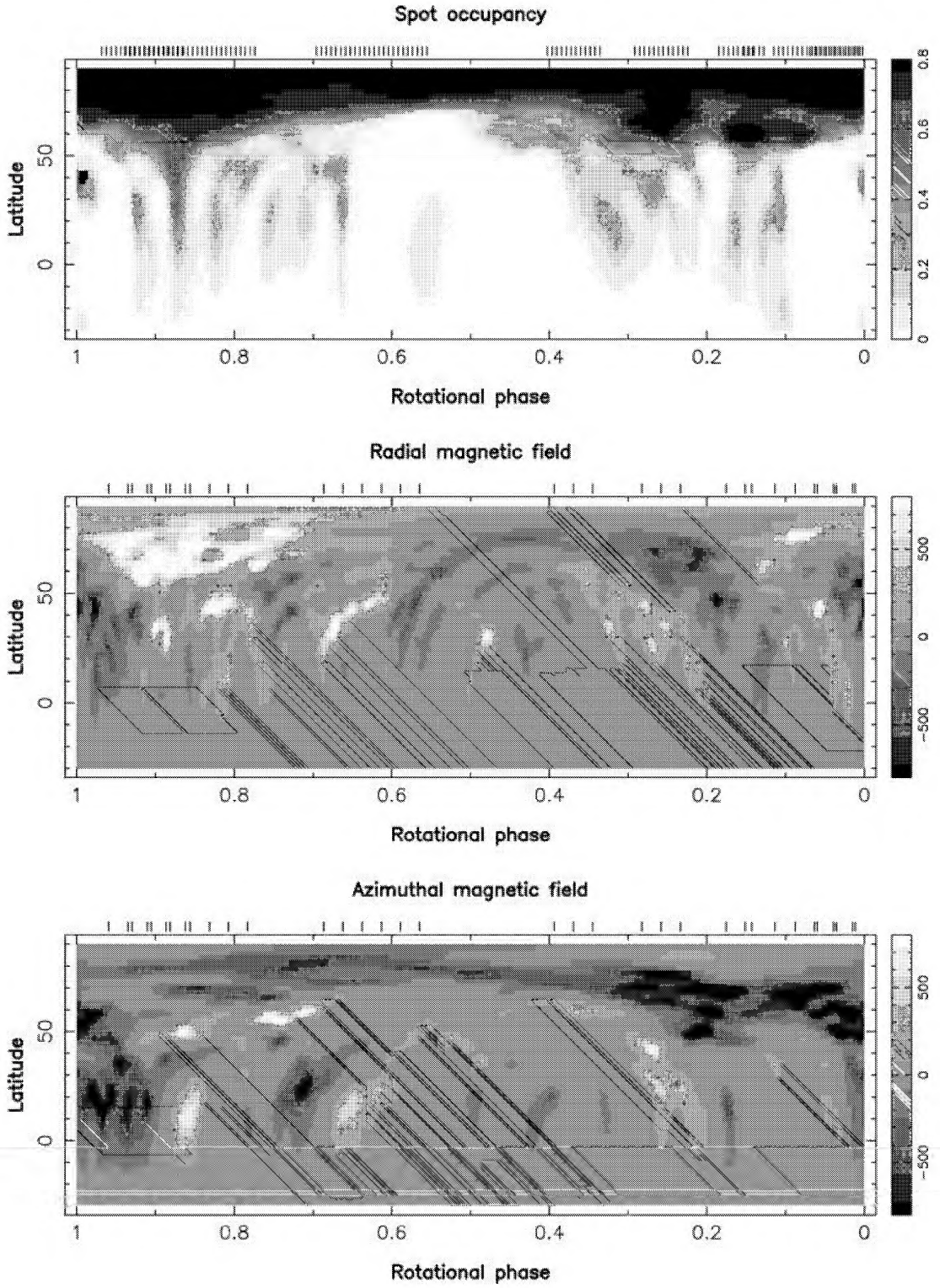

Figure 8. Same as in Fig. 2 for epoch 2000.93.

We also made the assumption that no surface differential rotation is present on LQ Hya; although this is most likely wrong (given, in particular, the increasing body of evidence that cool stars do indeed possess solar-like differential rotation; e.g. Donati & Cameron 1997; Donati et al. 2000), this is nevertheless not a major problem for us given the small time-span of our observations. The effect of assuming, in the reconstruction process, that the star rotates as a solid body (with a rate of 3.912 rad d^{-1}, i.e. close to that estimated

© Royal Astronomical Society • Provided by the NASA Astrophysics Data System

2003MNRAS.345.1145D

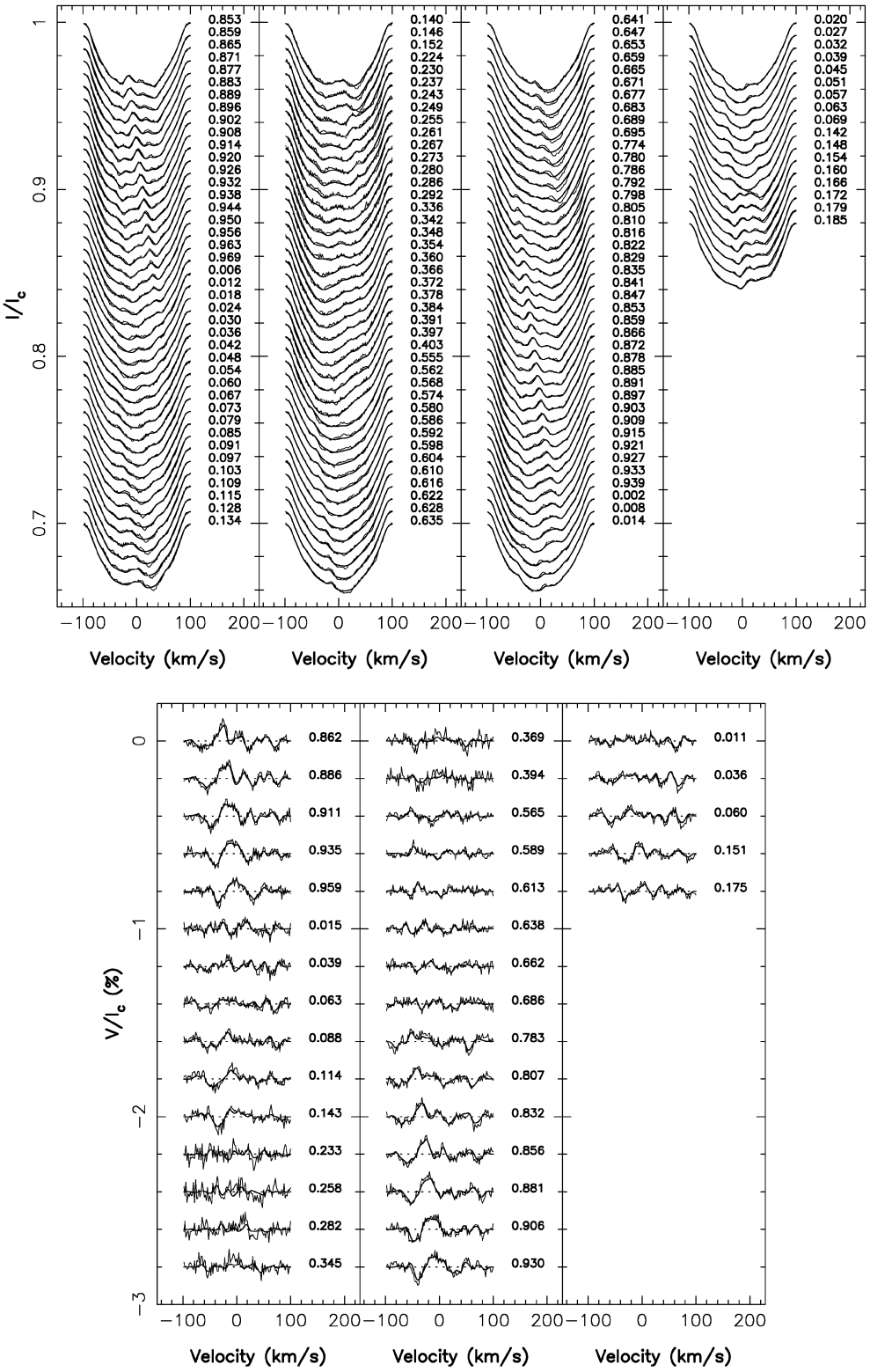

Figure 9. Same as in Fig. 3 for epoch 2000.93.

for the main non-axisymmetric spot groups, centred at a latitude of approximately 35°, see Donati et al. 2003) is indeed that the features we recover are slightly blurred, by an amount that depends on the latitudinal distance from 35°. For an average differential rotation rate between the equator and pole of approximately 0.1 rad d^{-1} (Donati et al. 2003) and a maximum time-span of 13 d, we find that spots located at latitudes of either 20° or 70° are azimuthally blurred by no more than a few per cent of the rotation

© Royal Astronomical Society • Provided by the NASA Astrophysics Data System

2003MNRAS.345.1145D

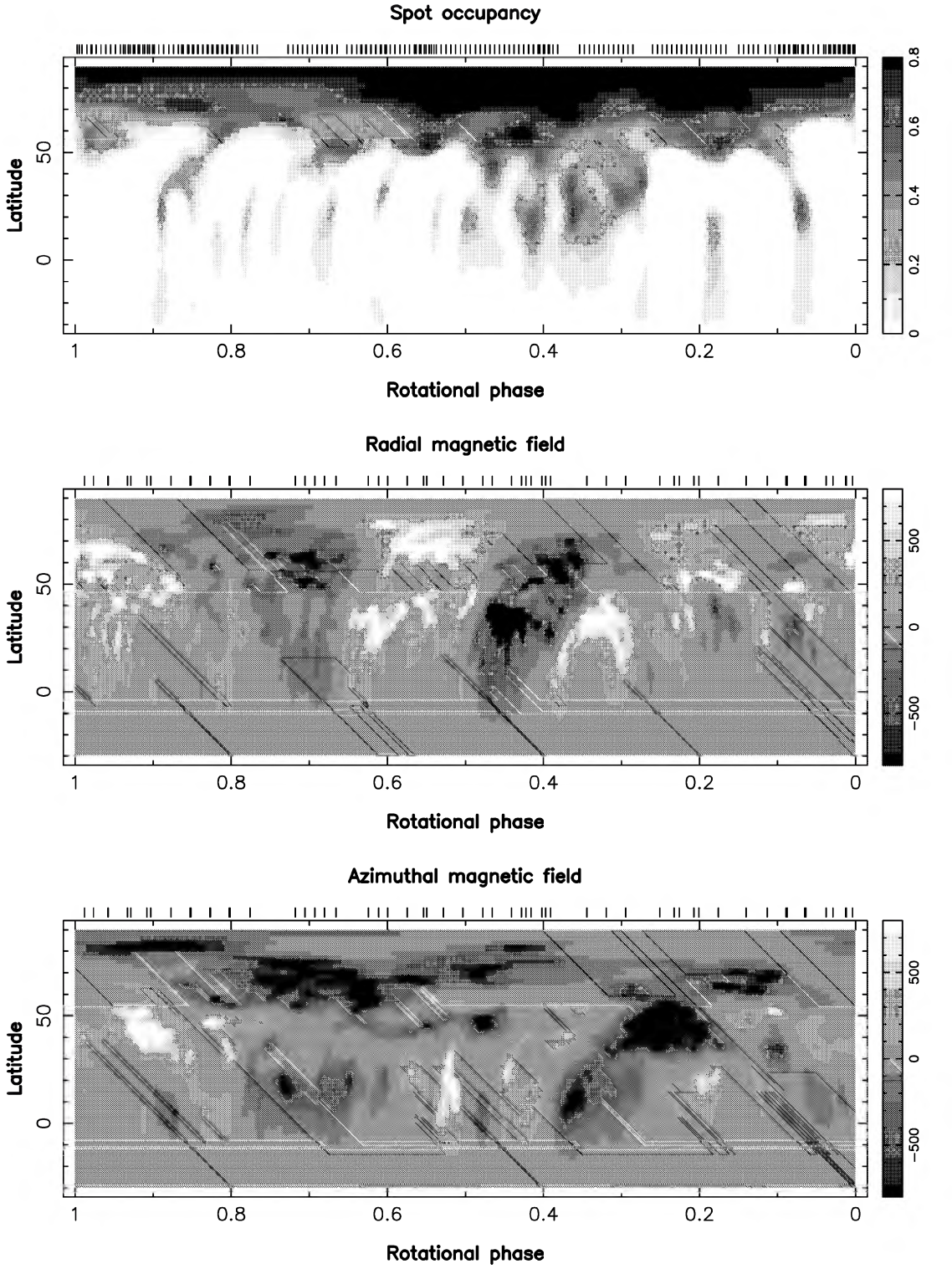

Figure 10. Same as in Fig. 2 for epoch 2001.99.

cycle towards both sides of the position at which they are imaged. This is not a very limiting factor in the particular case of LQ Hya; the low $v \sin i$ of this star and the spectral resolution of our observations indeed constrains the size of any spatially resolved structure reconstructed at its surface to be larger than 3 and 9 per cent in rotational phase, for latitudes of 20° and 70°, respectively. Moreover, this problem does not prevent us from examining the global structure of the magnetic field and its axisymmetric components, and from looking for the potential long-term evolution of the field. A careful investigation of these data to estimate the

© Royal Astronomical Society • Provided by the NASA Astrophysics Data System

2003MNRAS.345.1145D

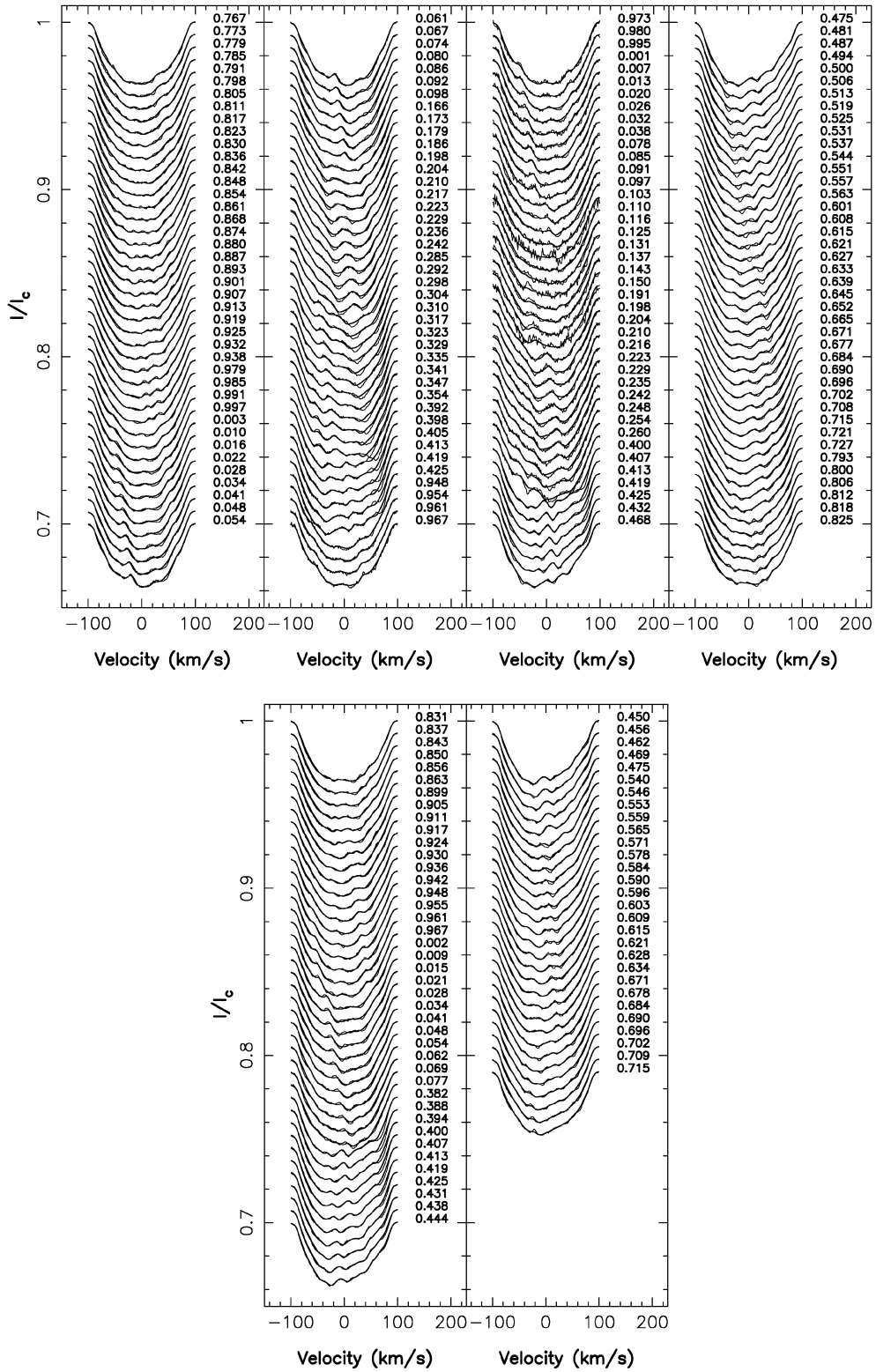

Figure 11. Same as in Fig. 3 for epoch 2001.99.

surface differential rotation of LQ Hya is presented in Donati et al. (2003).

The phase coverage that we achieved at each epoch essentially reflects the amount of clear time in each observing session (see Section 2.2), i.e. reasonable to excellent on 1999.00, 2000.93 and 1999.97, moderate on 1998.03 but very poor on 1999.97. The maximum entropy images we obtain from the different data sets are shown in Figs 13–17 for epochs 1998.03, 1999.00, 1999.97,

© Royal Astronomical Society • Provided by the NASA Astrophysics Data System

2003MNRAS.345.1145D

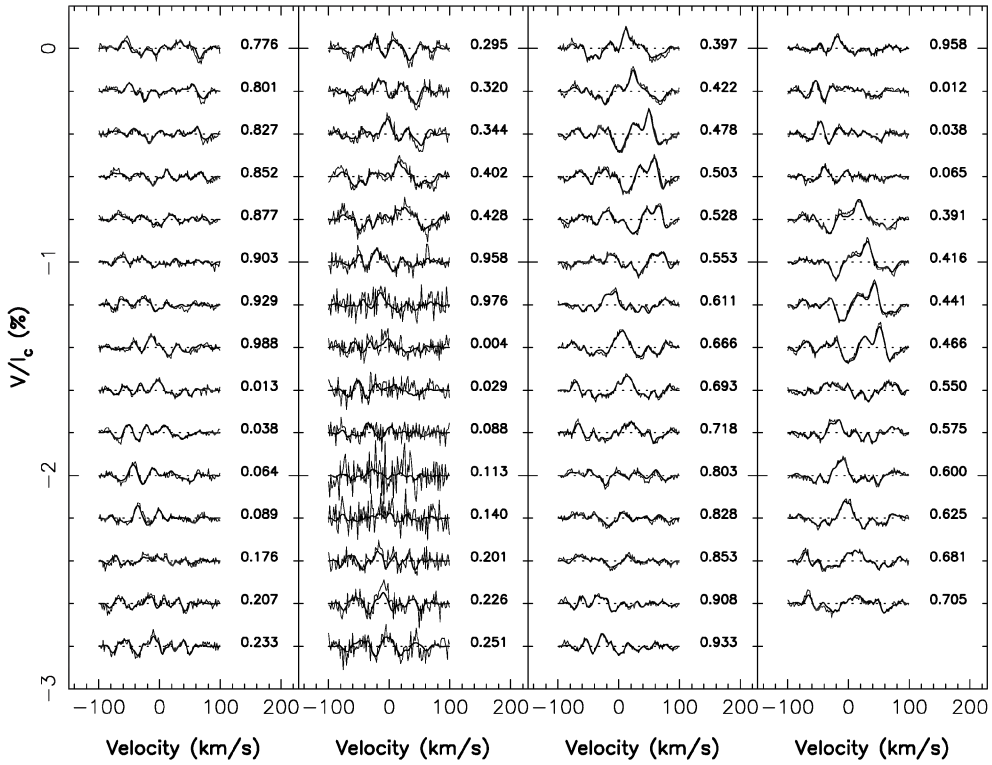

Figure 11 – *continued*

2000.93 and 2001.99, respectively, along with the corresponding fits to the observed LSD profiles. Unpolarized LSD profiles are fitted to an average accuracy level of approximately 0.1 per cent rms, while Stokes V LSD profiles are adjusted at unit reduced χ^2 level.

Again, the brightness images we reconstruct are structurally very similar to those presented in Donati (1999), featuring one main polar spot with a small number of (usually approximately five) low-latitude spots, either fully detached from, or appearing as extensions of, the cool polar cap. We also note that these images share some

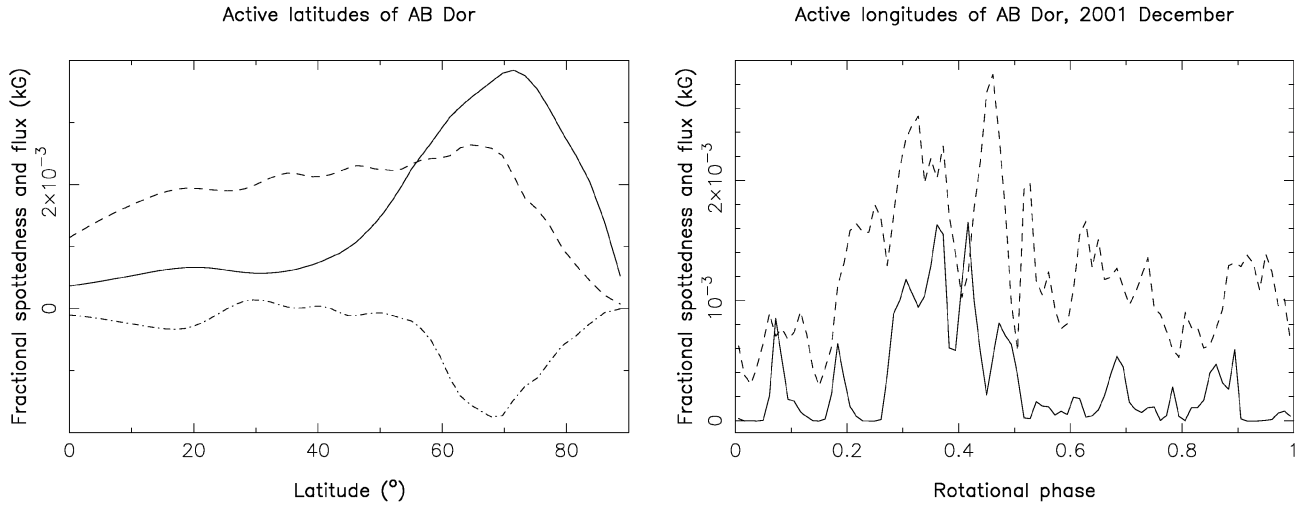

Figure 12. Fractional spot coverage (full line) and quadratic magnetic flux in kG (dashed line) per latitude bin (after integrating over longitudes, left-hand panel) or per rotational phase bin (after integrating over latitudes 0°–50°, right-hand panel). Note that the quadratic magnetic flux is defined here as the local field modulus times the local relative surface area, regardless of the field orientation. In the left-hand panel, the dash-dot line depicts the azimuthal field flux per latitude bin in kG, once integrated over longitudes (we do not show the average radial field flux with latitude, since this quantity is observed to vary significantly with time at high latitudes, see the text). The right-hand curves correspond to epoch 2001.99, while the left-hand ones represent an average over all observing epochs (including 1995 December and 1996 December). Note that the sharp decline of all curves towards the pole reflects no more than decreasing the relative surface of constant latitude belts with increasing latitude.

© Royal Astronomical Society • Provided by the NASA Astrophysics Data System

2003MNRAS.345.1145D

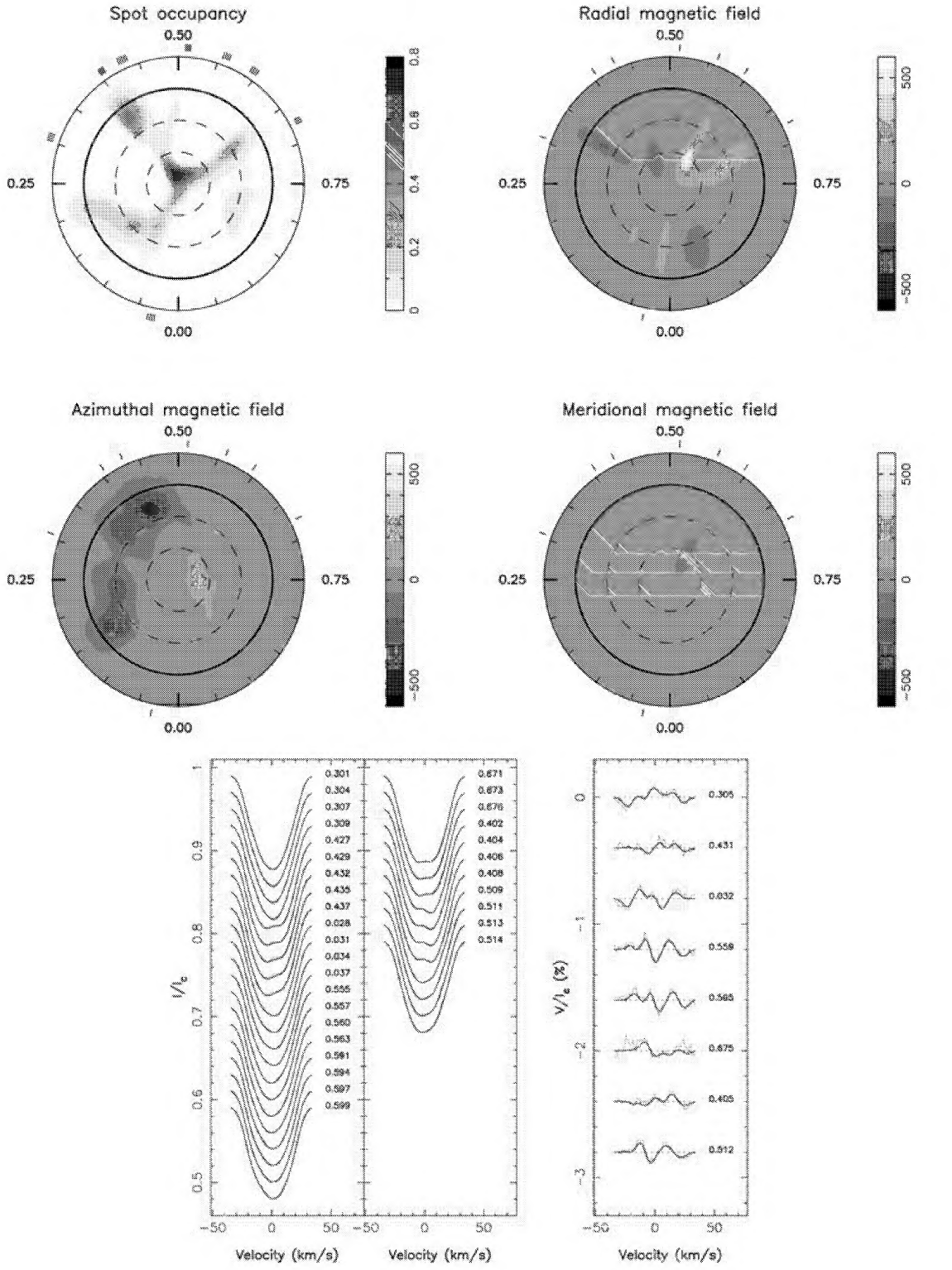

Figure 13. Top panel, maximum entropy brightness (upper left) and magnetic field images of the young K0 dwarf LQ Hya at epoch 1998.03. These images are flattened polar projections extending down to a latitude of -30° (the bold and thin circles depicting the equator and the 30° and 60° latitude parallels, respectively). The radial ticks around (and outside) each plot illustrate the phases at which the star was observed. Positive field values correspond to magnetic vectors directed outward, anticlockwise and poleward for radial, azimuthal and meridional field components, respectively (all labelled in G). Bottom panel: maximum entropy fit (thick line) to the observed (thin line) Stokes I (left) and V (right) data sets.

© Royal Astronomical Society • Provided by the NASA Astrophysics Data System

2003MNRAS.345.1145D

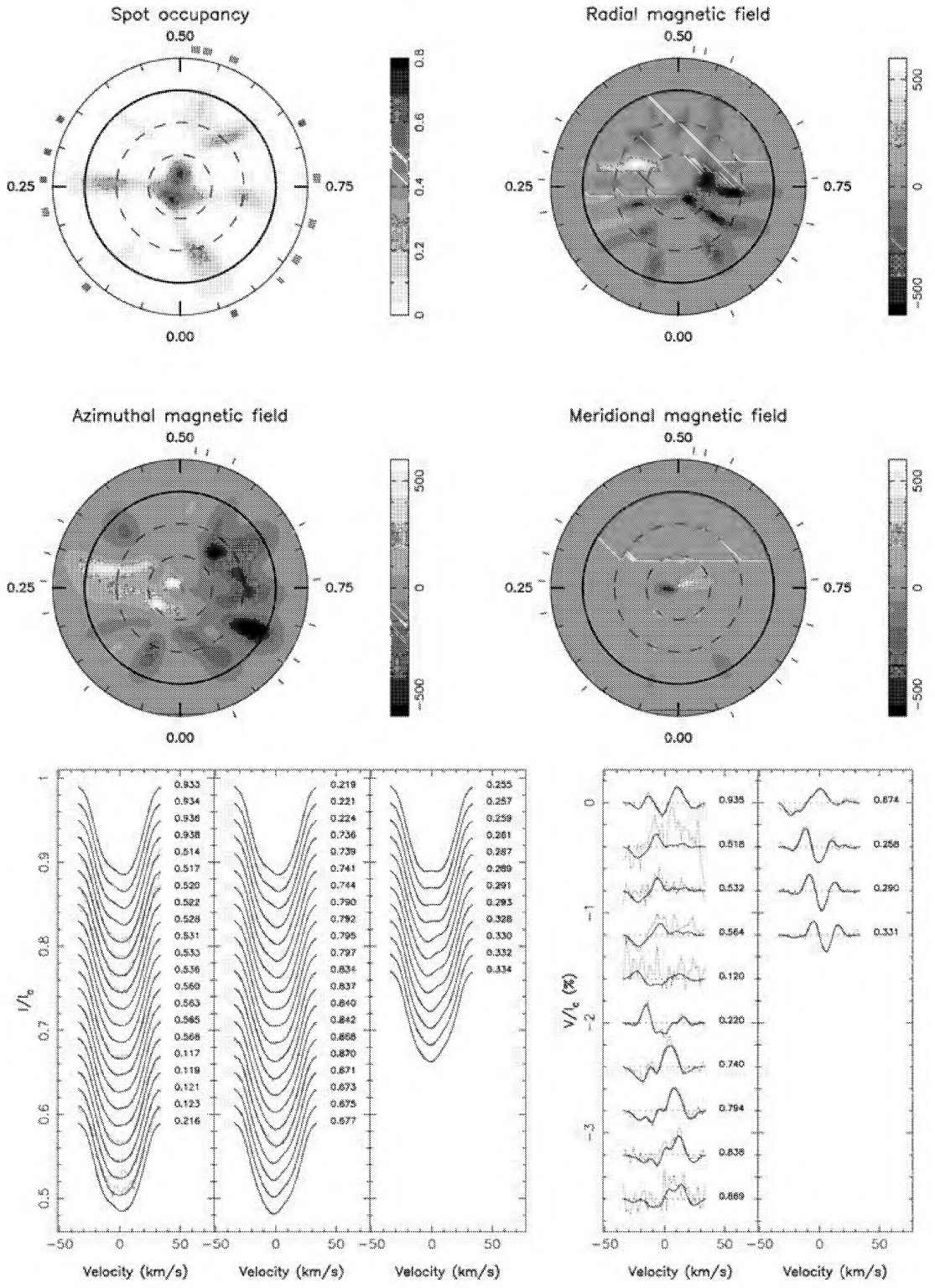

Figure 14. Same as in Fig. 13 for epoch 1999.00.

similarity with those derived for AB Dor, if we take into account the fact that the latter are much better spatially resolved, by a factor of at least 3.5 (assuming dense phase coverage) and often significantly more (within phase gaps of the data set). Another probable consequence of this different spatial resolution is that the amount of spot we recover is significantly smaller for LQ Hya than for AB Dor; while the first three epochs suggest a spot coverage of only approximately 3.2 per cent of the total stellar surface, the last two indicate a slightly higher value of approximately 4.4 per cent, probably reflecting the much better coverage obtained during these recent

© Royal Astronomical Society • Provided by the NASA Astrophysics Data System

2003MNRAS.345.1145D

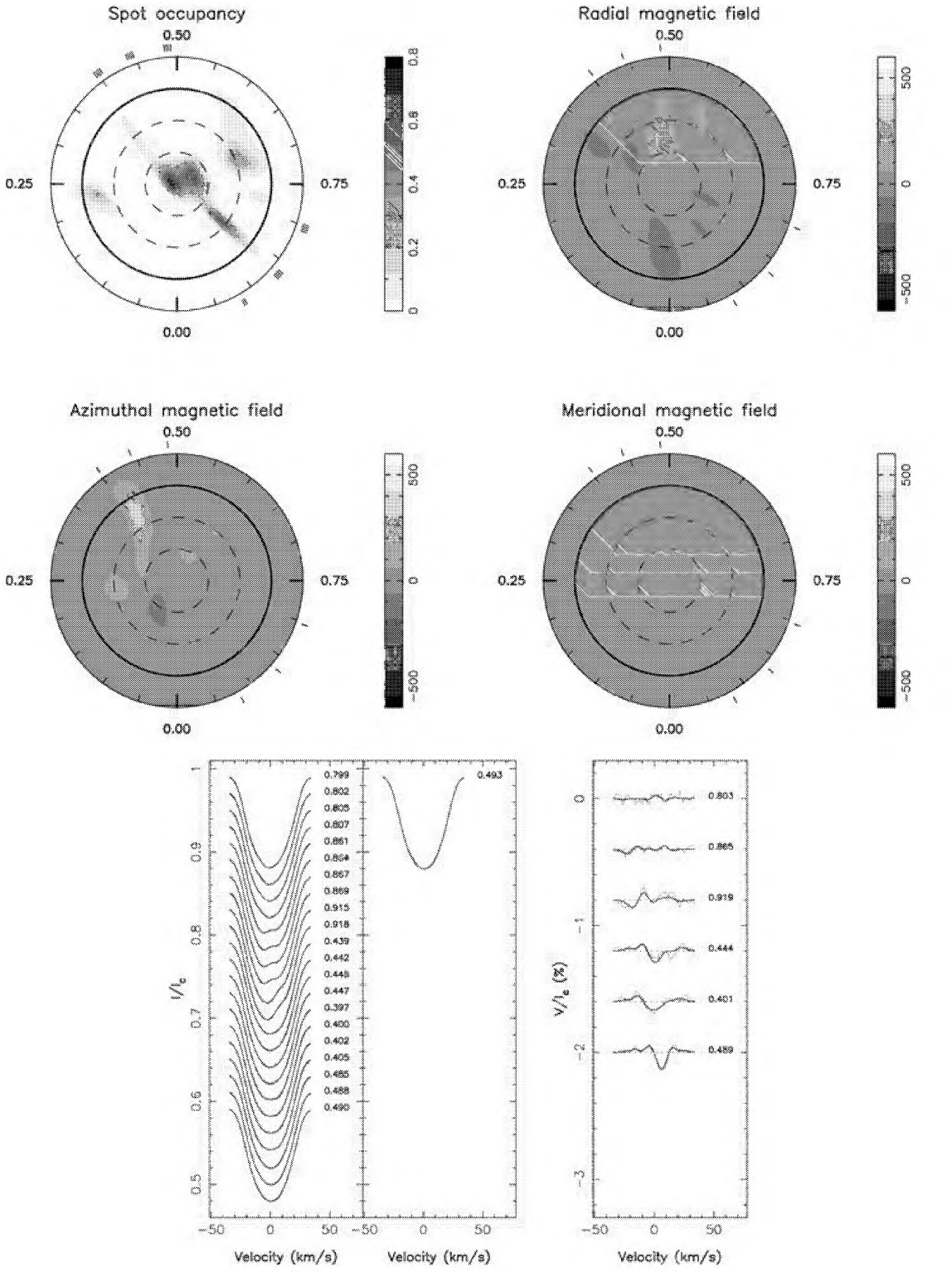

Figure 15. Same as in Fig. 13 for epoch 1999.97.

campaigns. Although this variation looks consistent with the global dimming of the integrated flux from LQ Hya between epoch 1995 and 2000 (Berdyugina et al. 2002), the actual decrease in brightness revealed by photometry (0.1 mag) is much larger that the 1 per cent increase in spot coverage that we derive here, strengthening the conclusion that Doppler images reconstructed without photometric information cannot be trusted for predicting long-term stellar irradiance variations.

© Royal Astronomical Society • Provided by the NASA Astrophysics Data System

2003MNRAS.345.1145D

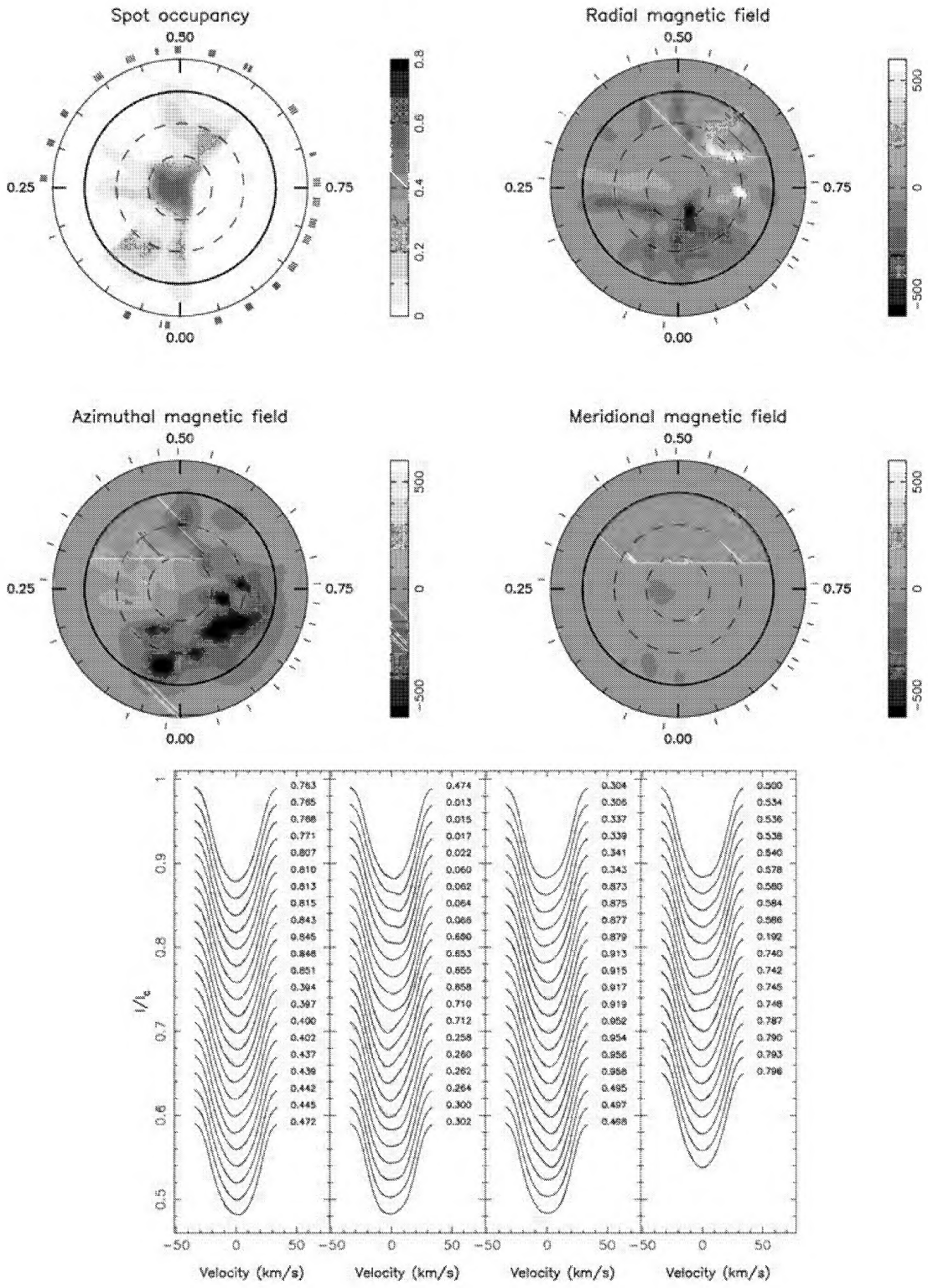

Figure 16. Same as in Fig. 13 for epoch 2000.93.

In the same spirit, comparing the images derived by Berdyugina et al. (2002) from photometric data only with ours (at least those obtained with very good phase coverage, i.e. at epoch 1999.00, 2000.93 and 2001.99) is very instructive as well. The light curve of LQ Hya around epoch 1999.00 is basically flat (slightly deeper in the first half rotation cycle in Jetsu et al.'s ephemeris, i.e. from phase 0.53 to 1.03 in the ephemeris we used), arguing in favour of a roughly axisymmetric distribution of low-latitude features at

© Royal Astronomical Society • Provided by the NASA Astrophysics Data System

2003MNRAS.345.1145D

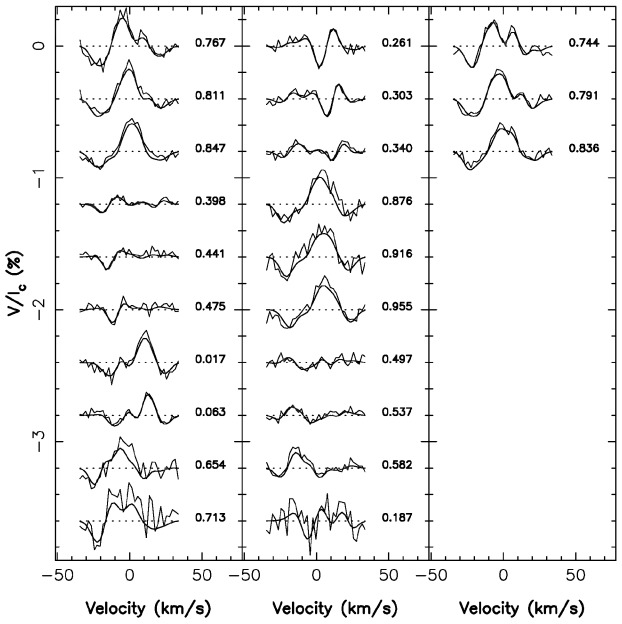

Figure 16 – *continued*

the surface of the star (with slightly more features in the second half rotation cycle in the ephemeris we used). This is indeed grossly what we obtain from our own image (see Fig. 14). At epoch 2000.93 and 2001.99, however, the situation is very different; while the light curves of Berdyugina et al. (2002) indicate that LQ Hya reaches maximum brightness (and thus presumably minimum low-latitude spottedness) around phases 0.70 and 0.55 at epochs 2000.93 and 2001.99, respectively (in Jetsu et al.'s ephemeris, corresponding to a phase of 0.58 and 0.15, respectively, in the ephemeris we used), our images demonstrate that, in both cases, this phase almost coincides with that of one of the main groups of low-latitude features reconstructed at the surface of the star (those at phase 0.55 and 0.20 at epoch 2000.93 and 2001.99, respectively, see Figs 16 and 17). Similarly, phases of minimum brightness (and thus presumably maximum low-latitude spottedness) at epoch 2001.99 (roughly equal to 0.25 and 0.75 in Jetsu et al.'s ephemeris, and to 0.85 and 0.35 in our ephemeris) appear to correspond with regions that are basically free of low-latitude spots in our reconstructed image (see Fig. 17). Note that our intention is certainly not to question the accuracy of Berdyugina et al.'s (2002) photometric data; our images demonstrate, however, that their implicit assumption that phases of maximum and minimum photometric brightness, respectively, correspond to regions with the highest and lowest density of low-latitude cool spots at the surface of the star is simply invalid. Our images point out that the shape of the resulting light curve results from many different factors, with high-latitude features (e.g. the off-centring of the polar spot) playing as important a role as that of low-latitude ones. A similar conclusion was reached in Vogt et al. (1999) from comparing light curves with Doppler images derived from spectroscopy.

The average latitudinal pattern of all spot distributions since 1995 December, shown on the left-hand panel of Fig. 18, is found to be rather similar to that of AB Dor, but with slightly more spots (approximately half of them) appearing at a latitude lower than 50°, the other half forming the polar cap. In particular, it is worth noting the fact that low-latitude spots seem to appear preferentially around latitude 25°. A closer look at these images, and those from epoch 1995.94 and 1996.99, reveals that the fractional spottedness associated with the polar cap actually varies slightly with time; after decreasing regularly down to a minimum (of approximately 40 per cent) reached at epoch 1998.03, it increased again back up to its apparently nominal value (of approximately 55 per cent) where it stayed for the last 3 yr. As for AB Dor, this long-term variation of the latitudinal spot repartition at the surface of LQ Hya does not seem to be caused by a progressive migration of high-latitude features towards the equator, but rather by a slow, possibly periodic, phenomenon of yet unknown origin that changes the respective average sizes of newly emerging low- and high-latitude features.

The magnetic images we reconstruct for LQ Hya are probably among the most enigmatic ones discussed in this paper, although essentially similar to those discussed in Donati (1999). The value of the mean quadratic magnetic field flux we recover increases progressively from approximately 50 G at epoch 1998.03 up to slightly more than 100 G at epochs 1999.00, 2000.93 and 2001.99. We caution, however, that the moderate phase coverage obtained at epoch 1998.03 could, at least partly, explain this variation. The flux value we recover at epoch 1999.97 (approximately 30 G) can only be considered as a lower limit given the very poor phase coverage achieved for this season. This apparent increase follows the decrease observed in previous years, and in particular between epochs 1995.94 (when the flux was larger than the value of 80 G derived from the sparse data set secured at this epoch) and 1996.99 (at which the flux is as low as 50 G despite the reasonably dense phase coverage obtained during this run). We also find that approximately 80 per cent of the quadratic flux reconstructed at the surface of LQ Hya concentrates at latitudes lower than 50° (and mostly around latitude 25°, see Fig. 18, left-hand panel), with only very little variation from this value (less than 5 per cent) with time. Part of the obvious difference with the latitudinal pattern of the brightness distribution may again be attributed, as for AB Dor, to the presence of the dark polar cap obscuring most magnetic information coming from these regions. We can nevertheless note that LQ Hya shows more magnetic field and more spots at low latitudes than AB Dor, as one can

© Royal Astronomical Society • Provided by the NASA Astrophysics Data System

2003MNRAS.345.1145D

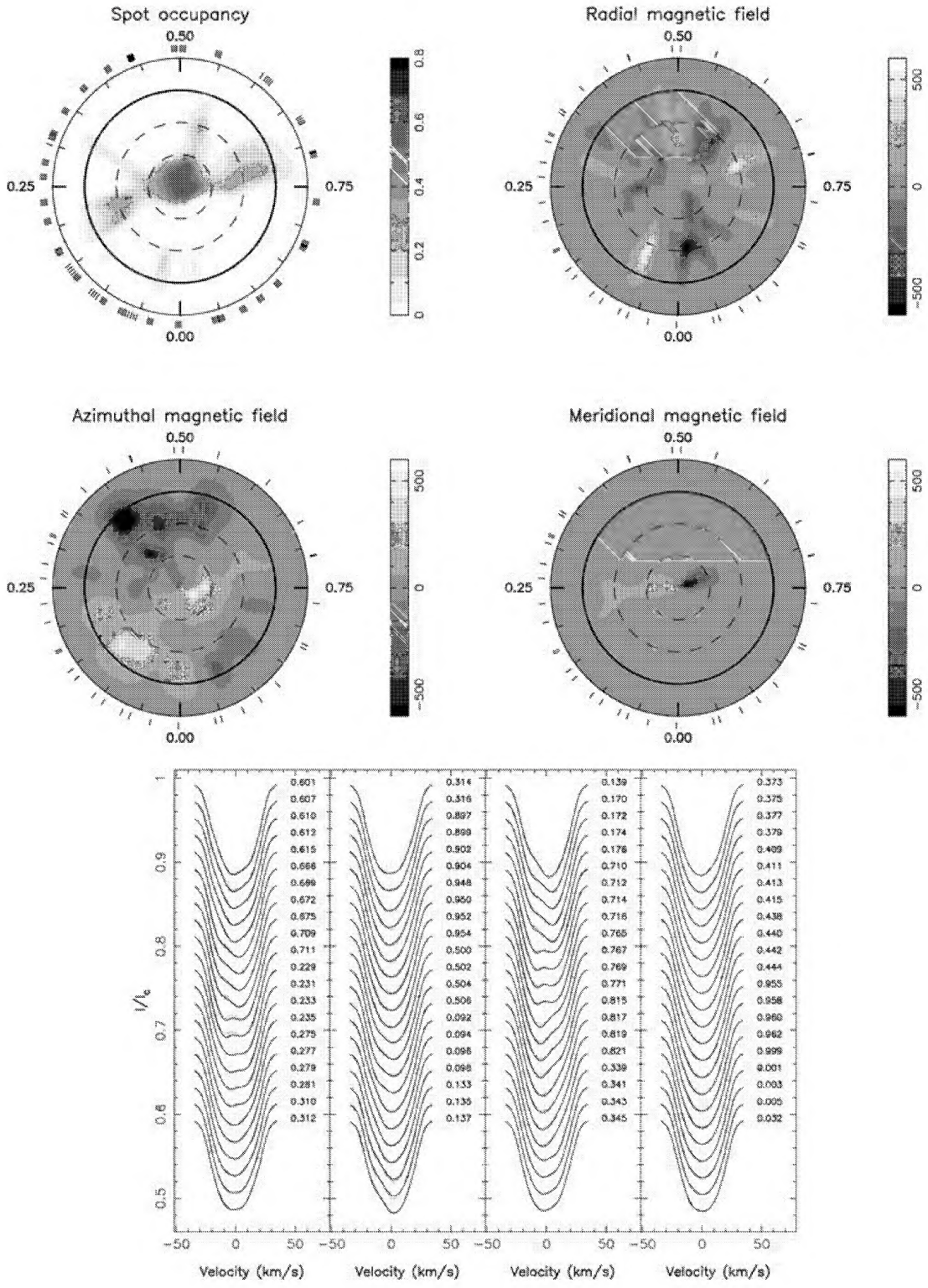

Figure 17. Same as in Fig. 13 for epoch 2001.99.

check very easily from comparing the left-hand panels of Figs 18 and 12.

Something we do not observe on LQ Hya are rings of azimuthal field encircling the star, similar to those we very clearly reconstruct on both AB Dor and HR 1099. The azimuthal field maps we obtain show a mixture of both polarities, with a preference for a counter-clockwise field to appear at high latitudes and a clockwise field to be present at low latitudes. This is most obvious at epoch 1998.03,

© Royal Astronomical Society • Provided by the NASA Astrophysics Data System

2003MNRAS.345.1145D

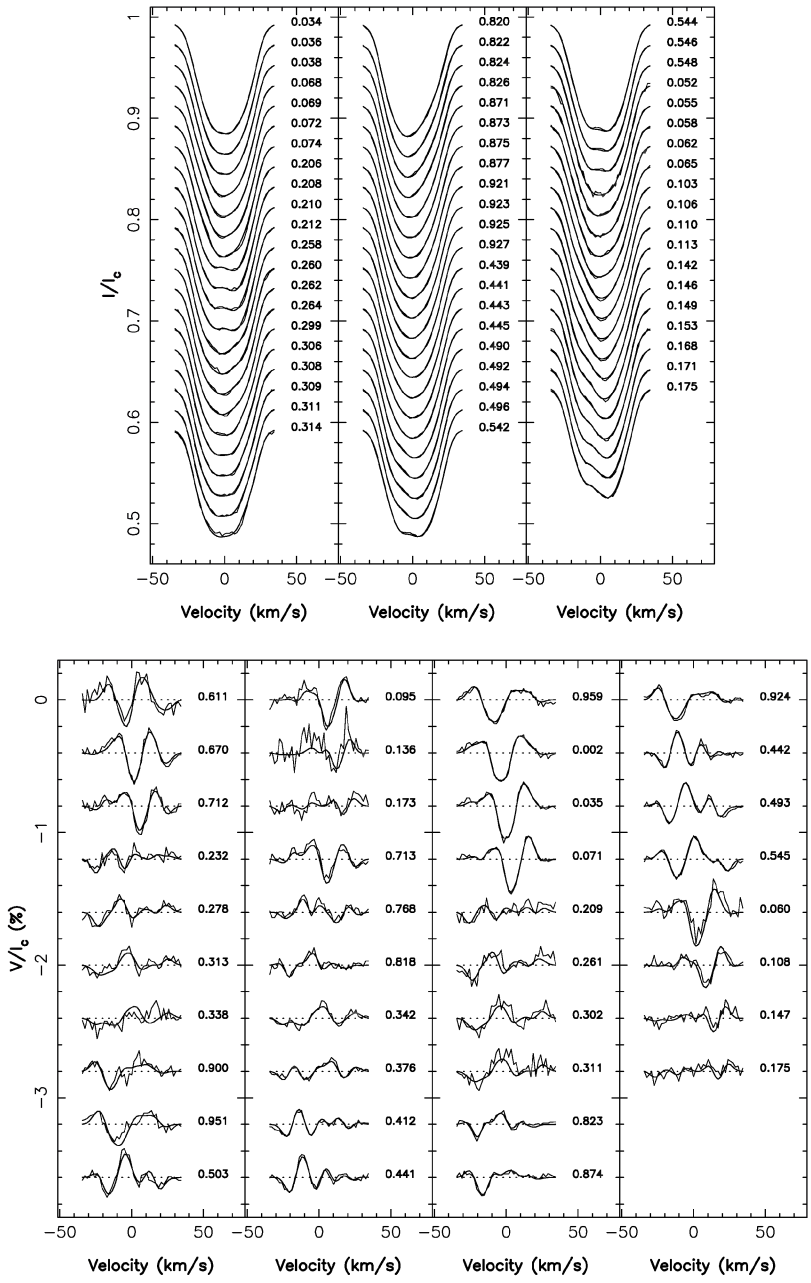

Figure 17 – *continued*

1999.00 and 2000.93 (the 1999.97 data set being too sparse to allow any meaningful conclusion). In particular, we confirm the initial observation of Donati (1999) that counterclockwise azimuthal field, essentially absent from all maps prior to epoch 1996.0, is becoming progressively more and more heavily represented at the surface of LQ Hya until it becomes roughly as important as the other azimuthal field polarity at epoch 2001.99. It may therefore suggest that a global polarity change of the azimuthal field structure (and thus of the underlying toroidal component of the large-scale dynamo field) is indeed taking place in LQ Hya, as initially proposed by Donati (1999). The latitudinal pattern of the mean azimuthal field map (averaged over epochs 1996.99–2001.99) indeed confirms that the axisymmetric component of the toroidal field structure now features two main polarities in the visible hemisphere (a positive one near the pole, peaking at a latitude of 70°, and a negative one close to the equator, at a latitude of 20°), instead of only one as was the case prior to epoch 1996.0 (Donati 1999). We emphasize that, as was the case for AB Dor, this axisymmetric component contains only a small fraction of the total azimuthal field energy reconstructed at each epoch, with most of the remaining energy being distributed in higher-order terms of the spherical harmonics expansion.

The radial field maps also feature at all epochs a number of spots of both polarities, but no apparent latitudinal preference for either polarities. At some epochs (1998.03 for instance), only very few

© Royal Astronomical Society • Provided by the NASA Astrophysics Data System

2003MNRAS.345.1145D

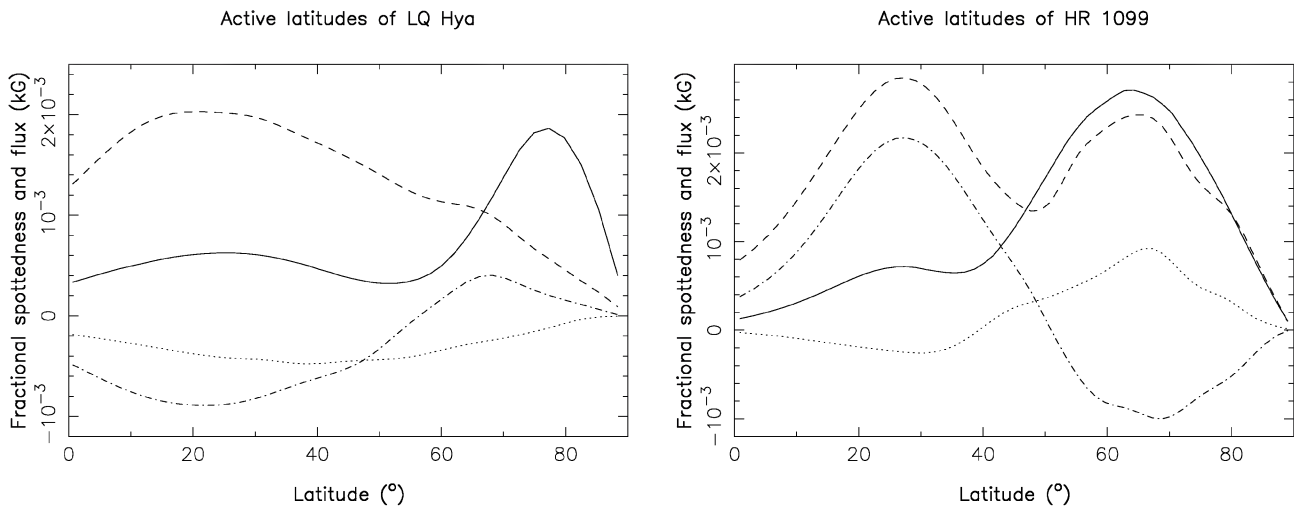

Figure 18. Same as the left-hand panel of Fig. 12 for LQ Hya (left-hand panel) and HR 1099 (right-hand panel). The dash-dot and dotted curves represent, respectively, the azimuthal field and radial field fluxes per latitude bin in kG, once integrated over longitudes and averaged over all epochs (except for the azimuthal field flux of LQ Hya, only averaged over epochs 1996.99–2001.99).

radial field spots are present at the stellar surface despite the reasonable phase coverage; at some others, however, a much larger number of regions with alternating polarities (up to 10) are reconstructed all around the star, as we often see on AB Dor. We therefore reach the same conclusion as that obtained for the azimuthal field, i.e. that most of the magnetic energy associated with the radial field component is stored in relatively high-order terms of the field structure. If we then average all maps together and produce a mean latitudinal polarity pattern for the radial field, we find that the axisymmetric component is essentially negative over the whole visible hemisphere (see the left-hand panel of Fig. 18), just as it used to be in previous years (Donati 1999).

When computing the relative fraction of the total magnetic energy stored in the different field components, we find that the field of LQ Hya is oriented most of the time azimuthally. If we exclude epochs 1995.94 and 1999.97 at which the very sparse data sets make this estimate rather unreliable, we find that more than 60 per cent of the magnetic energy is usually stored in the azimuthal field component. Only at epoch 1996.99 is the radial field dominant at the surface of LQ Hya, with no more than 20 per cent of the magnetic energy allocated to the toroidal field component. Although we cannot be sure whether this is significant or only a pure coincidence, we note that this epoch also corresponds to that at which the new azimuthal field polarity emerged at high latitudes (Donati 1999). We can conclude at least that, as for AB Dor, the relative energy content stored in the poloidal and toroidal components of the large-scale dynamo field of LQ Hya is found to undergo drastic changes with time, switching from regular situations when the field is essentially toroidal, to infrequent ones when the field is essentially poloidal. We return to this point in Section 6.

Conversely to what we see on AB Dor, there seems to be no evidence for active longitudes (in the sense defined in Section 3) at the surface of LQ Hya. The brightness and quadratic magnetic flux distributions integrated over latitudes 0°–50° usually feature several peaks randomly distributed in latitude; moreover, the longitudinal position of the peaks in both brightness and magnetic distributions do not usually coincide at any single epoch. Although this point does not necessarily contradict the conclusions of Berdyugina et al. (2002) given the fact that active longitudes are not defined in the same way in both studies, it nevertheless restricts the potential interest of the concept of active longitudes in LQ Hya, since these features (if real) do not seem to be associated there with any specific property of the magnetic field (supposed to be at the origin of most activity demonstrations in cool stars) as opposed to what we see on AB Dor. A definite answer to this question, however, requires the examination in detail of the properties of the large-scale magnetic field underlying the observed flux distributions of LQ Hya, with tools such as SHADE (Donati 2001); this is postponed for a forthcoming paper.

5 THE RS CVN SYSTEM HR 1099

For this study, we assume that the orbital parameters of the close RS CVn binary system HR 1099 are those recently redetermined by Donati (1999), assuming in particular a circular orbit and an inclination angle of 38° between the line of sight and both the orbital and spin rotation axes. As for the two previous stars, the $v \sin i$ we finally selected in this study for the primary system star (equal to 39 km s^{-1}) is slightly smaller (by 2 km s^{-1}) than that used by Donati (1999); this new estimate is found to produce a better fit to the observed LSD Stokes I profiles (especially in the wings), and thus to produce smaller residuals (and in particular smaller systematic differences) at the cost of a higher spot coverage.

Our data confirms the discovery of Donati (1999) that there is a systematic and time-dependent phase shift between the epochs of first conjunction (i.e. with the primary star closest to the observer) as derived from the observations and predicted by Fekel's (1983) ephemeris (giving HJD = 244 2766.080 + 2.837 74 E). As in Donati (1999), we define ϕ_0 as the phase (on Fekel's ephemeris) at which the observationally determined epoch of first conjunction occurs. The physical origin of the variability that ϕ_0 undergoes was tentatively attributed by Donati (1999) to changes in the quadrupolar moment of the primary star induced by its own activity cycle, as initially proposed by Applegate (1992). The value of ϕ_0 derived from the present data sets is found to decrease monotonically with time, from −0.0458 at epoch 1998.03 to −0.0784 at epoch 2001.99 (see Table 4). We find that the speed at which ϕ_0 decreases

© Royal Astronomical Society • Provided by the NASA Astrophysics Data System

2003MNRAS.345.1145D

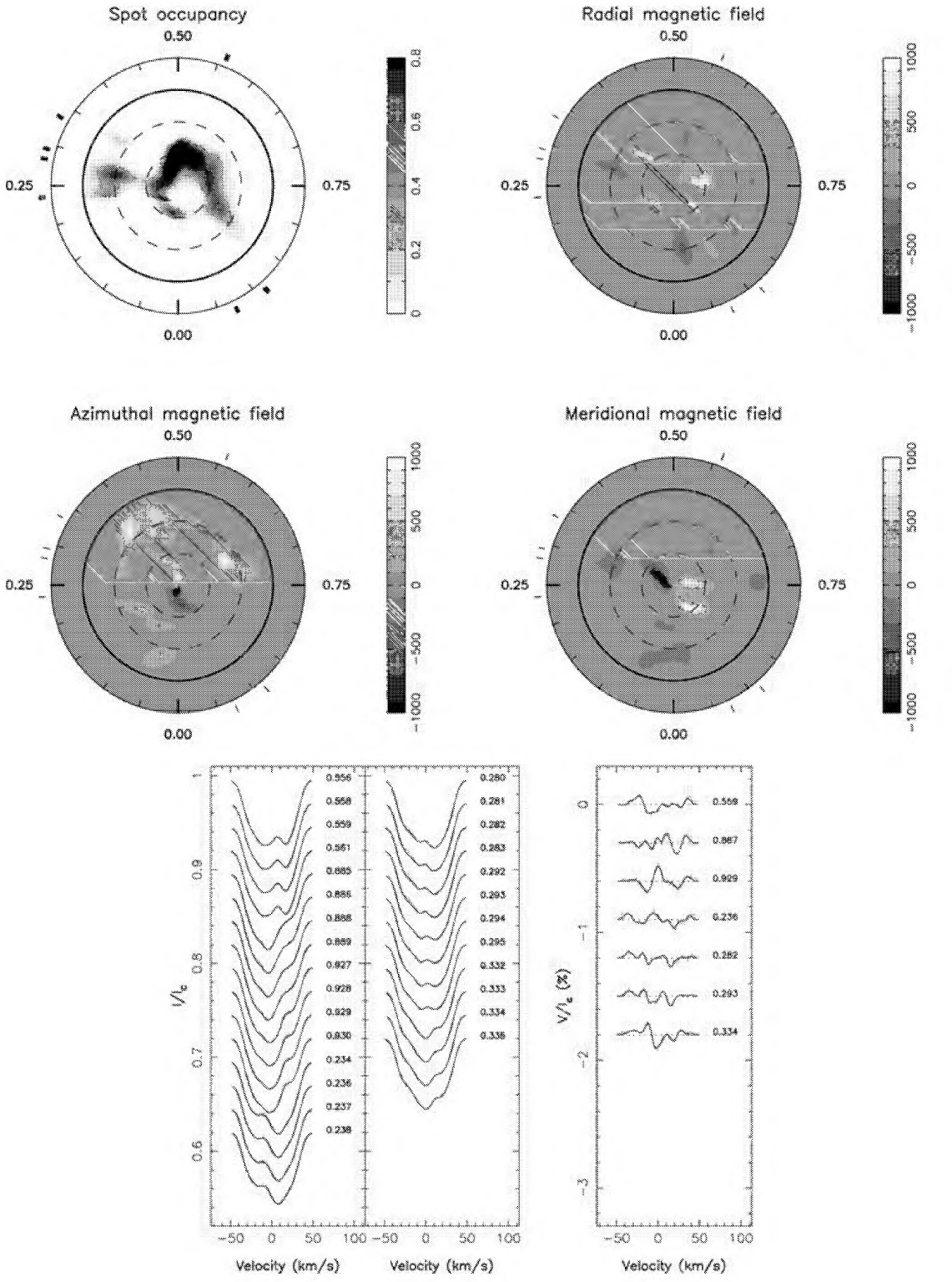

Figure 19. Same as in Fig. 13 for HR 1099 at epoch 1998.03.

with time (equal to 0.0083 cycle yr^{-1} in average between epoch 1995.94 and 2001.99) departs slightly (but significantly) from the average value depending on the epoch, but does not follow the evolution predicted by Donati (1999) from a sinusoidal extrapolation of the existing data; in particular, this speed did not switch sign at epoch 1999.3 (as the 18 yr sinusoidal variation proposed by Donati (1999) suggested), and shows no obvious intention to do so in the near future. It implies at least that the way ϕ_0 varies with time, if

© Royal Astronomical Society • Provided by the NASA Astrophysics Data System

2003MNRAS.345.1145D

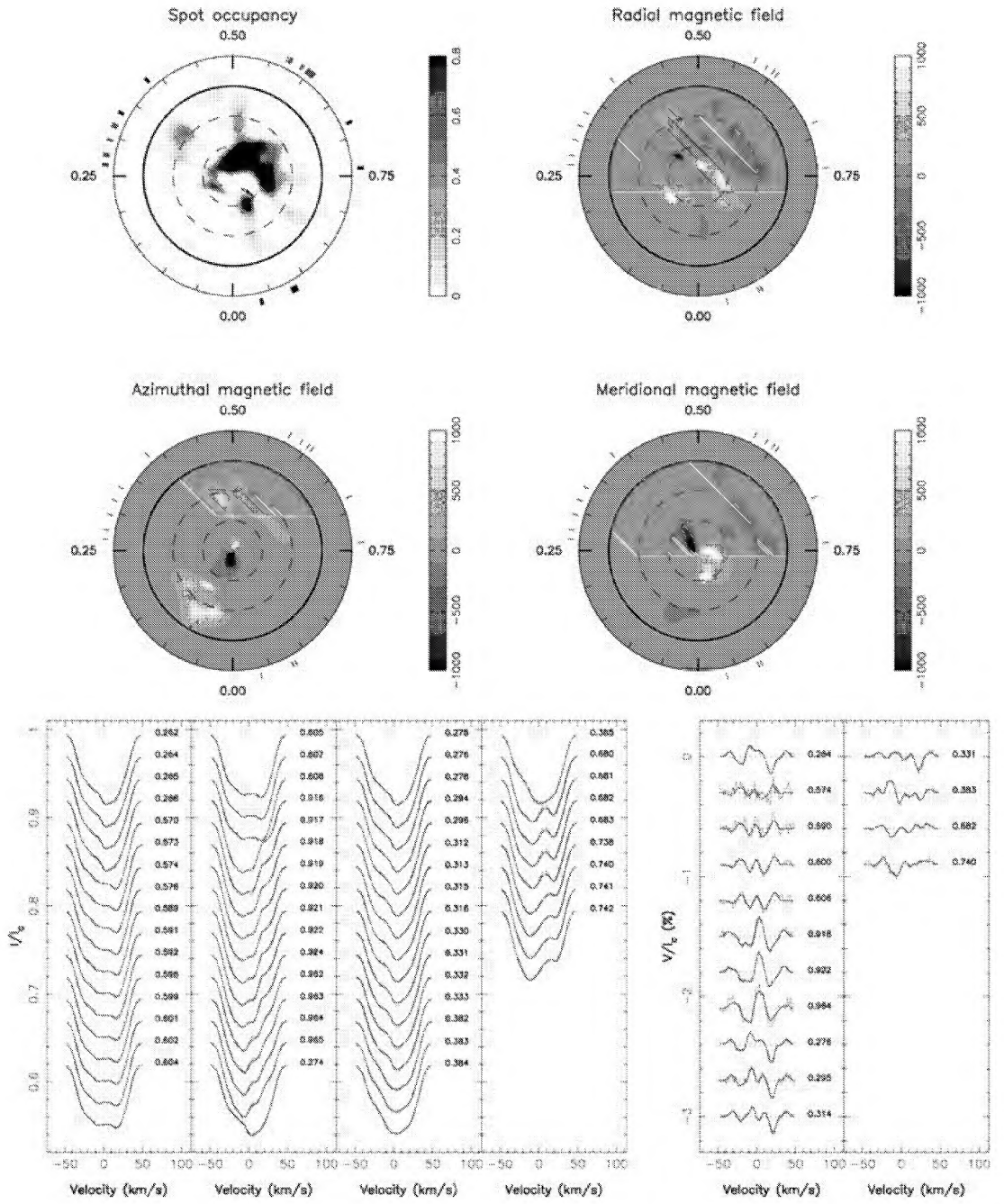

Figure 20. Same as in Fig. 19 for epoch 1999.00.

periodic,[4] is either strongly non-sinusoidal, or occurs on a period significantly longer than 18 yr, or both. To conclude on this specific point, we clearly need additional observations spanning at least one complete period of the fluctuations of ϕ_0 with time.

The semi-amplitude of the radial velocity curve and systemic velocity we obtain from a fit to the radial velocities of the secondary star (measured according to the method of Donati et al. 1992) are equal to 63.0 ± 0.1 and -14.8 ± 0.1 km s^{-1}, once averaged over epochs 1998.03–2001.99. We note, in particular, that the yearly variations we find on these two parameters are compatible with the accuracy we claim on the radial velocity measurements, confirming that there is no significant variation of the systemic velocity with time to an accuracy of approximately 0.1 km s^{-1}. We also mention that these new estimates are compatible with the previous, and less accurate, ones derived by Donati (1999, his table 2). This information is used to remove the (assumed Gaussian) profile of the secondary star from all our Stokes I LSD profiles of HR 1099. The results

[4] We consider that the variation of ϕ_0 is most likely periodic, to explain at least the fact that Fekel's (1983) ephemeris grossly reproduces the radial velocity observations of HR 1099 in the last two decades.

© Royal Astronomical Society • Provided by the NASA Astrophysics Data System

2003MNRAS.345.1145D

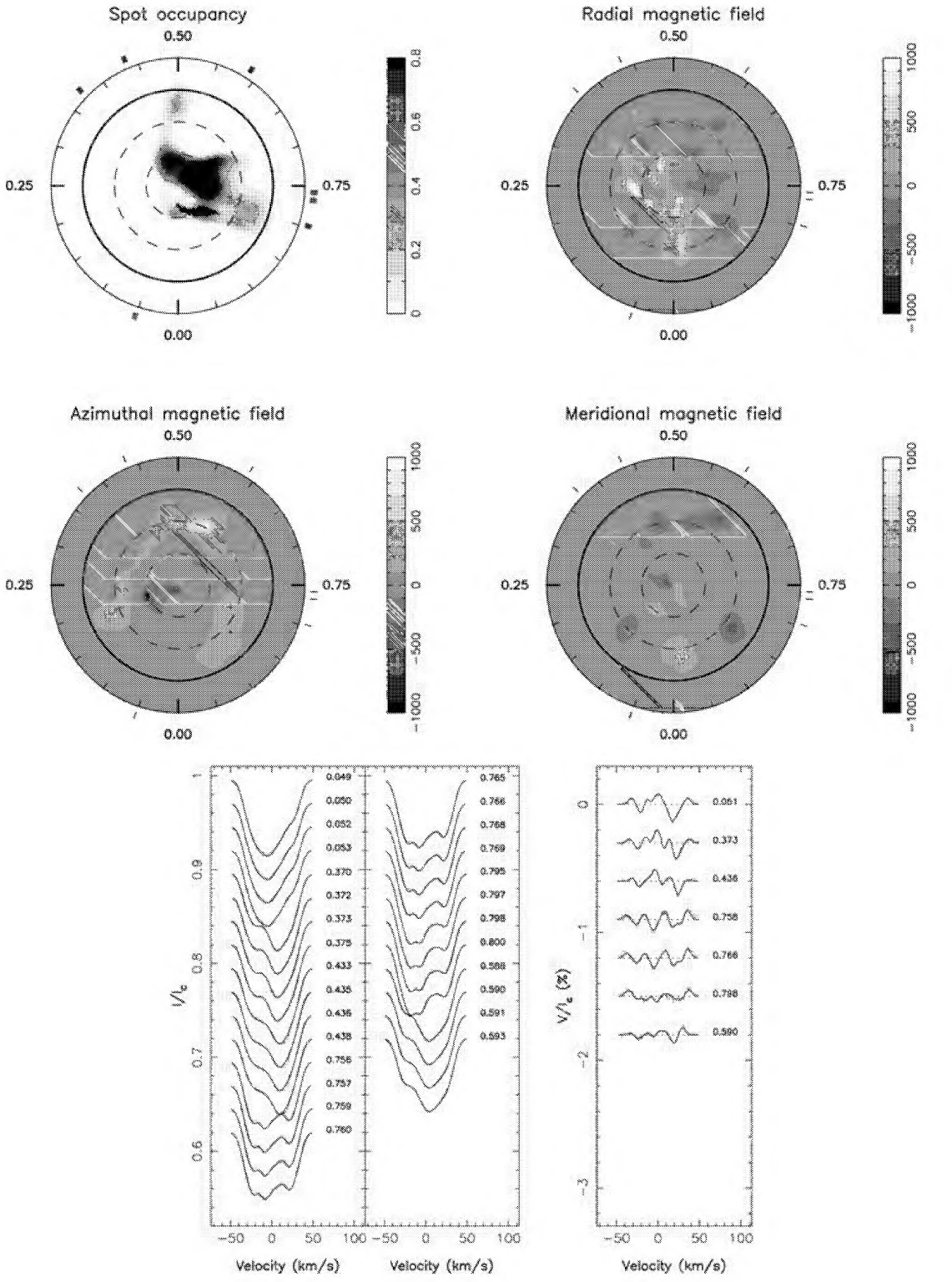

Figure 21. Same as in Fig. 19 for epoch 1999.97.

we obtain are found to be as satisfactory as those reported in Donati et al. (1992). We also repeated the experiment of Donati (1999) consisting in deriving, at each epoch, the mean LSD Stokes V signature of the secondary star by using observations of HR 1099 outside of system conjunction. We find that this mean signature is virtually identical to that obtained at previous epochs, featuring in particular both the same shape and amplitude as those depicted in fig. 2 of Donati (1999). We can thus conclude that no evidence yet exists that

© Royal Astronomical Society • Provided by the NASA Astrophysics Data System

2003MNRAS.345.1145D

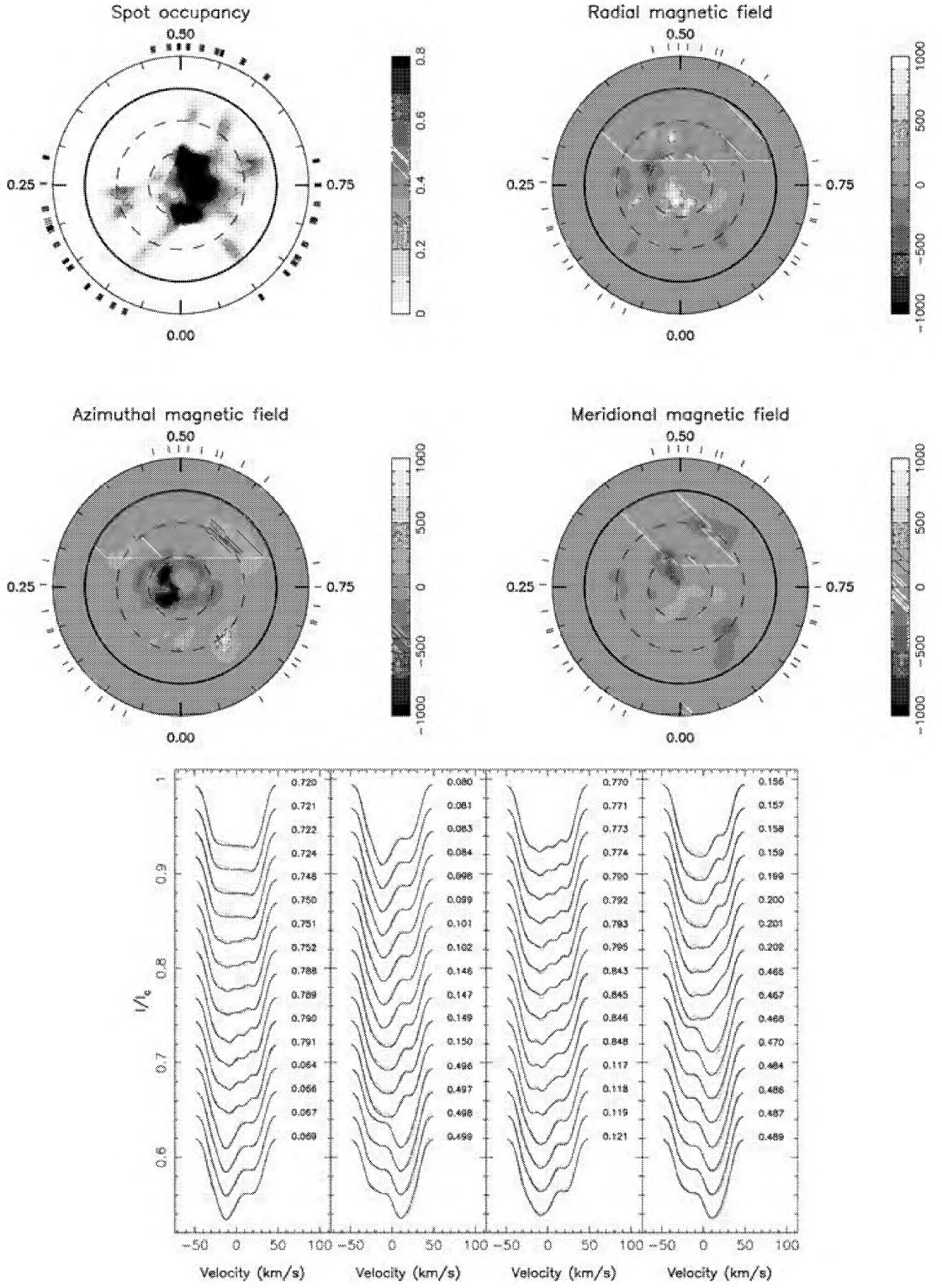

Figure 22. Same as in Fig. 19 for epoch 2000.93.

this mean signature (whatever its origin is) is variable on a long-term basis. Given the very small size of this average signature, we did not bother removing it from Stokes *V* LSD profiles of HR 1099 at conjunction phases prior to reconstructing the magnetic maps of the primary star, since previous experience (reported in Donati 1999) convinced us that this operation had virtually no impact on the recovered images.

In a second step, we derive, through fits to the Stokes *I* LSD profiles of the primary star with our imaging code, an estimate of the semi-amplitude K_p of the radial velocity curve for the primary

© Royal Astronomical Society • Provided by the NASA Astrophysics Data System

2003MNRAS.345.1145D

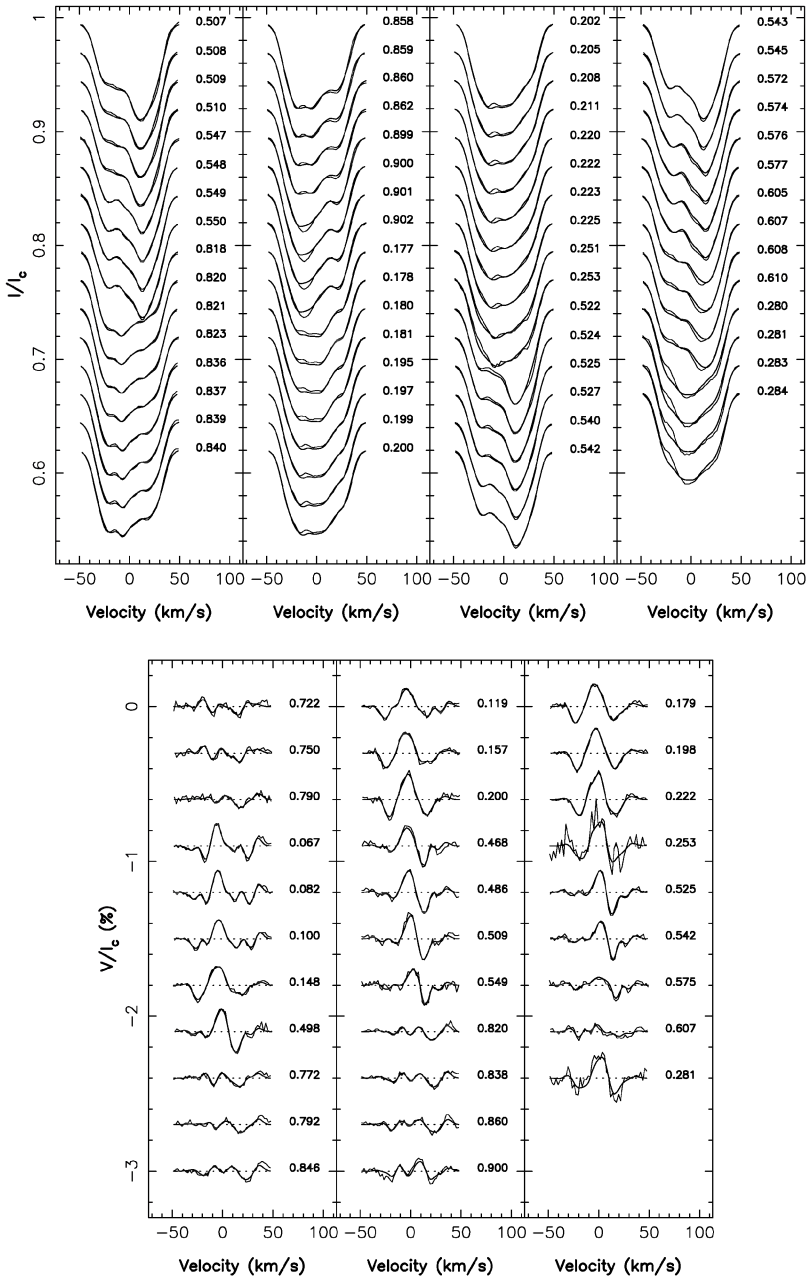

Figure 22 – *continued*

star, and a second (independent) measurement of the systemic velocity; these optimal parameters are selected by choosing the values that produce images with minimum spottedness at a given reduced χ^2 level (usually equal to one) between the observed and synthetic profiles at each epoch. Surprisingly enough, we find that this optimal value of the systemic velocity, equal on average to -14.5 ± 0.2 km s^{-1} over epochs 1998.03–2001.99, is slightly (but systematically) larger than that obtained from fitting the radial velocities of the secondary component. If this effect is real, we have no obvious explanation for it; given the fact that the difference is rather small and produces only negligible differences on reconstructed images, we simply averaged both estimates at each epoch to obtain our reference systemic velocity (listed in Table 4). The grand average over our total observing period yields a value of -14.6 ± 0.2 km s^{-1}, with (again) no significant variation with time. The estimate we obtain for K_p is on average equal to 49.1 ± 0.5 km s^{-1}; however, the values derived at different epochs now show a significant scatter with no apparent long-term trend, with a standard deviation (approximately 0.5 km s^{-1}) larger than the expected error bar (of the order of 0.2 km s^{-1}, see Table 4). Moreover, this new estimate is slightly smaller than that obtained previously by Donati (1999), equal to 50 ± 0.5 km s^{-1}. Since we have no obvious explanation of why this parameter should vary with time by as much as 2 per cent, and since it has no direct consequence on the topic discussed in the present paper, we keep this problem open for future work when a more extensive data set is available.

© Royal Astronomical Society • Provided by the NASA Astrophysics Data System

2003MNRAS.345.1145D

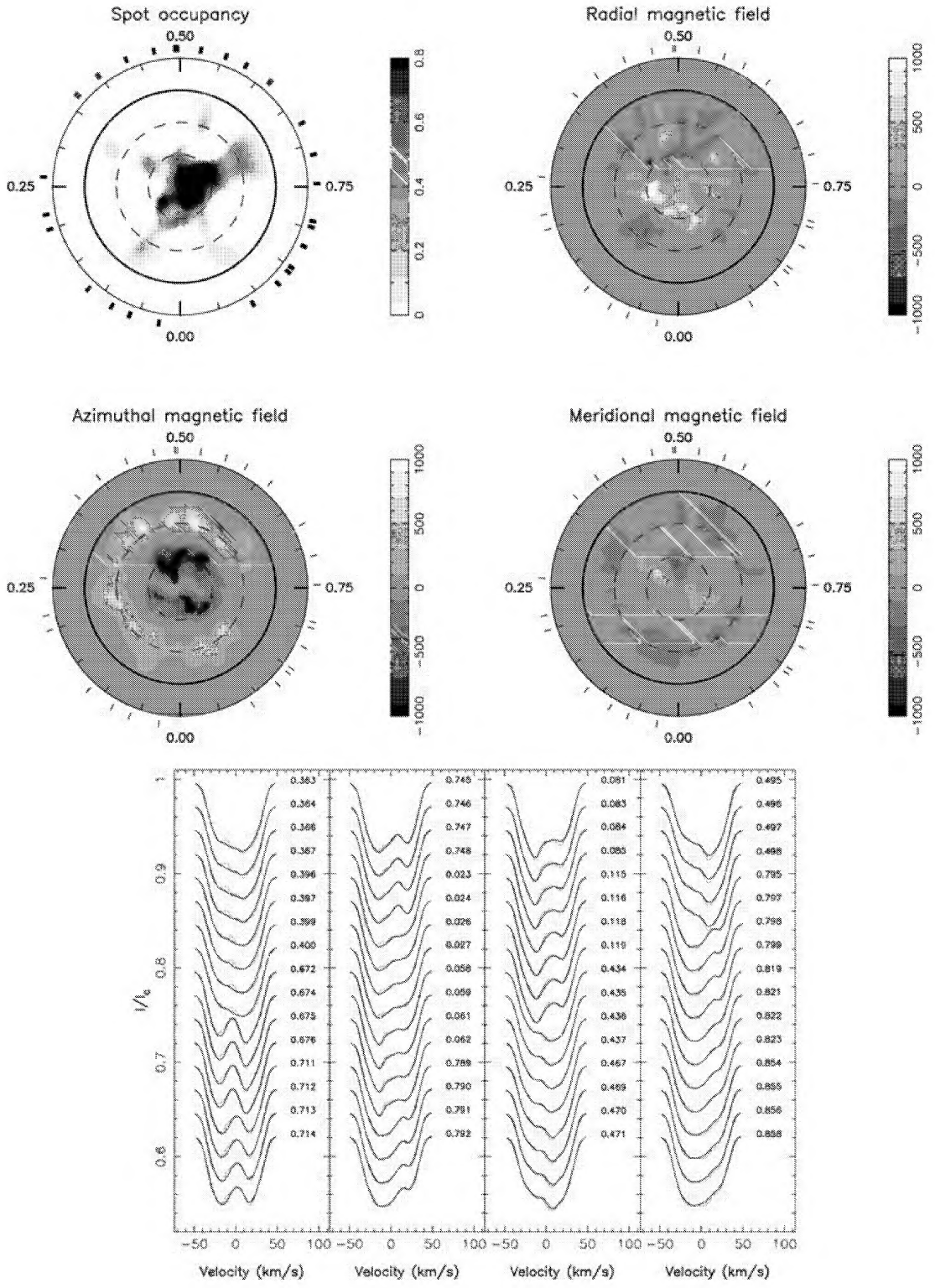

Figure 23. Same as in Fig. 19 for epoch 2001.99.

As for LQ Hya, all images of HR 1099 presented in this paper assume that no differential rotation distorts the brightness and magnetic surface distribution of spots. The most recent results concerning differential rotation at the surface of HR 1099 indicate that the photospheric shear that the primary star suffers is rather weak (with a time of approximately 1.3 yr for the equator to lap the pole by one complete rotation cycle, i.e. four times smaller than that of the Sun; Petit et al. 2001, 2003a), invalidating at the same time previous

© Royal Astronomical Society • Provided by the NASA Astrophysics Data System

2003MNRAS.345.1145D

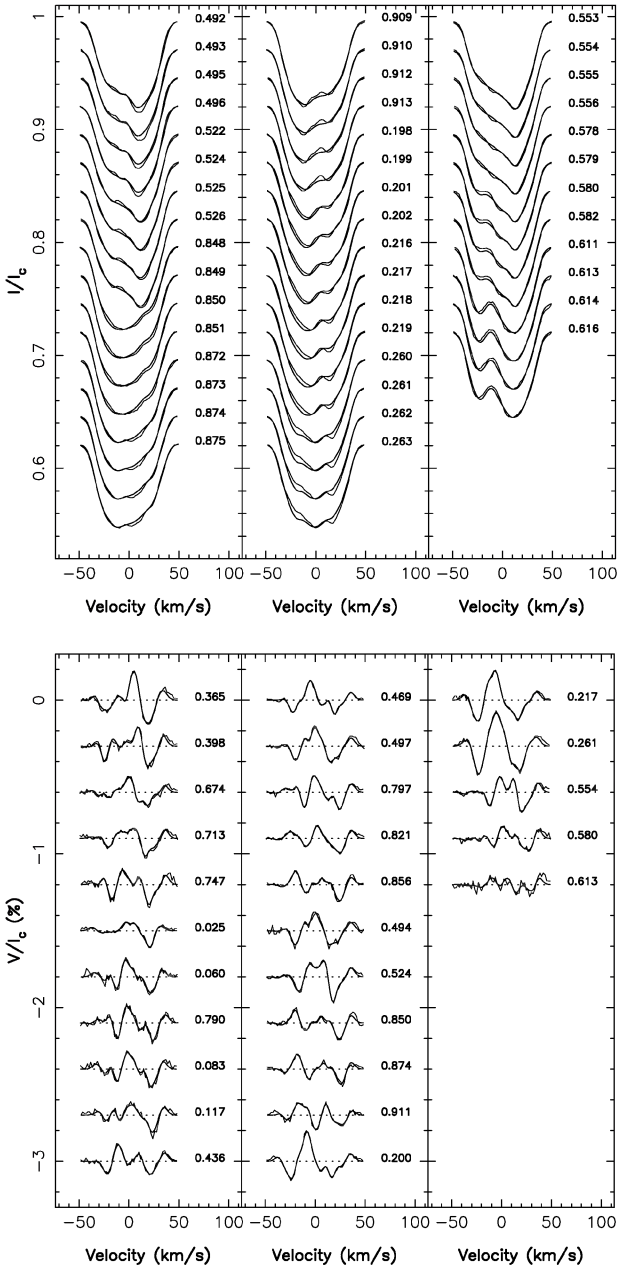

Figure 23 – *continued*

claims that surface differential rotation was antisolar on this star (with a pole rotating faster than the equator; e.g. Vogt et al. 1999). For our particular purpose, it tells us at least that image distortion over the maximum time-span of our observations should never blur reconstructed surface features by more than 0.8 per cent of the rotation cycle towards both sides of the position at which they are imaged, ensuring that the assumption that no differential rotation is present should have only a very small impact for our analysis.

The phase coverage achieved is sparse at epochs 1998.03 and 1999.97, but ensures at least that every point of the upper hemisphere was seen once. At other epochs, phase coverage is usually good on at least half the rotation cycle (in 1999.00) to very good (in 2000.93 and 2001.99). The maximum entropy images we derive from the different data sets are shown in Figs 19–23, along with the corresponding fits to the observed LSD profiles. Unpolarized LSD profiles are fitted to an average accuracy level of approximately 0.10–0.13 per cent rms (depending on the epoch) while Stokes V LSD profiles are adjusted at a reduced χ^2 level ranging from 1.0 to 1.5 (again depending on the epoch); we find, in particular, that data sets recorded over a longer time-span tend to yield larger fit residuals (see, for instance, the mediocre fit to the first eight Stokes I LSD profiles at epoch 2001.99 in Fig. 23), suggesting that temporal variability, caused by star spots emerging or disappearing, could be occurring on time-scales as short as a fortnight.

All brightness images we derive include essentially a main polar cap, usually strongly offcentred and very complex in shape, and

© Royal Astronomical Society • Provided by the NASA Astrophysics Data System

2003MNRAS.345.1145D

several extensions to lower latitudes and detached spots close to the equator. Their structure is very much the same as those presented in Donati (1999) and reconstructed from similar (though usually less densely sampled) data sets. We note, in particular, that the polar spot of HR 1099 is fairly different from that of AB Dor and LQ Hya and presents an extremely intricate aspect, making it sometimes even closer to a partial ring than to a real cap (e.g. at epoch 1998.03). The overall spot coverage we derive ranges between 6 per cent (at most epochs) to slightly larger than 8 per cent (at epoch 1995.94 and 2000.93) and does not seem to depend obviously on the phase coverage of the corresponding data set.

The average latitudinal pattern of all spot distributions since 1995 December, shown on the right-hand panel of Fig. 18, features a relatively broad peak at high latitudes (reflecting the fact that the polar cap is often strongly offcentred), and a smaller hump close to the equator. As for AB Dor, approximately 70 per cent of all spots are found at a latitude larger than 50°, with the rest of them forming essentially around an average latitude of 25°. The long-term behaviour seems to indicate a gradual decrease of the spottedness at low latitude, peaking at approximately 40 per cent at epoch 1996.99 and decreasing regularly since then down to approximately 20 per cent in our most recent image. We suspect that this observation reflects essentially the tendency of the polar spot to become progressively more centred and symmetric during the last 5 yr, and therefore to fit more completely within the 50° lower latitude limit we chose for this measurement, rather than to some putative migration of low-latitude features towards the pole. As pointed out in Petit et al. (2003a), we also note that the phase towards which the polar spot is decentred seems to shift slightly but steadily with time, from approximately phase 0.5 at epoch 1998.03 up to phase 0.8 at epoch 2001.99.

The new magnetic images of HR 1099 we present in this paper essentially confirms and extends the earlier conclusions reached in Donati et al. (1992) and Donati (1999). The value of the mean quadratic magnetic flux we recover is most of the time of the order of 90 G, except at epoch 2001.99 where it reaches almost 140 G (and is therefore back to the level it had at epoch 1995.94). Since minimal phase coverage (i.e. featuring at least three main phase groups evenly spaced throughout the rotation cycle) is secured at every single epoch on HR 1099, we are confident that this flux variation reflects a real phenomenon operating within HR 1099 rather than some spurious instrumental or observational effect; this conclusion is further confirmed by the fact that two extreme values of the magnetic flux (80 and 140 G) are obtained at epochs at which very dense phase coverage is achieved (2000.93 and 2001.99, respectively, see Figs 22 and 23). We also find that approximately 60 per cent of the quadratic magnetic flux we reconstruct at the surface of the star appears to be located at latitudes lower than 50°. One significant difference worth noting with respect to AB Dor and LQ Hya is that the magnetic flux distribution with latitude no longer appears as a continuum spreading out smoothly from the equator to the pole, but clearly features a double-peak structure, with one peak at a latitude of 65° and another one at 25°.

Among the three stars studied in this paper, HR 1099 is definitely the one on which the rings of azimuthal field encircling the star are most obvious; at epoch 2001.99 in particular, the azimuthal field map we reconstruct shows two prominent belt-like structures, one with a clockwise field at high latitude and another one with a counterclockwise field closer to the equator. This map is very reminiscent of that obtained at epoch 1995.94 for which both azimuthal field rings were also very clearly reconstructed (see Donati 1999). All the new maps presented here essentially repeat this information, featuring spots, arcs or rings of azimuthal field with a polarity that strictly obeys the same law (i.e. positive field below latitude 45° and negative field above this limit). We confirm, in particular, the observation of Donati (1999) that the high-latitude ring of clockwise azimuthal field usually forms a belt around the polar cap (e.g. at epoch 2000.93 and 2001.99), or at least a partial arc or an elongated region close to its outer edge.[5] Producing the latitudinal pattern of the mean azimuthal field map (averaged over all epochs, see the right-hand panel of Fig. 18) clearly shows the two main azimuthal field polarities that occupies the upper hemisphere of HR 1099. The only long-term evolution of this pattern worth reporting here is the fact that the high-latitude ring of the azimuthal field became progressively better centred (with the twin spots of meridional field close to the pole vanishing simultaneously). The visual impression that this ring became stronger is only a graphical illusion; if we count all meridional field regions poleward of latitude 45° as part of the toroidal field structure, and all those below latitude 45° as part of the poloidal field structure (as performed by Donati 1999), we indeed find that approximately half of the toroidal field quadratic flux is reconstructed at a latitude larger than 50° at all times (except at epoch 1999.97, most probably due to the sparse phase coverage achieved).

The radial field maps we recover for HR 1099 include a number of spots where the polarities also exhibit a very clear dependence with latitude; the radial field in high-latitude spots is indeed mostly emerging from the surface, while radial field regions at low latitudes almost always feature a negative polarity. This trend appears very clearly on the mean latitudinal polarity pattern of the radial field, averaged over both epochs and longitudes (see the right-hand panel of Fig. 18). It is interesting to note, in particular, that the latitudinal polarity patterns for both radial and azimuthal fields feature the same number of extrema, and are found to reach these extrema and to switch sign at roughly the same latitudes. As opposed to what is reported in Donati (1999), we no longer find any evidence that radial magnetic fields close to the pole are penetrating the photosphere. This is obvious, not only from the average latitudinal polarity pattern (i.e. the mean axisymmetric component) of the radial field, but also from most individual images, and in particular from the last two (featuring the densest phase sampling), for which no evidence of negative radial field is found above a latitude of 70°. Note, however, that some uncertainty still remains concerning the exact radial field polarity at the pole due to the fact that this region is indeed so cool with respect to the quiet photosphere that only a very few polarized photons are available to provide a fully reliable diagnosis on this point.

Given the fact that the inclination angle of HR 1099 is much lower than that of AB Dor and LQ Hya, we find that a significant amount of the magnetic energy reconstructed on HR 1099 is attributed to the meridional field component, in agreement with the results of Donati & Brown (1997). We find, in particular, that this fraction has been regularly decreasing from epoch 1998.03 up to now (from as much as 35 per cent to less than 10 per cent), reflecting essentially the fact that the high-latitude ring of clockwise azimuthal field encircling the cool polar spot became progressively better centred during the

[5] Note that the bipolar spot groups observed very close to the pole in both azimuthal and meridional field maps (especially prominent at epochs 1998.03 and 1999.00), are actually all part of the same magnetic feature, containing a field directed roughly homogeneously throughout the whole region; as already explained in Donati (1999, Section 3.4), its split appearance is no more than a visual artefact resulting from the fact that the pole is a singular point in spherical coordinates.

© Royal Astronomical Society • Provided by the NASA Astrophysics Data System

2003MNRAS.345.1145D

last 5 years. The images of Donati (1999) indicate that this recent decrease in the strength of the meridional field actually followed a symmetric increase of roughly equal amplitude, which occurred between epoch 1991.96 and 1996.99. It suggests at least that the main axis of symmetry of the azimuthal field component (and thus of the underlying toroidal structure) is varying in orientation with time, but on a rather long-term basis (at least one decade).

If we again count all meridional field regions as part of the poloidal or toroidal field structures depending on whether their latitudes are smaller or larger than 45° (see above), we find that the large-scale toroidal component usually contains more than 70 per cent of the total amount of magnetic energy. Only at epoch 1999.97 does the poloidal component dominate, with as much as 60 per cent of the total magnetic energy. We caution, however, that this epoch corresponds to one at which phase coverage, although not poor (with seven Stokes *V* observations in three evenly spaced phase groups, see Fig. 22), is one of the worst achieved since epoch 1991.96 (see Donati 1999). We do not think, however, that this explains our observation, since no such effect is observed at the other epoch at which phase coverage is equally sparse (i.e. 1998.03). Moreover, this effect is also observed in magnetic images obtained at roughly the same epoch from another totally independent data set with much denser coverage (Petit et al. 2003a). We actually rather suspect that these fluctuations are, as for AB Dor and LQ Hya, a direct consequence of the dynamo processes operating in the star and converting the poloidal field into a toroidal field and vice versa, as discussed more extensively in Section 6.

Looking at the distribution of spots and magnetic flux with longitude (once averaged over latitudes 0° to 60°), we find no clear correlation between local brightness and magnetic flux, nor any clue that spots or magnetic fields do gather at specific longitudes, as they seem to do on AB Dor (see Section 3). We therefore conclude that our data contain no evidence for active longitudes (as defined in Section 3) on HR 1099.

6 SUMMARY AND DISCUSSION

In this paper we have presented yearly brightness and magnetic images for three cool active stars, namely AB Dor, LQ Hya and HR 1099, derived from data secured throughout a total observing allocation of 50 nights (28 clear nights) on the Anglo-Australian Telescope, spread out on a period of approximately 5 yr. Along with the data already published by Donati & Cameron (1997), Donati (1999) and Donati et al. (1999), we now have in our hands a data base of brightness and magnetic images covering an interval of as much as 11 yr for HR 1099 and LQ Hya, and 7 yr for AB Dor. These images represent the only such data base available for observational studies of dynamo processes in convective zones of cool stars, and for investigations of activity cycles in stars other than the Sun.

6.1 Dynamo processes

This paper first confirms that the three very active stars discussed here persistently show magnetic regions in which the field is mostly azimuthal. Our new data thus bring further evidence that the initial discovery of Donati et al. (1992), and repeated since in Donati & Cameron (1997), Donati (1999) and Donati et al. (1999), undoubtedly corresponds to something inherent to the dynamo processes operating in very active stars, rather than to some spurious effect in either the data collection procedure, the reduction pipeline or the imaging software. Moreover, our new study demonstrates that these azimuthal field features include, most of the time, the main fraction of the energy corresponding to the surface magnetic field we reconstruct.

We also observe that these structures are stable on time-scales of at least 2 weeks, as we can judge from the fact that data collected over this period of time can usually be fitted as a whole down to the noise level (i.e. at unit reduced χ^2 level) without the need to assume that the magnetic structure is subject to intrinsic variability (apart from the photospheric shear resulting from differential rotation that is implemented as part of the imaging process). Note that we do not yet pretend to explain how these horizontal field structures detected at photospheric level can survive magnetic field buoyancy on such a long time-scale, but just tell that this is what the observations indicate; although intriguing, this result nevertheless needs to be given proper account, simply from the large body of evidence that we now have accumulated in favour of these apparently stable horizontal field regions.

For all three stars discussed here, the axisymmetric part of the azimuthal component of the magnetic field we recover is found to obey a strict latitudinal polarity pattern. This dependence is sometimes so obvious (in particular, when the axisymmetric part of the azimuthal field dominates) that it can be observed readily from the individual images; this is for instance the case of HR 1099 where two prominent azimuthal field rings are repeatedly observed encircling the star (at low and high latitudes, respectively) at basically all epochs. In other cases, this latitude dependence is less apparent (e.g. when the non-axisymmetric part of the azimuthal field dominates); averaging the azimuthal field distribution over longitudes nevertheless yields very clearly the polarity pattern that we mention, and that most of the time repeats identically from one year to the next. As already mentioned above and argued in several previous papers, we interpret this pattern as the photospheric imprint of the toroidal component of the large-scale dynamo field.

Note that this conclusion does not result from any kind of sophisticated modelling, but only reflects the logical fact that nearly axisymmetric azimuthal field rings encircling the star such as those we detect can simply not be attributed to something other than to the toroidal component of the large-scale dynamo field; it also witnesses the obvious deduction that such horizontal field structures could possibly not preserve their integrity while rising up to the surface and show up as they do at a photospheric level if they had been produced deep within the star. In particular, our idea is not necessarily compatible with the recent model of Schrijver & Title (2001) trying to explain the formation of polar spots in Sun-like stars and predicting the formation of radial field rings around the pole, rather than that of azimuthal field rings at all latitudes such as what we see on most stars observed to date.[6] The fact that this toroidal component is not deeply buried within the star, as in the Sun, but is rather readily visible at a photospheric level yet remains a very intriguing puzzle, and must probably be related to a new type of dynamo processes able to generate fields directly in the subsurface region (e.g. Dikpati et al. 2002) where strong radial gradients in angular rotation may also be present (e.g. Corbard & Thompson 2002), and possibly even distributed throughout the whole convective zone (e.g. Lanza, Rodonò & Rosner 1998).

The same observation applies for the radial field, the axisymmetric component of which also seems to obey a strict latitudinal

[6] Note that this statement does not mean that Schrijver & Title's (2001) model is inapplicable to active stars such as AB Dor, but rather implies that it is still too simple (if valid) to reproduce the main characteristics of the large-scale magnetic field observed on such stars.

© Royal Astronomical Society • Provided by the NASA Astrophysics Data System

2003MNRAS.345.1145D

polarity pattern. By analogy with our conclusions concerning the azimuthal field, and following the interpretation presented in previous papers, we propose that the radial field corresponds essentially to the poloidal component of the large-scale dynamo field. As far as the reconstructed meridional field is concerned (only significant in stars with low inclination angles, Donati & Brown 1997), we observe that it usually relates to the poloidal field component at low to medium latitudes (due to potential crosstalk problems between radial and meridional fields at these latitudes when imaging is performed from Stokes *V* data alone, see Donati & Brown 1997; Donati 2001), but must be associated with the toroidal field component at high latitudes (most often due to offcentred azimuthal field structures close to the pole, see Section 5).

Comparing the respective latitudinal polarity patterns of both poloidal and radial fields is potentially very instructive on the type of dynamos operating in these stars. In the Sun for instance, observations indicate that the poloidal and toroidal fields vary in time with a phase shift roughly equal to 180° all over the surface, a very useful and challenging constraint for testing theoretical dynamo models (e.g. Rüdiger & Brandenburg 1995; Schlichenmaier & Stix 1995; Dikpati & Charbonneau 1999; Dikpati & Gilman 2001). This is roughly what we see on HR 1099 as well, with radial and azimuthal fields featuring opposite signs at all latitudes (see the right-hand panel of Fig. 18). On LQ Hya, however, the situation (since epoch 1996.99 at least) is different, with radial and azimuthal field components featuring opposite polarities only at latitudes higher than approximately 55°. Both field components are negative at lower latitudes, as they used to be over the whole visible hemisphere prior to epoch 1995.94 (see Donati 1999). On AB Dor, the situation is even more complex; while the azimuthal field exhibits up to three different polarities in the upper hemisphere (with no apparent temporal evolution of the polarity pattern), the radial field showed no more than two up to epoch 1999.5 and even only one (since then). The situation is therefore far more complicated than that of the Sun, resulting probably from the fact that several dynamos (and probably several types of dynamo, e.g. an overshoot layer dynamo and a distributed dynamo) are operating at the same time within the convective zone of these stars.

It is also likely that the spatial structure of the axisymmetric dynamo field component depends on the fundamental parameters of the star. In this respect, AB Dor and LQ Hya are very similar in mass (1 $M_\odot$ for AB Dor and 0.95 $M_\odot$ for LQ Hya) and age (approximately 40–50 Myr for both), according to the pre-main-sequence evolutionary models of Siess, Dufour & Forestini (2000). The depth of their convective zone is also almost the same (approximately 30 per cent of the stellar radius), and roughly equal to that of the Sun. Both stars differ, however, very significantly in their rotation rate, with AB Dor spinning approximately 3.4 times faster than LQ Hya (and up to 50 times faster than the Sun). Although HR 1099 is also as massive as the Sun (according to Donati 1999), it is, however, much more evolved (with an age of approximately 10 Gyr, Charbonnel et al. 1996) and thus hosts a much deeper convective zone (approximately 85 per cent of the total radius). An important difference with the two other stars studied in this paper is that HR 1099 is a member of a close binary system, and suffers (as a likely consequence of the close binarity and the strong tidal forces that result) a much weaker rotational shear of its photosphere (Petit et al. 2001).

From the corresponding models of the stellar structure, we can estimate both the Rossby number (characterizing the strength of the interaction between rotation and convection) and the dynamo number (measuring the efficiency of the dynamo processes) across the convective zone, using the equations mentioned in, for example, Mangeney & Praderie (1984) and assuming that the characteristic velocity α (describing the effect of fluid helicity on the large-scale magnetic field) is of the order of the stellar rotation rate times the local mixing length (as approximated in Mangeney & Praderie 1984). We find, in particular, that the inverse Rossby number exceeds 10 in most of the convective zone for all three stars (up to approximately 5 per cent of the stellar radius below the surface), whereas this situation occurs in the Sun only in a very thin layer at the bottom of the convective zone. Assuming the same differential rotation shear for LQ Hya and AB Dor (which is roughly valid at least when averaged over several years, Donati et al. 2003), we moreover find that the diffusive damping time of the magnetic field exceeds the amplification time by a factor larger than 40 (and thus that the dynamo number is larger than 10^3) throughout the whole region in which the inverse Rossby number exceeds 10, indicating that dynamo processes will certainly be very active within most of the convective zone. Note that this certainly does not explain how such fields can survive buoyancy forces on time-scales longer than the activity cycle itself, i.e. of the order of at least one decade.

We find in particular that AB Dor and HR 1099 roughly share the same dynamo efficiency, the lower rotation and differential rotation rates of HR 1099 being compensated by its much larger convective depth. The dynamo number of LQ Hya is approximately half that of the other two stars, as a result of the smaller rotation rate. We caution, however, that this ranking is still largely uncertain, most parameters used to estimate the dynamo number being model dependent (and, in particular, the depth of the convective zone) and therefore subject to potentially large errors. It is nevertheless reassuring to find that what we obtain is at least compatible with the observed spatial structure of the axisymmetric toroidal/poloidal field components (the higher the dynamo number, the larger the number of toroidal/poloidal field rings).

Comparing the dashed curves of Figs 12 and 18, we also note that the integrated quadratic magnetic flux at high latitudes with respect to that at low latitudes seems to rank on the same scale. While the low-latitude magnetic flux dominates its high-latitude counterpart on LQ Hya, both are roughly equal on HR 1099, and the high-latitude component is significantly stronger than the low-latitude one on AB Dor. This again directly reflects the structural differences in the way dynamo processes operate in stars with different dynamo numbers, and suggests, in particular, that magnetic fields concentrate at higher latitudes in stars with higher dynamo numbers. Note that this effect is probably not a consequence of, or at least not fully attributable to, the phenomenon described by Schüssler et al. (1996) in which flux tubes emerging from the base of the convective zone are deflected to higher latitudes by the Coriolis force in very rapidly rotating stars. The effect we report here is indeed readily visible on the axisymmetric component of the azimuthal magnetic field themselves (see the dash-dot curves of Figs 12 and 18); given the fact that this field component must be generated very close to the surface (since it would not be visible as an azimuthal field otherwise), we conclude that the observed magnetic field concentration towards higher latitude in stars with higher dynamo numbers very likely reflects some intrinsic property of the dynamo processes operating in these very active stars (and, in particular, the spatial structure of the excited dynamo modes), rather than an indirect consequence of how the field emerges to the surface as proposed by Schüssler et al. (1996).

Another important difference worth noticing between HR 1099 and the two other targets studied here is that its magnetic structure is much closer to axisymmetry. As detailed in Section 5, the latitudinal

© Royal Astronomical Society • Provided by the NASA Astrophysics Data System

2003MNRAS.345.1145D

polarity patterns of both radial and azimuthal field components of HR 1099 are readily visible from the individual images themselves, while they are actually much more tricky to identify unambiguously for AB Dor and LQ Hya (being essentially hidden under the stronger non-axisymmetric components). Note, in particular, that this observation refers to basically all epochs, and not just to a few selected ones. We speculate that it reflects some major difference between the stars themselves, and in particular in their convective zones. The main difference is the thickness of the envelope itself, being in proportion almost three times larger in HR 1099 than in the other two stars. It may suggest that the non-axisymmetric component (or at least most of it) is mainly caused by a magnetic field deeply rooted at the base of the convective zone, that consequently hardly shows up at the stellar surface (or only at very high latitudes, e.g. Schüssler et al. 1996) or ends up being trapped within the star (Holzwarth, Schüssler & Solanki 2001) when the convective zone is as deep as in HR 1099. This is of course only a speculation that must be tested with observations of other rapidly rotating evolved stars with very deep convective zones (such as FK Com stars for instance, e.g. Petit et al. 2003b) prior to deriving any meaningful conclusion on this point. This requires, in particular, the use of quantitative tools (such as SHADE, Donati 2001) to study the relative strength of the various spatial modes excited by the dynamo processes, and the respective weight of axisymmetric versus non-axisymmetric components.

6.2 Activity cycles

As reported in the description of the reconstructed images (see Sections 3–5), we observe that the magnetic field configuration of all three stars undergo long-term structural changes with time. The most obvious aspects of these changes are of course the major brightness and magnetic spot rearrangements that we observe from year to year. In most cases, these modifications reflect no more than the limited lifetime of stellar surface structures, estimated to be of the order of 1 month from long-term monitoring of these targets (e.g. Petit et al. 2003a).

One noticeable exception concerns the polar spots of all three stars, and the rings of azimuthal field encircling the rotation axis (especially obvious on both HR 1099 and AB Dor). These features, even though they display some level of variability, are globally stable on a long-term basis. While their evolution with time does not seem to follow any kind of regular trend in AB Dor and LQ Hya, the situation looks different in HR 1099, the cool polar cap of which seems to obey some long-term transformation, as already mentioned in Section 5 and discussed in Petit et al. (2003a). By looking at the images presented in this paper along with those published in Donati (1999), one can indeed clearly note a regular evolution in the rotational phase towards which the polar cap is tilted, raising progressively from 0.05 at epoch 1992.94 to 0.75 at epoch 2001.99; the only brightness image in the series that does not fit this pattern is that corresponding to epoch 1991.96 (for which the polar spot is tilted towards phase 0.40). It may suggest that some cyclic evolution is taking place in HR 1099 on a typical time-scale of 12 yr, with some abrupt events taking place from time to time (e.g. between epoch 1991.96 and 1992.94 in our case). This scenario seems, however, incompatible with the assumption that the orbital period fluctuations (showing perfect smoothness all the way from epoch 1991.96 to 2001.99, with no hint of discontinuities between epoch 1991.96 and 1992.94) are caused by the activity cycle of the primary star, as proposed by Applegate (1992) and discussed at length in Donati (1999).

Something we cannot confirm is the general existence of one main, well-defined, stellar active longitude at which star spots and magnetic fields tend to cluster preferentially at a given epoch. Most images indeed show a large number of features at any single epoch, but no clustering towards specific longitudes of both magnetic fields and star spots at any given epoch; only on AB Dor do we marginally observe this trend at certain epochs (see Section 3), but nothing similar on either HR 1099 nor LQ Hya. Moreover, even when hints of such clustering is observed, we note no obvious temporal evolution of these active longitudes, and, in particular, do not observe the sudden and recurrent 180° phase shift (usually designated under the name of 'flip-flop', e.g. Jetsu et al. 1993) that these features are reported to undergo. A detailed examination of the most accurate brightness images we reconstructed for LQ Hya at the specific phases where active longitudes (as defined by Jetsu et al. 1993) are supposed to be located in this star (Berdyugina et al. 2002) gives no support to their existence either. Of course, this does not imply that active longitudes do not exist, but it tells us at least that their existence is still essentially a matter of speculation at the moment; investigating the large-scale magnetic topology underlying the observed magnetic field distributions (with tools such as SHADE, Donati 2001) is certainly a promising avenue to progress in this direction and attempt at revealing any slowly varying low-order structures that potentially hide beneath the observed rapidly variable spatially complex surface maps derived from the observations.

No clear secular change is detected yet in the axisymmetric component of the magnetic field of either stars. In particular, no global polarity switch was observed in the very obvious azimuthal field ring pattern of HR 1099, nor in the high-latitude azimuthal field ring of AB Dor, the topology of which has thus remained essentially constant for the last 11 and 7 yr, respectively. Some modifications of the magnetic field structure can nevertheless be reported for both LQ Hya and AB Dor. As announced in Donati (1999) and confirmed in this study, the axisymmetric component of the azimuthal field switched from negative to positive at high latitudes on LQ Hya between epoch 1995.94 and epoch 1996.99; similarly, the axisymmetric component of the radial field at high latitudes on AB Dor switched from strongly negative at epoch 1998.03 to strongly positive at epoch 2000.93 (with no apparent evolution in the polarity of the high-latitude azimuthal field ring). These variations obviously represent strong evidence that partial polarity switches do indeed occur on these stars; it is, however, premature to diagnose whether these changes actually occur on a regular basis and can be considered as cyclic or are essentially random in nature, and whether these partial changes are the forerunners of a global polarity switch or the signature of a multiperiodic variability of the large-scale magnetic structure. Only further observations can provide answers to these questions.

One thing we can note as well are the secular changes in the total spottedness and quadratic magnetic flux of these stars. The solar analogy suggests, in particular, that these parameters may vary with the activity cycle as well. Both quantities are indeed observed to vary for all three stars, even between epochs at which data sets are very densely sampled (e.g. epochs 2000.93 and 2001.99), demonstrating that these fluctuations are indeed genuine. While this conclusion was already well established for the total stellar irradiance from the long photometric records existing in the literature for all three stars, we can now safely claim that this is also the case for the quadratic magnetic flux (at least that corresponding to the visible fraction of the stellar surface). This variability, even though expected for a number of reasons, does, however, not seem to correlate with any of the structural changes in the magnetic field reported above, and, in particular, the polarity switches observed in the axisymmetric field components. This may, in particular, explain why previous

© Royal Astronomical Society • Provided by the NASA Astrophysics Data System

2003MNRAS.345.1145D

investigations on long-term photometric variations of active stars yielded only very discrepant (and therefore probably spurious) values for the cycle period.

Another kind of variability worth reporting here is the temporal evolution in the relative fraction of reconstructed azimuthal and radial field that we detect on all three stars. Note that this observation is only based on the large-scale magnetic features that our imaging technique was able to reconstruct from the rotationally modulated Zeeman signatures detected in the stellar spectra. If the azimuthal and radial field patterns we observe for all three stars do indeed represent the large-scale toroidal and poloidal components of the dynamo field as we suspect, and if the modifications we observe in the field structure somehow relate to an activity cycle, then we would expect to see, at some stages, demonstrations of the physical processes underlying dynamo action, i.e. the successive transformation of the poloidal field into the toroidal field and vice versa. We speculate that the temporal evolution we report in the fractional magnetic energies stored in the medium- to large-scale radial and azimuthal field structures reconstructed at the surface of all three stars may be a direct illustration of this phenomenon. On LQ Hya, we observe that the field is mostly poloidal at epoch 1996.99, i.e. when the azimuthal polarity initiated its sign switch at high latitudes. On AB Dor, we find that the poloidal field component dominates the toroidal one at epochs 1995.94 and 1999.97, slightly before the axisymmetric component of the radial field showed a strong unipolar feature at high latitude (epochs 1998.03 and 2000.99). On HR 1099, the only epoch at which the poloidal field seems to dominate is 1999.97, but no obvious sign of polarity switch in any of the field components can be associated with it.

Finally, looking at the mean magnetic signature associated with the secondary star of HR 1099 (see Section 5) can also provide some information concerning a possible magnetic cycle of the primary star; if we indeed assume that this average magnetic signature results from the effect of the magnetic field of the primary star on to the photosphere of the secondary star (as suggested by Donati 1999 from the fact that this mean signature is extremely simple, much simpler, in particular, than what it ought to be for an active star with a $v \sin i$ of 12 km s^{-1}), the non-variability of this mean signature argues in favour of the fact that the global poloidal dynamo field of the subgiant (the strength of which is of the order of 200 G) did not change significantly over the last 12 yr, and in particular did not switch sign. Still further evidence in this direction can be obtained from the observation that the phase of the first system conjunction decreases steadily with time (see again Section 5), suggesting that the orbital motion is roughly stable and therefore that the large-scale dynamo field of the subgiant (assumed to be at the origin of the orbital motion fluctuations, Applegate (1992) has been approximately constant over the last 8 yr or so.

Again, we emphasize the fact that the various hints of global magnetic polarity switches that we report in this paper are only very fragmentary at the moment. If these clues are further confirmed, it would indicate that magnetic polarity switches indeed occur on these very active stars and that their dynamo magnetic fields are likely to vary periodically. For the moment, we can only conclude that the full magnetic cycles of LQ Hya and HR 1099 (if any) are longer than approximately twice the total observation time-span, i.e. of the order of, or larger than, approximately two decades. We can at least safely state that it rules out the periods of approximately 5 and 16 yr proposed for LQ Hya by Berdyugina et al. (2002), the signatures of which are clearly not found in our data set. The situation of AB Dor is more ambiguous; from the observed polarity switch at high latitudes in the poloidal field component, one could invoke a cycle length of only 6–8 yr, while the non-variability of the toroidal field component suggests at the same time a cycle period at least twice as long. A possible way out of this apparent contradiction is that the magnetic cycles of these very active stars are multiperiodic, with several dynamo modes simultaneously present at the surface of the star, each fluctuating with its specific time-scale.

7 CONCLUSIONS AND PROSPECTIVES

The observational material presented in this paper, along with previously published results on the same stars (Donati & Cameron 1997; Donati 1999; Donati et al. 1999), constitute the first long-term data set on the temporal variations in the magnetic topologies of a few very active stars. All reconstructed magnetic images indicate that large regions hosting predominantly azimuthal magnetic fields are continuously present at the surfaces of these stars. We take this as evidence that the underlying dynamo processes that produce them are operating throughout their entire convective zone (and, in particular, close to the surface as well), rather than being confined at its base as in the Sun.

We speculate that the radial and azimuthal field maps that we recover correspond, respectively, to the poloidal and toroidal components of the large-scale dynamo field. In the series of images, we find that some specific signatures, and, in particular, the relative fraction of magnetic energy stored in the poloidal and toroidal field components, and the polarity of the axisymmetric component of the field, are variable with time, and provide potentially fruitful diagnostics to investigate magnetic cycles in active stars other than the Sun. We report here the detection of partial polarity switches in some of the axisymmetric components of two of our programme stars (AB Dor and LQ Hya), suggesting that the dynamo operating in these stars may be cyclic.

Although very promising, the results presented here are nevertheless still very fragmentary and require confirmation from the addition of new data that will provide longer time bases for studying stellar activity cycles. Optimally, the aim would be to cover at least one full magnetic cycle of each star, estimated to be of the order of approximately two decades. More high-resolution spectropolarimeters, similar to that used for the present study, but more efficient in throughput (to allow them to operate on smaller, more available, telescopes) are required in this aim. A good strategy would consist in replicating ESPaDOnS (Donati et al. 1998) for 2-m class telescopes in both hemispheres, such as Telescope Bernard Lyot at Pic du Midi (a project called NARVAL, mostly funded already), to allow the long, repeated and if possible multisite, observational campaigns that are necessary for continuing this kind of investigation and improving our knowledge on how stellar dynamos operate.

ACKNOWLEDGMENTS

We thank the ATAC and PATT committees for generous allocations of observing time over the last five years. We are also very grateful to Corinne Charbonnel for computing specific models of the internal structure for the various stars discussed in this paper and to the referee, Nikolai Piskunov, for suggesting modifications that significantly improved the clarity of the paper.

REFERENCES

Applegate J.H., 1992, ApJ, 385, 621
Basri G., Marcy G.W., Valenti J.A., 1992, ApJ, 390, 622
Bennett J.M., 1970, Appl. Opt., 9, 2123

© Royal Astronomical Society • Provided by the NASA Astrophysics Data System

2003MNRAS.345.1145D

Berdyugina S.V., Pelt J., Tumoninen I., 2002, A&A, 394, 505
Borra E.F., Landstreet J.D., 1980, ApJS, 42, 421
Brown S.F., Donati J.-F., Rees D.E., Semel M., 1991, A&A, 250, 463
Cameron A.C., 1992, in Byrne P.B., Mullan D.J., eds, Surface Inhomogeneities on Late-Type Stars. Springer-Verlag, Berlin, p. 33
Cameron A.C., Donati J.-F., 2002, MNRAS, 329, L23
Charbonnel C., Meynet G., Maeder A., Schaerer D., 1996, A&AS, 115, 339
Corbard T., Thompson M.J., 2002, Solar Phys., 205, 211
Dikpati M., Charbonneau P., 1999, ApJ, 518, 508
Dikpati M., Corbard T., Thompson M.J., Gilman P.A., 2002, ApJ, 575, L41
Dikpati M., Gilman P.A., 2001, ApJ, 559, 428
Donati J.-F., 1999, MNRAS, 302, 457
Donati J.-F., 2001, in Boffin H.M.J., Steeghs D., Cuypers J., eds, Lect. Notes Phys. 573, Astrotomography, Indirect Imaging Methods in Observational Astronomy. Springer-Verlag, Berlin, p. 207
Donati J.-F., Brown S.F., 1997, A&A, 326, 1135
Donati J.-F., Cameron A.C., 1997, MNRAS, 291, 1
Donati J.-F., Brown S.F., Sernel M., Rees D.E., Dempsey R.C., Matthews J.M., Henry G.W., Hall D.S., 1992, A&A, 265, 682
Donati J.-F., Semel M., Carter B.D., Rees D.E., Cameron A.C., 1997, MNRAS, 291, 658
Donati J.-F., Catala C., Landstreet J.D., 1998, in Martin P., Rucinski S., eds, Proc. fifth CFHT Users Meeting, p. 50
Donati J.-F., Cameron A.C., Hussain G.A.J., Semel M., 1999, MNRAS, 302, 437
Donati J.-F., Mengel M., Carter B.D., Marsden S.C., Cameron A.C., Wichmann R., 2000, MNRAS, 316, 699
Donati J.-F., Cameron A.C., Petit P., 2003, MNRAS, 345, 1187 (this issue)
Fekel F.C., 1983, ApJ, 268, 274
Guirado J.C. et al., 1997, ApJ, 490, 835
Hatzes A.P., Penrod G.D., Vogt S.S., 1989, ApJ, 341, 456
Holzwarth V., Schüssler M., Solanki S.K., 2001, in Mathys G., Solanki S., Wickramasinghe D., eds,, Magnetic Fields throughout the HR diagram. Astron. Soc. Pac., San Francisco, p. 259
Hussain G.A.J., Donati J.-F., Cameron A.C., Barnes J.R., 2000, MNRAS, 318, 961
Jardine M., Cameron A.C., Donati J.-F., 2002, MNRAS, 333, 339
Jetsu L., Pelt J., Tuominen I., 1993, A&A, 278, 449
Kurucz R.L., 1993, CDROM no 13 (ATLAS9 atmospheric models) and no 18 (ATLAS9 and SYNTHE routines, spectral line database)
Lanza A.F., Rodonò M., Rosner R., 1998, MNRAS, 296, 893
Mangeney A., Praderie F., 1984, A&A, 130, 143
Petit P. et al., 2001, in Boffin H.M.J., Steeghs D., Cuypers J., eds, Lect. Notes Phys. 573, Astrotomography, Indirect Imaging Methods in Observational Astronomy. Springer-Verlag, Berlin, p. 232
Petit P. et al., 2003a, MNRAS, submitted
Petit P. et al., 2003b, MNRAS, submitted
Piskunov N., Kochukhov O., 2002, A&A, 381, 736
Robinson R.D., 1980, ApJ, 239, 961
Rüdiger G., Brandenburg A., 1995, A&A, 296, 557
Schlichenmaier R., Stix M., 1995, A&A, 302, 264
Schrijver C.J., Title A.M., 2001, ApJ, 551, 1099
Schüssler M., Caligari P., Ferriz-Mas A., Solanki S.K., Stix M., 1996, A&A, 314, 503
Semel M., 1989, A&A, 225, 456
Siess L., Dufour E., Forestini M., 2000, A&A, 358, 593
Skilling J., Bryan R.K., 1984, MNRAS, 211, 111
Stenflo J.O., 1992, in Tuominen I., Moss D., Rüdiger G., eds, IAU Coll. 130, The Sun and Cool Stars: Activity, Magnetism, Dynamos. Springer-Verlag, Berlin, p. 193
Strassmeier K.G., Rice J.B., Wehlaw W.H., Hill G.M., Matthews J.M., 1993, A&A, 268, 671
Unruh Y.C., Cameron A.C., 1995, MNRAS, 273, 1
Vogt S.S., Penrod G.D., Hatzes A.P., 1987, ApJ, 321, 496
Vogt S.S., Hatzes A.P., Misch A.A., Kürster M., 1999, ApJS, 121, 547

This paper has been typeset from a TEX/LATEX file prepared by the author.

© Royal Astronomical Society • Provided by the NASA Astrophysics Data System